Controls on Mixing and Non-Mixing Dependent Denitrification in River Hyporheic Zones

Katherine I. Young

Thesis submitted to the faculty of the Virginia Polytechnic Institute
and State University in partial fulfillment of the requirements for the
degree of

Master of Science
In
Civil Engineering

Erich T. Hester, Chair
Mark A. Widdowson
Madeline E. Schreiber

December 2, 2013
Blacksburg, VA

Keywords: hyporheic, surface water-groundwater exchange, pollutant attenuation, nitrate, denitrification, streams, contaminants, sediments

Controls on Mixing and Non-Mixing Dependent Denitrification in River Hyporheic Zones

Katherine I. Young

Abstract

Increases in reactive nitrogen from human actions have led to negative impacts on surface water (SW) and groundwater (GW) quality, and it is important to better understand denitrification processes in aquatic systems. The hyporheic zone has unique biogeochemical conditions, and is known to attenuate contaminants originating from SW and traveling through the hyporheic zone, together with necessary reactants. However, the ability of the hyporheic zone to attenuate contaminants from deeper upwelling GW plumes as they exit to SW is less understood. I used MODFLOW and SEAM3D to simulate hyporheic flow cells induced by riverbed dunes and upwelling GW together with mixing dependent denitrification of an upwelling nitrate (NO_3^-) plume. My basecase model scenario entailed dissolved organic carbon (DOC) and dissolved oxygen (DO) advecting from SW and DO and NO_3^- advecting from GW, which is typical of water in agricultural land uses. I conducted a sensitivity analysis to determine controls on mixing dependent denitrification. Mixing dependent denitrification increased with increasing hydraulic conductivity, decreasing lower bottom flux, as well as increasing DOC in SW and NO_3^- in GW. Non-mixing dependent denitrification also occurred when there was SW NO_3^-, and I found its magnitude was much greater than mixing dependent denitrification. Nevertheless, potential for hyporheic zones to attenuate upwelling NO_3^- plumes seems to be substantial, though highly variable depending on biogeochemical reaction rates as well as geomorphic, hydraulic and biogeochemical conditions. Stream and river restoration efforts may be able to increase both mixing and non-mixing dependent reactions by increasing hyporheic zone residence times.

Acknowledgements

I would like to thank the Charles E. Via, Jr. Endowment at Virginia Tech for providing support while completing my M.S. thesis. I thank Milko Maykowskyj for assisting me in using FORTRAN, Michael Mobile for assisting me in using codes within GMS, Jay Zarnetske for assisting me with Monod kinetics, and Andrew Tompson for providing the Turning Bands Codes. Additionally, I would like to thank my family friends and research group for all of their support. Finally, I would like to thank my advisor Erich Hester, as well as my committee members Mark Widdowson and Madeline Schreiber.

Table of Contents

List of Figures

List of Tables

List of Abbreviations

DOC	Dissolved organic carbon
DO	Dissolved oxygen
SW	Surface water
GW	Groundwater
K_{xx}	Value of hydraulic conductivity (L/T) along the *x* coordinate axis
K_{yy}	Value of hydraulic conductivity (L/T) along the *y* coordinate axis
K_{zz}	Value of hydraulic conductivity (L/T) along the *z* coordinate axis
h	Potentiometric head (L)
W	Volumetric flux per until volume representing sources and/or sinks of water (T^{-1})
S_S	Specific storage of the porous media (L^{-1})
t	Time (T)
θ	Porosity of the subsurface medium (-)
C^k	Dissolved concentration of species *k* (ML^{-3})
$x_{i,j}$	Distance along the respective Cartesian coordinate axis (L)
D_{ij}	Hydrodynamic dispersion coefficient tensor (L^2T^{-1})
v_i	Seepage or linear pore water velocity (LT^{-1})
q_s	Volumetric flow rate per unit volume of aquifer representing fluid sources (positive) and sinks (negative) (T^{-1})
C_s^k	Concentration of the source or sink flux for species *k* (ML^{-3})
$\sum R_k$	Reaction term ($ML^{-3}T^{-1}$)
R_{DO}	Total biological DO reaction rate ($ML^{-3}T^{-1}$)
R_{NO3}	Total biological NO3- reaction rate ($ML^{-3}T^{-1}$)
R_{DOC}	Total biological DOC reaction rete ($ML^{-3}T^{-1}$)
M_n	Biomass concentration for reaction *n* (either aerobic respiration or denitrification) (ML^{-3})
M_{AR}	Biomass concentration for aerobic respiration (ML^{-3})
M_{DN}	Biomass concentration for denitrification (ML^{-3})
$\gamma_{k,n}$	The use coefficient for species *k* in reaction *n* (-)
$\gamma_{DO,\,AR}$	Use coefficient for DO in aerobic respiration (-)
$\gamma_{NO3,\,DN}$	Use coefficient for NO_3^- in denitrification (-)
v_n	The maximum specific rate of utilization for reaction *n* (T^{-1})
v_{AR}	Maximum specific rate of utilization for aerobic respiration (T^{-1})
v_{DN}	Maximum specific rate of utilization for denitrification (T^{-1})
C_{ED}	Electron donor (DOC) concentration (ML^{-3})
C_{EA}	Electron acceptor (DO or NO_3^-) concentration (ML^{-3})
C_{DOC}	DOC concentration (ML^{-3})
C_{DO}	DO concentration (ML^{-3})
C_{NO3}	NO_3^- concentration (ML^{-3})
K_{ED}	Half saturation constant for the electron donor (ML^{-3})
K_{EA}	Half saturation constant for the electron acceptor (ML^{-3})
K_{DOC}	Half saturation constant for DOC (ML^{-3})
K_{DO}	Half saturation constant for DO (ML^{-3})
K_{NO3}	Half saturation constant for NO_3^- (ML^{-3})
I	Inhibition function (-)
K_I	Inhibition constant for denitrification (ML^{-3})

1. Introduction

1.1 Literature Review

Human actions such as combustion of fossil fuels, production of nitrogen fertilizers, and cultivation of nitrogen-fixing legumes have approximately doubled the rate of transfer of unreactive nitrogen (N_2) to reactive nitrogen species (e.g., NO_3^-), resulting in extensive alterations to the natural global nitrogen cycle [*Galloway et al.*, 1995; *Vitousek et al.*, 1997]. Production and application of reactive nitrogen in the form of synthetic fertilizers has enabled humans to increase crop yields and support larger populations; however at the same time, the use of such fertilizers has released considerable amounts of reactive nitrogen to the water supply through agriculture runoff and seepage, and through additional sewage from humans and livestock [*Braun*, 2007]. Human derived increases in the supply of reactive nitrogen has led to negative impacts on water quality and aquatic ecosystems including groundwater (GW) contamination [*Howden et al.*, 2011], eutrophication [*Galloway et al.*, 2003], biodiversity loss [*Sala et al.*, 2000] and increased hypoxic events [*Diaz and Rosenberg*, 2008]. Denitrification, an important process in the nitrogen cycle, is the reduction of nitrate (NO_3^-) to nitrogen gasses (N_2O and N_2) by denitrifying heterotrophic bacteria. This process occurs under anaerobic conditions in the presence of electron donors such as dissolved organic carbon (DOC). Denitrification is important because it is the only way reactive nitrogen can be converted back to unreactive nitrogen. It is thus important to better understand denitrification processes in aquatic systems.

1.1.1 Excess Nitrate from Inorganic Fertilizers

The use of synthetic fertilizers is the largest source of reactive nitrogen in the world, representing approximately half of the total human derived reactive nitrogen inputs [*Howarth et al.*, 2002]. Land applications of reactive nitrogen from fertilizer has increased in the United States (US) from 3.1 billion kg N a^{-1} in 1961 to 11.2 billion kg N a^{-1} in 1999, and in 2002 the US used 13.1% of the total inorganic nitrogen fertilizer used globally [*Howarth et al.*, 2002]. In the US, more than 50% of reactive nitrogen inputs are removed as harvested crops [*Howarth et al.*, 2002], with the remainder running off into waterways or leaching into the GW primarily as NO_3^-. If underlying aquifers are anoxic and contain labile DOC, NO_3^- can be denitrified and converted back to unreactive nitrogen through denitrification. If dissolved oxygen (DO) is present, denitrification is inhibited and the NO_3^- is capable of being transported to surface water (SW). It is estimated that in the US, about 23% of total reactive nitrogen inputs to agricultural fields are denitrified or stored in the soil, and about 20% are leached to water either by directly running off into SW or by leaching into GW and then eventually discharging into the SW [*Howarth et al.*, 2002].

The median NO_3^- concentration in GW underlying agriculture land across the US is 13.2 mg/L, and the range is ~0 to 70.9 mg/L (10^{th}-90^{th} percentile) [*Dubrovsky et al.*, 2010]. The composition of a "typical" NO_3^- GW plume varies considerably depending on the properties of the underlying aquifer. If the aquifer is anoxic (GW DO < 0.5 mg/L) the plume will likely have NO_3^- concentrations just at detection levels (~0.9 mg/L) [*Dubrovsky et al.*, 2010]. Extremely low NO_3^- concentrations in anoxic GW has been seen as the "norm" across the U.S. underlying agricultural regions and other land uses (e.g., urban) [*Dubrovsky et al.*, 2010], and is likely because denitrification is occurring. However, if the underlying aquifer is oxic, the plume will likely contain much higher amounts of NO_3^-, because DO inhibits denitrification. The median concentration of NO_3^- in oxic aquifers in the U.S. in agriculture land uses is 24.8 mg/L [*Dubrovsky et al.*, 2010], which is much higher than the median concentration of all aquifers.

It is clear that in aquifers, NO_3^- concentrations are related to DOC and DO concentrations. Similarly, DOC and DO in aquifers are functionally related, and the concentration of one often affects the concentration of the other. *Chapelle et al.* [2012] presents data for the DOC and DO concentrations for 1552 well samples from 17 different NAWQA study areas located throughout the US. They found that the relationship between DOC and DO was not random, and that typically, when DO concentrations are high, DOC concentrations tend to be lower, and vice-versa (Figure 1-1). The pattern described regarding DOC and DO in GW makes sense, because if there is excess DO, aerobic respiration has probably already depleted the DOC, and if there is excess DOC, aerobic respiration has probably already depleted the DO. Aerobic respiration is microbial respiration using DO as an electron acceptor and DOC as an electron donor. Data from *Chapelle et al.* [2012] also showed that often GW is depleted of both DOC and DO, but the data did not show any cases where there were significant amounts of both DOC and DO.

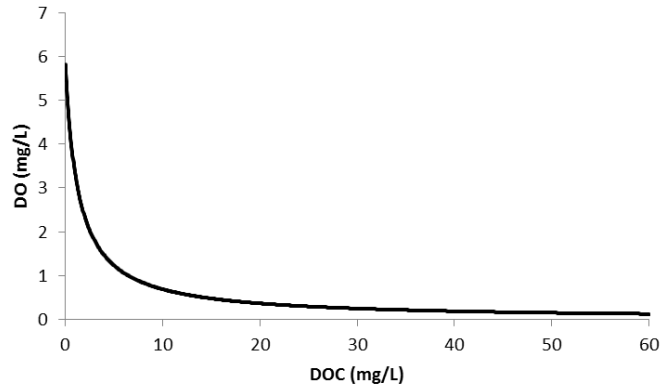

Figure 1-1: Trend *Chapelle et al.* [2012] found between concentrations of DOC versus DO for 1552 wells sampled in 17 NAWQA study areas located throughout the United States.

1.1.2 Excess Nitrate from Human and Animal Waste

As noted previously, in the US, more than 50% of the reactive nitrogen from fertilizers is removed from fields as harvested crops and then fed to animals and humans [*Howarth et al.*, 2002]. About 17% of reactive nitrogen is then exported to GW and SW as animal waste [*Howarth et al.*, 2002]. One situation where high amounts of animal waste get into the GW is in the vicinity of concentrated animal feeding operations (CAFO). *Toetz* [2006] described the distribution of NO_3^- in wells in the proximity of a CAFO, and found high amounts of NO_3^- (>106 mg/L) in the wells just below the waste spray area of the CAFO. It was determined that the CAFO was the source of the contaminant plume. Reactive nitrogen can also get into the water supply from human waste. Approximately 8% of reactive nitrogen (removed from fields) is exported as human waste to wastewater treatment plants and onsite treatment systems, where some of the reactive nitrogen is eventually discharged back into SW and GW [*Howarth et al.*, 2002]. It is likely that a considerable portion of the reactive nitrogen from human and animal waste is denitrified along the way, however the exact amount is unknown.

In the US about 26 million homes, businesses and recreational facilities use onsite wastewater treatment systems which collect, treat, and release about 4 billion gallons of effluent daily[*Schwartz*, 2010]. Such systems consist of septic tanks and drain distribution fields, which release the effluent to the shallow subsurface [*United States Census Bureau*, 1993]. Septic system effluent typically contains high ammonium (NH_4^+), high DOC and some DO. DOC is consumed via aerobic respiration and NH_4^+ is consumed by nitrification and converted to NO_3^-. Additionally, DO is typically consumed by both nitrification and aerobic respiration. The resulting contaminant plumes from septic systems typically have depleted DO (<1 mg/L), high NO_3^--N (22-180 mg/L) and low to medium DOC-C (1.9 - 3.4 mg/L) [*Robertson et al.*, 1991; *Robertson and Cherry*, 1992; *DeSimone and Howes*, 1998] (Table 1-1).

Table 1-1: Typical concentration ranges of solutes in aquifers with various contamination sources.

Contamination Source	Typical Concentration (mg/L)		
	DOC-C	DO	NO_3^-
Agriculture (Oxic Aquifer)	0-5	>0.5	0-70.9
Agriculture (Anoxic Aquifer)	0-50	<0.5	<0.9
Septic System	1.9-3.4	<1	22-180

1.1.3 Mixing Dependent Denitrification in the Hyporheic Zone

All nitrogen sources within watersheds eventually flow through streams and rivers, which control nitrogen exports via internal nitrogen source and sink processes (e.g., mineralization, denitrification). Yet the nitrogen cycle in aquatic systems is complex and it is often difficult to predict if, where and when sources and sinks of reactive nitrogen will occur. Thus there is a need to determine the key factors

controlling sources and sinks of reactive nitrogen in stream and river ecosystems. The hyporheic zone is the area beneath and adjacent to streams, rivers and riverine estuaries where SW and GW meet in sediments [*Brunke and Gonser*, 1997; *Harvey and Wagner*, 2000]. Hyporheic zones typically contain strong hydrologic and biogeochemical gradients which control rates of many chemical reactions [*Hedin et al.*, 1998]. Additionally, hyporheic zones and are known to be important locations for many reactions, including nitrogen transformations [*Triska et al.*, 1989; *Duff and Triska*, 1990; *Hill and Lymburner*, 1998; *Zarnetske et al.*, 2011a].

Biogeochemical reactions in the hyporheic zone can be categorized as either mixing dependent or non-mixing dependent. Non-mixing dependent reactions are reactions where all reactants come from the same source water and travel together such that mixing among source waters is not required for reactions to occur. In other words, for non-mixing dependent reactions, all reactants come from the SW and travel in the same hyporheic flow paths or alternatively all reactants come from GW and upwell along the same flow paths. By contrast, mixing dependent reactions are reactions where reactants come from different source waters [*Cirpka et al.*, 1999; *Cirpka et al.*, 2006; *Werth et al.*, 2006]. In the hyporheic zone, mixing dependent reactions occur where some reactants come from downwelling SW and some reactants come from upwelling GW. For mixing dependent reactions to occur, different source waters must mix.

Many studies of nitrogen reactions in the hyporheic zone have focused on predicting the fate of SW nitrogen, where reactants (i.e., DOC, DO, NO_3^-, NH_4^+) are transported together into the hyporheic zone along the same flow paths and undergo non-mixing dependent reaction [*Boano et al.*, 2010; *Marzadri et al.*, 2011; *Zarnetske et al.*, 2011a; *Bardini et al.*, 2012; *Zarnetske et al.*, 2012]. Other studies have focused on the fate within the hyporheic zone of nitrogen species originating from GW as they upwell into streams and rivers [*Kennedy et al.*, 2009a; b; *Krause et al.*, 2009; *Stelzer and Bartsch*, 2012; *Krause et al.*, 2013]. In this case, mixing dependent reactions are possible, as reactants originating in both SW and GW mix, yet these types of reactions have not been distinguished and their controls have not been quantified. For example, *Kennedy et al.* [2009b] used field data to quantify nitrogen fluxes from GW to SW in an agriculture watershed. They quantified NO_3^- lost to non-mixing dependent denitrification in upwelling GW before it mixed with the SW, but did not quantify denitrification at shallower depths where SW and GW mixed. In another example, *Krause et al.* [2013] investigated the impacts of streambed physical properties on the fate of NO_3^- in GW upwelling through a streambed of a lowland river. They found that there was significant NO_3^- transformations in both the first 15 cm of the river sediment (i.e., where SW and GW mix) and at depths of 15-150 cm (which was all upwelling GW) but did not describe processes behind the observed patterns. *Robertson et al.* [1991] monitored GW contamination from a private resident septic system, and studied the plume as it migrated towards a river. They found that in the last 1 m before the plume discharged into the river, NO_3^- decreased from 89 mg/L

to 2.2 mg/L. They attributed the consumed NO_3^- to vigorous denitrification that occurred in the riverbed sediments as a result of higher DOC in the riverbed sediments and the development of anaerobic conditions (the plume core had between 0-1 mg/L DO and near the river DO was completely depleted). However they did not distinguish mixing-dependent from non-mixing-dependent reactions. We are not aware of studies that have separated and quantified the relative dominance of mixing-dependent and non-mixing dependent reactions in general, or nitrogen reactions in particular, within the hyporheic zone.

1.1.4 Purpose of Study

Mixing of SW and GW within the hyporheic zone occurs under neutral to moderately gaining conditions when flow paths originating from SW create hyporheic flow cells and meet with upwelling flow paths originating from deeper GW. Hyporheic flow cells are induced by riverbed morphology (e.g., bedforms, submerged bars, riffles, debris dams) through hydrostatic head variations and form drag [*Storey et al.*, 2003; *Gooseff et al.*, 2006; *Hester and Doyle*, 2008; *Sawyer et al.*, 2011]. When upwelling GW flow paths divert around hyporheic flow cells, water from two different sources (i.e., SW and GW) meets within a thin mixing zone [*Hester et al.*, 2013]. A few other studies have included mixing as a process, however all used dispersivities that were too large to accurately model mixing dependent reactions [*Lautz and Siegel*, 2006; *Bardini et al.*, 2012]. Here I use numerical modeling to quantify denitrification in the hyporheic zone of a gaining river, where SW is induced into the sediment bed from dune-type bedforms. Such bedforms are typical in medium to large waterways, have widespread distribution and their hydraulics are well understood [*Thibodeaux and Boyle*, 1987; *Elliott and Brooks*, 1997; *Cardenas and Wilson*, 2007]. My specific objectives are to:

1. Quantify denitrification in the hyporheic zone due to mixing dependent and non-mixing dependent reactions induced by riverbed dunes.
2. Determine how various biogeochemical conditions control mixing dependent denitrification.
3. Determine how physical parameters such as hydraulic conductivity (K), heterogeneity of K and upwelling GW flux control mixing dependent denitrification.

1.2 Organization of Thesis

This thesis is organized around a journal article that will likely be submitted for publication in *Water Resources Research*. The journal article is located in Section 2 of this document. The introduction of the journal article (Section 2.1) is a slightly condensed version of the literature review in this section. Section 3 contains engineering applications and significance of the study. Section 2.4.2 in the journal article is a condensed version of Section 3 of the thesis. Finally, the Appendix contains supporting

material, including a more detailed description of modeling methodology, as well as additional figures and plots beyond those that could be included in the journal article.

1.3 References

Bardini, L., F. Boano, M. Cardenas, R. Revelli, and L. Ridolfi (2012), Nutrient cycling in bedform induced hyporheic zones, *Geochimica et Cosmochimica Acta*, *84*, 47-61.

Boano, F., A. Demaria, R. Revelli, and L. Ridolfi (2010), Biogeochemical zonation due to intrameander hyporheic flow, *Water Resources Research*, *46*(2).

Braun, E. (2007), *Reactive Nitrogen in the Environment: Too Much Or Too Little of a Good Thing*, United Nations Publications.

Brunke, M., and T. Gonser (1997), The ecological significance of exchange processes between rivers and groundwater, *Freshwater Biology*, *37*(1), 1-33.

Cardenas, M. B., and J. L. Wilson (2007), Dunes, turbulent eddies, and interfacial exchange with permeable sediments, *Water Resources Research*, *43*(8).

Chapelle, F. H., P. M. Bradley, P. B. McMahon, K. Kaiser, and R. Benner (2012), Dissolved Oxygen as an Indicator of Bioavailable Dissolved Organic Carbon in Groundwater, *Ground Water*, *50*(2), 230-241.

Cirpka, O. A., E. O. Frind, and R. Helmig (1999), Numerical simulation of biodegradation controlled by transverse mixing, *Journal of Contaminant Hydrology*, *40*(2), 159-182.

Cirpka, O. A., Å. Olsson, Q. Ju, M. Rahman, and P. Grathwohl (2006), Determination of transverse dispersion coefficients from reactive plume lengths, *Ground Water*, *44*(2), 212-221.

DeSimone, L. A., and B. L. Howes (1998), Nitrogen transport and transformations in a shallow aquifer receiving wastewater discharge: A mass balance approach, *Water Resources Research*, *34*(2), 271-285.

Diaz, R. J., and R. Rosenberg (2008), Spreading dead zones and consequences for marine ecosystems, *Science*, *321*(5891), 926-929.

Dubrovsky, N. M., K. R. Burow, G. M. Clark, J. Gronberg, P. A. Hamilton, K. J. Hitt, D. K. Mueller, M. D. Munn, B. T. Nolan, and L. J. Puckett (2010), *The Quality of Our Nation's Water: Nutrients in the Nation's Streams and Groundwater, 1992-2004*, US Department of the Interior, US Geological Survey.

Duff, J. H., and F. J. Triska (1990), Denitrifications in sediments from the hyporheic zone adjacent to a small forested stream, *Canadian Journal of Fisheries and Aquatic Sciences*, *47*(6), 1140-1147.

Elliott, A. H., and N. H. Brooks (1997), Transfer of nonsorbing solutes to a streambed with bed forms: Theory, *Water Resources Research*, *33*(1), 123-136.

Galloway, J. N., W. H. Schlesinger, H. Levy, A. Michaels, and J. L. Schnoor (1995), Nitrogen fixation: Anthropogenic enhancement-environmental response, *Global Biogeochemical Cycles*, *9*(2), 235-252.

Galloway, J. N., J. D. Aber, J. W. Erisman, S. P. Seitzinger, R. W. Howarth, E. B. Cowling, and B. J. Cosby (2003), The nitrogen cascade, *BioScience*, *53*(4), 341-356.

Gooseff, M. N., J. K. Anderson, S. M. Wondzell, J. LaNier, and R. Haggerty (2006), A modelling study of hyporheic exchange pattern and the sequence, size, and spacing of stream bedforms in mountain stream networks, Oregon, USA, *Hydrological Processes*, *20*(11), 2443-2457.

Harvey, J. W., and B. Wagner (2000), Quantifying hydrologic interactions between streams and their subsurface hyporheic zones, *Streams and Ground Waters*, *344*.

Hedin, L. O., J. C. von Fischer, N. E. Ostrom, B. P. Kennedy, M. G. Brown, and G. P. Robertson (1998), Thermodynamic Constraints on Nitrogen Transformations and Other Biogeochemical Processes at Soil-Stream Interfaces, *Ecology*, *79*(2), 684-703.

Hester, E. T., and M. W. Doyle (2008), In-stream geomorphic structures as drivers of hyporheic exchange, *Water Resources Research*, *44*(3).

Hester, E. T., K. I. Young, and M. A. Widdowson (2013), Mixing of Surface and Groundwater Induced by Riverbed Dunes: Implications for Hyporheic Zone Definitions and Pollutant Reactions, *Water Resources Research*.

Hill, A. R., and D. J. Lymburner (1998), Hyporheic zone chemistry and stream-subsurface exchange in two groundwater-fed streams, *Canadian Journal of Fisheries and Aquatic Sciences*, *55*(2), 495-506.

Howarth, R. W., E. W. Boyer, W. J. Pabich, and J. N. Galloway (2002), Nitrogen use in the United States from 1961-2000 and potential future trends, *AMBIO: A Journal of the Human Environment*, *31*(2), 88-96.

Howden, N. J., T. P. Burt, F. Worrall, S. Mathias, and M. J. Whelan (2011), Nitrate pollution in intensively farmed regions: What are the prospects for sustaining high-quality groundwater?, *Water Resources Research*, *47*(6).

Kennedy, C. D., D. P. Genereux, D. R. Corbett, and H. Mitasova (2009a), Relationships among groundwater age, denitrification, and the coupled groundwater and nitrogen fluxes through a streambed, *Water Resources Research*, *45*(9), W09402.

Kennedy, C. D., D. P. Genereux, D. R. Corbett, and H. Mitasova (2009b), Spatial and temporal dynamics of coupled groundwater and nitrogen fluxes through a streambed in an agricultural watershed, *Water Resources Research*, *45*(9).

Krause, S., L. Heathwaite, A. Binley, and P. Keenan (2009), Nitrate concentration changes at the groundwater-surface water interface of a small Cumbrian river, *Hydrological Processes*, *23*(15), 2195-2211.

Krause, S., C. Tecklenburg, M. Munz, and E. Naden (2013), Streambed nitrogen cycling beyond the hyporheic zone: Flow controls on horizontal patterns and depth distribution of nitrate and dissolved oxygen in the upwelling groundwater of a lowland river, *Journal of Geophysical Research: Biogeosciences*.

Lautz, L. K., and D. I. Siegel (2006), Modeling surface and ground water mixing in the hyporheic zone using MODFLOW and MT3D, *Advances in Water Resources*, *29*(11), 1618-1633.

Marzadri, A., D. Tonina, and A. Bellin (2011), A semianalytical three-dimensional process-based model for hyporheic nitrogen dynamics in gravel bed rivers, *Water Resources Research*, *47*(11).

Robertson, W., and J. Cherry (1992), Hydrogeology of an unconfined sand aquifer and its effect on the behavior of nitrogen from a large-flux septic system, *Applied Hydrogeology*, 32-44.

Robertson, W., J. Cherry, and E. Sudicky (1991), Ground-water contamination from two small septic systems on sand aquifers, *Ground Water*, *29*(1), 82-92.

Sala, O. E., F. S. Chapin, J. J. Armesto, E. Berlow, J. Bloomfield, R. Dirzo, E. Huber-Sanwald, L. F. Huenneke, R. B. Jackson, and A. Kinzig (2000), Global biodiversity scenarios for the year 2100, *Science*, *287*(5459), 1770-1774.

Sawyer, A. H., M. Bayani Cardenas, and J. Buttles (2011), Hyporheic exchange due to channel-spanning logs, *Water Resources Research*, *47*(8).

Schwartz, A. F. (2010), *Housing policy in the United States*, Routledge.

Stelzer, R. S., and L. A. Bartsch (2012), Nitrate removal in deep sediments of a nitrogen-rich river network: A test of a conceptual model, *Journal of Geophysical Research: Biogeosciences (2005–2012)*, *117*(G2).

Storey, R. G., K. W. Howard, and D. D. Williams (2003), Factors controlling riffle-scale hyporheic exchange flows and their seasonal changes in a gaining stream: A three-dimensional groundwater flow model, *Water Resources Research*, *39*(2), 1034.

Thibodeaux, L. J., and J. D. Boyle (1987), Bedform-generated convective transport in bottom sediment.

Toetz, D. (2006), Nitrate in ground and surface waters in the vicinity of a concentrated animal feeding operation, *Archiv für Hydrobiologie*, *166*(1), 67-77.

Triska, F. J., V. C. Kennedy, R. J. Avanzino, G. W. Zellweger, and K. E. Bencala (1989), Retention and transport of nutrients in a third-order stream in northwestern California: hyporheic processes, *Ecology*, 1893-1905.

United States Census Bureau. (1993), 1990 Census Of Housing: Detained Housing Characteristics., edited, Housing and Economic Statistics Divisions, Bureau of the Census Washington, D.C.

Vitousek, P. M., J. D. Aber, R. W. Howarth, G. E. Likens, P. A. Matson, D. W. Schindler, W. H. Schlesinger, and D. G. Tilman (1997), Human alteration of the global nitrogen cycle: sources and consequences, *Ecological Applications*, *7*(3), 737-750.

Werth, C. J., O. A. Cirpka, and P. Grathwohl (2006), Enhanced mixing and reaction through flow focusing in heterogeneous porous media, *Water Resources Research*, *42*(12).

Zarnetske, J. P., R. Haggerty, S. M. Wondzell, and M. A. Baker (2011), Dynamics of nitrate production and removal as a function of residence time in the hyporheic zone, *Journal of Geophysical Research: Biogeosciences (2005–2012)*, *116*(G1).

Zarnetske, J. P., R. Haggerty, S. M. Wondzell, V. A. Bokil, and R. González-Pinzón (2012), Coupled transport and reaction kinetics control the nitrate source-sink function of hyporheic zones, *Water Resources Research*, *48*(11).

2 Controls on Mixing and Non-Mixing Dependent Denitrification in River Hyporheic Zones

In Preparation for Water Resources Research

Katherine I. Young, Erich T. Hester*, and Mark A. Widdowson

Department of Civil and Environmental Engineering, Virginia Tech, Blacksburg, VA 24060

Corresponding Author:
Erich T. Hester
Department of Civil and Environmental Engineering
Virginia Tech
220-D Patton Hall
Blacksburg, VA 24061

Email: ehester@vt.edu
Phone: 540-231-9758

Other Authors:
Katherine I. Young
Department of Civil and Environmental Engineering
Virginia Tech
200 Patton Hall
Blacksburg, VA 24061

Mark A. Widdowson
Department of Civil and Environmental Engineering
Virginia Tech
220-A Patton Hall
Blacksburg, VA 24061

2.1 Introduction

Human actions such as combustion of fossil fuels, production of nitrogen fertilizers, and cultivation of nitrogen-fixing legumes have approximately doubled the rate of transfer of unreactive nitrogen (N_2) to reactive nitrogen species (e.g., nitrate (NO_3^-)) [*Galloway et al.*, 1995; *Vitousek et al.*, 1997]. Production and application of reactive nitrogen in the form of synthetic fertilizers has released significant amounts of reactive nitrogen to the water supply through agriculture runoff and seepage, and through additional sewage from humans and livestock [*Braun*, 2007]. Human derived increases in the supply of reactive nitrogen has led to negative impacts on water quality and aquatic ecosystems including groundwater (GW) contamination [*Howden et al.*, 2011], eutrophication [*Galloway et al.*, 2003], biodiversity loss [*Sala et al.*, 2000] and increased hypoxic events [*Diaz and Rosenberg*, 2008]. Denitrification is the reduction of NO_3^- to nitrogen gasses (N_2O and N_2) by denitrifying heterotrophic bacteria. This process occurs under anaerobic conditions in the presence of electron donors such as dissolved organic carbon (DOC). Denitrification is important because it is the only way reactive nitrogen can be converted back to unreactive nitrogen. It is thus important to better understand denitrification processes in aquatic systems.

2.1.1 Excess Nitrate from Inorganic Fertilizers

The use of synthetic fertilizers is the largest source of reactive nitrogen in the world, representing approximately half of the total human derived reactive nitrogen inputs [*Howarth et al.*, 2002]. Land applications of reactive nitrogen from fertilizer have more than tripled in the United States (US) from 1961 to 1999. Only about half of this reactive nitrogen applied to fields is removed as harvested crops, with the remainder running off into waterways or leaching to GW primarily as NO_3^-. About 23% of total reactive nitrogen inputs to agricultural fields are denitrified or stored in the soil, and about 20% are leached to surface water (SW) either directly or by traveling first through GW [*Howarth et al.*, 2002].

The composition of NO_3^- GW plumes vary considerably depending on the properties of the aquifer. In anoxic conditions (GW DO < 0.5 mg/L) with labile DOC, NO_3^- can be denitrified. However, if dissolved oxygen (DO) is present, denitrification is inhibited and NO_3^- can be transported SW. Anoxic aquifers typically have NO_3^- concentrations just at detection levels (~0.9 mg/L) in both agricultural land uses and urban land uses [*Dubrovsky et al.*, 2010]. In contrast, the median concentration of NO_3^- in oxic aquifers with agriculture land uses in the US is 24.8 mg/L [*Dubrovsky et al.*, 2010].

NO_3^- concentrations in aquifers are related to DOC and DO concentrations. Similarly, DOC and DO concentrations are functionally related. *Chapelle et al.* [2012] present data for DOC and DO concentrations for 1552 well samples from throughout the US and found that typically, when DO concentrations are high, DOC concentrations tend to be lower, and vice-versa *Chapelle et al.* [2012].

This pattern makes sense, because if there is excess DO, aerobic respiration has probably already depleted the DOC, and if there is excess DOC, aerobic respiration has probably already depleted the DO. Data from *Chapelle et al.* [2012] also showed that GW is often depleted of both DOC and DO, but there were no cases with elevated amounts of both DOC and DO.

2.1.2 Excess Nitrate from Human and Animal Waste

As noted previously, in the US, about 50% of the reactive nitrogen from fertilizers is removed from fields as harvested crops and then fed to animals and humans [*Howarth et al.*, 2002]. About 17% of reactive nitrogen is then exported to GW and SW as animal waste. For example, *Toetz* [2006] found high amounts of NO_3^- in wells just below the waste spray area of a concentrated animal feeding operation (CAFO). Similarly, approximately 8% of reactive nitrogen originally removed from fields as crops is eventually exported as human waste to wastewater treatment plants and onsite treatment systems, where some is eventually discharged back into SW and GW [*Howarth et al.*, 2002]. It is likely that a significant portion of the reactive nitrogen from human and animal waste is denitrified along the way; however the exact amount is unknown.

In the US about 26 million homes, businesses and recreational facilities use onsite wastewater treatment systems which collect, treat, and release about 4 billion gallons of effluent daily [*Schwartz*, 2010]. Such systems consist of septic tanks and drain distribution fields, which release the effluent to the shallow subsurface [*United States Census Bureau*, 1993]. Septic system effluent typically contains high ammonium (NH_4^+), high DOC and some DO. DOC and DO are consumed via aerobic respiration and DO and NH_4^+ are consumed by nitrification and converted to NO_3^-. The resulting contaminant plumes from septic systems typically have depleted DO (<1 mg/L), high NO_3^--N (22-180 mg/L) and low to medium DOC-C (1.9 - 3.4 mg/L) [*Robertson et al.*, 1991; *Robertson and Cherry*, 1992; *DeSimone and Howes*, 1998].

2.1.3 Mixing dependent Denitrification in the Hyporheic Zone

All nitrogen sources within watersheds eventually flow through streams and rivers, which control nitrogen export via internal nitrogen source and sink processes (e.g., mineralization, denitrification). Yet the nitrogen cycle in aquatic systems is complex and it is often difficult to predict if, where and when sources and sinks of reactive nitrogen will occur. Thus there is a need to determine the key factors controlling sources and sinks of reactive nitrogen in stream and river ecosystems. The hyporheic zone is the area beneath and adjacent to streams, rivers and riverine estuaries where SW and GW meet in sediments [*Brunke and Gonser*, 1997; *Harvey and Wagner*, 2000]. Hyporheic zones contain strong hydrologic and biogeochemical gradients which control rates of many chemical reactions [*Hedin et al.*,

1998]. Additionally, hyporheic zones and are known to be important locations for many reactions, including nitrogen transformations [*Triska et al.*, 1989; *Duff and Triska*, 1990; *Hill and Lymburner*, 1998; *Zarnetske et al.*, 2011a].

Such reactions in the hyporheic zone can be categorized as either mixing dependent or non-mixing dependent. Non-mixing dependent reactions are reactions where all reactants come from the same source water and travel together such that mixing among source waters is not required for reactions to occur. Non-mixing dependent reactions in the hyporheic zone involve all reactants coming from SW and travelling in the same hyporheic flow paths, or alternatively all reactants coming from GW and upwelling along the same flow paths. By contrast, mixing dependent reactions are reactions where reactants come from different source waters [*Cirpka et al.*, 1999; *Cirpka et al.*, 2006; *Werth et al.*, 2006]. In the hyporheic zone, mixing dependent reactions occur where some reactants come from downwelling SW and some reactants come from upwelling GW. For mixing dependent reactions to occur, different source waters must mix.

Many studies of nitrogen reactions in the hyporheic zone have focused on predicting the fate of SW nitrogen, where reactants are transported together into the hyporheic zone along the same flow paths and undergo non-mixing dependent reaction [*Boano et al.*, 2010; *Marzadri et al.*, 2011; *Zarnetske et al.*, 2011a; *Bardini et al.*, 2012; *Kessler et al.*, 2012; *Zarnetske et al.*, 2012]. Other studies have focused on fate within the hyporheic zone of nitrogen species originating from GW as they upwell into streams and rivers [*Kennedy et al.*, 2009a; b; *Krause et al.*, 2009; *Stelzer and Bartsch*, 2012; *Krause et al.*, 2013]. In this case, mixing dependent reactions are possible, as reactants originating in both SW and GW mix, yet these types of reactions have not been distinguished and their controls have not been quantified. We are not aware of studies that have separated and quantified the relative dominance of mixing dependent and non-mixing dependent reactions in general, or nitrogen reactions in particular, within the hyporheic zone.

2.1.4 Purpose of Study

Mixing of SW and GW within the hyporheic zone occurs under neutral to moderately gaining conditions when flow paths originating from SW create hyporheic flow cells and meet with upwelling flow paths originating from deeper GW. Hyporheic flow cells are induced by riverbed morphology (e.g., bedforms, submerged bars, riffles, debris dams) through hydrostatic head variations and form drag [*Storey et al.*, 2003; *Gooseff et al.*, 2006; *Hester and Doyle*, 2008; *Sawyer et al.*, 2011]. When upwelling GW flow paths divert around hyporheic flow cells, water from two different sources (i.e., SW and GW) meets within a thin mixing zone [*Hester et al.*, 2013]. A few modeling studies simulate mixing as a process, however all used dispersivities that were too large to accurately model mixing dependent reactions [*Lautz and Siegel*, 2006; *Bardini et al.*, 2012]. Here we use numerical modeling to quantify denitrification in the

hyporheic zone of a gaining river, where SW is induced into the sediment bed from dune-type bedforms. Such bedforms are typical in medium to large waterways, have widespread distribution, and their hyporheic hydraulics are well understood [*Thibodeaux and Boyle*, 1987; *Elliott and Brooks*, 1997; *Cardenas and Wilson*, 2007]. Our specific objectives are to (1) quantify denitrification in the hyporheic zone due to mixing dependent and non-mixing dependent reactions induced by riverbed dunes, (2) determine how various biogeochemical conditions control mixing dependent denitrification and (3) determine how physical parameters such as hydraulic conductivity (K), heterogeneity of K and upwelling GW flux control mixing dependent denitrification.

2.2 Methods

2.2.1 Model Overview and Governing Equations

We numerically modeled flow, transport, and biogeochemical reactions in saturated sediments beneath a riverbed exhibiting a series of dune-like bedforms [*Savant et al.*, 1987; *Garcia*, 2008]. Interstitial flow and transport in the model was driven by upwelling groundwater (GW) and pressure variations along the dune surfaces due to form drag from the overlying water column [*Thibodeaux and Boyle*, 1987; *Elliott and Brooks*, 1997; *Cardenas and Wilson*, 2006] (Figure 2-1).

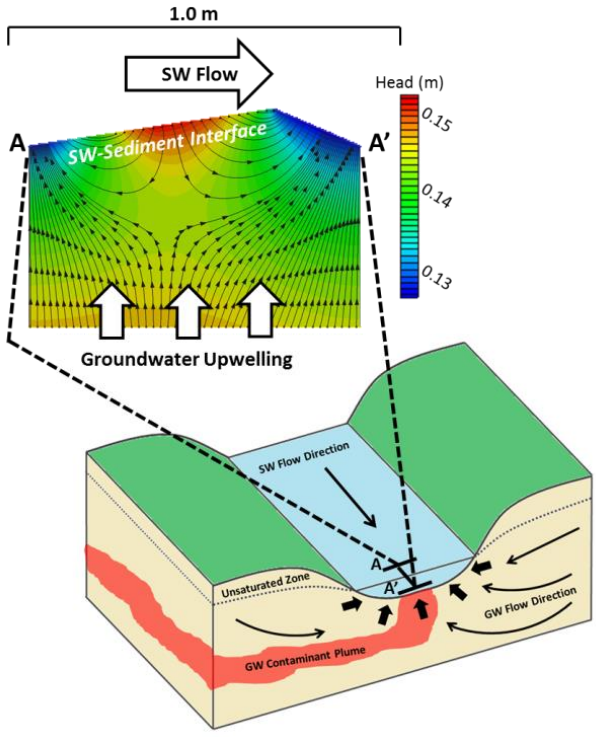

Figure 2-1: Conceptual figure of contaminant plume upwelling toward a river with example riverbed dune.

We used the same flow and transport model as in *Hester et al.* [2013], with some minor changes and the addition of multiple Monod biologically-mediated chemical reactions. The previous model used MODFLOW and MT3DMS within Groundwater Model Software (GMS). MODFLOW was developed by the United States Geological Survey (USGS) and is a modular finite-difference flow model. The code solves the three-dimensional GW flow equation [*Harbaugh*, 2005]:

$$\frac{\partial}{\partial x}\left(K_{xx}\frac{\partial h}{\partial x}\right)+\frac{\partial}{\partial y}\left(K_{yy}\frac{\partial h}{\partial y}\right)+\frac{\partial}{\partial z}\left(K_{zz}\frac{\partial h}{\partial z}\right)+W=S_s\frac{\partial h}{\partial t} \quad (1)$$

where K_{xx}, K_{yy}, and K_{zz} are hydraulic conductivity values (L/T) along the *x*, *y*, and *z* coordinate axes respectively, h is the potentiometric head (L), *W* is volumetric flux per unit volume representing sources and/or sinks of water (T^{-1}), S_s is the specific storage of the porous media (L^{-1}), and *t* is time (T).

MT3DMS is a modular three-dimensional transport model that solves the advection, dispersion, and chemical reaction equation for dissolved constituents in GW systems using the output of MODFLOW [*Zheng and Wang*, 1999]:

$$\frac{\partial(\theta C^k)}{\partial t}=\frac{\partial}{\partial x_i}\left(\theta D_{ij}\frac{\partial C^k}{\partial x_j}\right)-\frac{\partial}{\partial x_i}\left(\theta v_i C^k\right)+WC_s^k+\sum R_k \quad (2)$$

where θ is porosity (-), C^k is the dissolved concentration of species *k* (ML^{-3}), *t* is time (T), $x_{i,j}$ is the distance along the respective Cartesian coordinate axis (L), D_{ij} is the hydrodynamic dispersion coefficient tensor (L^2T^{-1}), v_i is seepage or linear pore water velocity (LT^{-1}), *W* is the volumetric flux per unit volume representing sources and/or sinks (T^{-1}), C_s^k is the concentration of the source or sink flux for species *k* (ML^{-3}) and $\sum R_k$ is the reaction term ($ML^{-3}T^{-1}$).

We included multiple Monod biological reactions using SEAM3D. SEAM3D is a reactive transport model used to simulate complex biodegradation problems involving multiple substrates and multiple electron acceptors [*Widdowson et al.*, 2002] in addition to advection and dispersion within the dissolved phase (equation (2)). SEAM3D simulates aerobic respiration and denitrification. Using formaldehyde as the form of dissolved organic carbon (DOC) [*Hunter et al.*, 1998; *Boano et al.*, 2010; *Bardini et al.*, 2012] aerobic respiration can be written as:

$$CH_2O + O_2 \rightarrow CO_2 + H_2O \quad (3)$$

and denitrification, also using formaldehyde as DOC, can be written as:

$$5CH_2O + 4NO_3^- + 4H^+ \rightarrow 5CO_2 + 2N_2 + 7H_2O \quad (4)$$

Biodegradation is represented by the last term in equation (2), and for each species (DOC, dissolved oxygen (DO), and nitrate (NO_3^-)) has the following general form:

$$R_k = \sum_n \left(\frac{M_n}{\theta}\right)(\gamma_{n,k})(v_n)\left(\frac{C_{ED}}{K_{ED}+C_{ED}}\right)\left(\frac{C_{EA}}{K_{EA}+C_{EA}}\right) I \quad (5)$$

where R_k is the total biological reaction for the *kth* species (DOC, DO or NO_3^-) due to the sum of all reaction components acting on the common *kth* species ($ML^{-3}T^{-1}$), M_n is the biomass concentration (ML^{-3}) for reaction *n* (either aerobic respiration or denitrification), $\gamma_{k,n}$ is the use coefficient for species *k* in reaction *n*, v_n is the maximum specific rate of utilization of substrate for reaction *n*, C_{ED} is the electron donor (DOC) concentration (ML^{-3}), K_{ED} is the half saturation constant for the electron donor (ML^{-3}), C_{EA} is the electron acceptor (DO or NO_3^-) concentration (ML^{-3}), K_{EA} is the half saturation constant for the electron acceptor (ML^{-3}) and *I* is the inhibition function (-). The use coefficient represents the mass of solute *k* used per unit mass of electron donor for reaction *n*. If one were calculating consumption of DOC for either aerobic respiration or denitrification, the use coefficient would be 1. From stoichiometry, the use coefficient for biodegradation of DO from aerobic respiration using CH_2O is 1.07, and the use coefficient for biodegradation of NO_3^- from denitrification using CH_2O is 1.65. The inhibition function is used to represent inhibition of denitrification given DO availability:

$$I = \frac{K_I}{K_I + C_{DO}} \quad (6)$$

where K_I is the inhibition constant for the denitrification reaction (ML^{-3}) and C_{DO} is the DO concentration (ML^{-3}). The inhibition function is 1 for aerobic respiration because there is no inhibition for this reaction. Therefore, the consumption of DO from aerobic respiration is defined as:

$$R_{DO} = -\left(\frac{M_{AR}}{\theta}\right)(\gamma_{DO,AR})(v_{AR})\left(\frac{C_{DOC}}{K_{DOC}+C_{DOC}}\right)\left(\frac{C_{DO}}{K_{DO}+C_{DO}}\right) \quad (7)$$

The consumption of NO_3^- from denitrification is defined as:

$$R_{NO3} = -\left(\frac{M_{DN}}{\theta}\right)(\gamma_{NO3,DN})(v_{DN})\left(\frac{C_{DOC}}{K_{DOC}+C_{DOC}}\right)\left(\frac{C_{NO3}}{K_{NO3}+C_{NO3}}\right)\left(\frac{K_I}{K_I+C_{DO}}\right) \quad (8)$$

And finally, the consumption of DOC from both aerobic and denitrification is defined as:

$$R_{DOC} = -\left(\frac{M_{AR}}{\theta}\right)(v_{AR})\left(\frac{C_{DOC}}{K_{DOC}+C_{DOC}}\right)\left(\frac{C_{DO}}{K_{DO}+C_{DO}}\right) - \left(\frac{M_{DN}}{\theta}\right)(v_{DN})\left(\frac{C_{DOC}}{K_{DOC}+C_{DOC}}\right)\left(\frac{C_{NO3}}{K_{NO3}+C_{NO3}}\right)\left(\frac{K_I}{K_I+C_{DO}}\right) \quad (9)$$

Our approach of modeling both physical transport and reaction kinetics has been used in previous studies of reactive nitrogen transformations and transport in hyporheic environments [*Gu et al.*, 2007; *Zarnetske et al.*, 2011a; *Zarnetske et al.*, 2012].

We modeled a two-dimensional vertical slice through a single dune, using the same dune geometry as *Hester et al.* [2013] and *Fehlman* [1985] with a model domain length in the downstream direction of 0.914 m and a dune height of 0.138 m. *Hester et al.* [2013] set the depth of the model (from bottom of the dune to the lower model boundary) in the vertical direction to 1.0 m. We set the depth of model to 0.5 m in order to cut down run times and because decreasing the model depth to 0.5 m had minimal effects on the hyporheic flow cell. The total domain depth was 0.638 m and model area was 0.52 m^2, including the dune.

We used two different grid sizes, a coarse grid and a fine grid as discussed later in Section 2.2.2 and 2.2.3. Both were two dimensional and one cell thick (10 mm) in the third dimension. The fine grid was uniform size at 4.0 mm by 4.0 mm, giving 229 model cells in the downstream direction and 160 cells in the vertical direction. The fine grid had a total model volume of 0.0052 m^3 and total of 36,623 model cells. The coarse grid was uniform size at 6.3 mm by 6.3 mm, giving 145 model cells in the downstream direction and 101 cells in the vertical direction. The coarse grid had a total model volume of 0.0052m^3 and a total of 14,692 model cells. *Hester et al.* [2013] uses a grid size of 2.5 mm by 2.5 mm in order to minimize numerical dispersion, however our fine grid was slightly larger. It was necessary to use a slightly larger grid size than *Hester et al.* [2013] in order to cut model run times down from >7 days (with 2.5 mm gird size) to ~24 hours (with 4.0 mm grid size). We varied grid size over a range of values and found that there was only a 2.2% increase in numerical dispersion between the 2.5 mm grid and the 4.0 mm grid. Additionally, this grid size is still smaller than those used to model transport in similar settings [*Cardenas et al.*, 2008a; *Sawyer and Cardenas*, 2009].

2.2.2 Hydraulic Model Boundary Conditions and Parameters

We ran a total of four sensitivity analyses, each of which involved varying sensitivity parameters one at a time in deviation from four respective basecases (Table 2-1, 2-2). Three of these sensitivity analyses used the coarse grid (Table 2-1) and one used the fine grid (Table 2-2). The three coarse grid

sensitivity analyses were done first and used to determine which basecase to use for the fine grid sensitivity analysis. For this reason we refer to the coarse grid sensitivity analyses as preliminary (Table 2-1) and the fine grid sensitivity analysis as final (Table 2-2). The rationale for doing three separate preliminary sensitivity analyses/basecases, the rationale for the specific basecases we used, and the rationale for picking the one specific basecase that we used for the final sensitivity analysis are all related to biogeochemical boundary conditions and are discussed below in Section 2.2.3.

Table 2-1: Summary table of basecase inputs and ranges for parameters varied in the preliminary sensitivity analyses (utilizing the coarse grid), including literature sources[a].

Parameter	Abbreviation	Unit	Coarse Grid Basecase 1 Value	Coarse Grid Basecase 2 Value	Coarse Grid Basecase 3 Value	Range Varied in Coarse Grid Sensitivity Analyses	Source
Hydraulic Model (MODFLOW)							
Hydraulic Conductivity	K	m/d	84.4	84.4	84.4	25-150	18
Biogeochemical Boundary Conditions (SEAM3D)							
Surface Water Dissolved Organic Carbon	SW DOC	mg/L	50	50	50	0-50	2, 12, 13, 14, 15
Groundwater Dissolved Organic Carbon[b]	GW DOC	mg/L	0	0	0	0-50	1, 2, 9, 10
Surface Water Dissolved Oxygen	SW DO	mg/L	5	5	5	0-10	4, 14, 16, 17
Groundwater Dissolved Oxygen[b]	GW DO	mg/L	3	3	0	0-8	1, 2, 3, 4, 5, 6, 9, 10
Surface Water Nitrate	SW NO_3^-	mg/L	4.9	0	0	0-47.8	8
Groundwater Nitrate	GW NO_3^-	mg/L	24.8	24.8	24.8	0-70.9	2, 4, 5, 6, 7, 8, 11

[a]Literature sources: 1.*Chapelle et al.* [2012], 2. *Puckett and Hughes* [2005], 3. *USGS* [2009], 4. *Krause et al.* [2013], 5. *Cey et al.* [1999], 6. *Kennedy et al.* [2009a], 7. *Gu et al.* [2007], 8. *Dubrovsky et al.* [2010], 9. *DeSimone and Howes* [1998], 10. *Robertson et al.* [1991], 11. *Barbaro* [2013], 12. *Bardini et al.* [2012], 13. *Spencer et al.* [2012], 14. *Boano et al.* [2010], 15. *Tian et al.* [2013], 16. *Corsi et al.* [2011], 17. *Wilcock et al.* [1998], 18. *Hester et al.* [2013].
[b]GW DOC and GW DO were varied simultaneously such that as GW DOC increases, GW DO decreases. The relationship between GW DOC and GW DO was taken from *Chapelle et al.* [2012].

Table 2-2: Summary table of basecase inputs and ranges for parameters varied in the final sensitivity analysis (utilizing the fine grid).

Parameter	Abbreviation	Unit	Fine Grid Basecase 2 Value	Range Varied in Fine Grid Sensitivity Analyses
Hydraulic Model (MODFLOW)				
Hydraulic Conductivity	K	m/d	84.4	25-150
Lower boundary groundwater (Darcy) flux	Lower Bdy q	m/d	1.09	0.55-5.47
Variance[a]	σ^2_{lnK}	-	0	0.0-2.5
Biogeochemical Boundary Conditions (SEAM3D)				
Surface Water Dissolved Organic Carbon	SW DOC	mg/L	50	0-50
Groundwater Dissolved Organic Carbon[b]	GW DOC	mg/L	0	0-50
Surface Water Dissolved Oxygen	SW DO	mg/L	5	0-10
Groundwater Dissolved Oxygen[b]	GW DO	mg/L	3	0-8
Surface Water Nitrate	SW NO_3^-	mg/L	0	0-47.8
Groundwater Nitrate	GW NO_3^-	mg/L	24.8	0-70.9

[a]Applies to heterogeneous K fields.
[b]GW DOC and GW DO were varied simultaneously such that as GW DOC increases, GW DO decreases. The relationship between GW DOC and GW DO was taken from *Chapelle et al.* [2012].

For all four basecases, we modeled GW hydraulics in steady state mode, such that the transient term on the right-hand side of equation (1) was set to zero. The top boundary was a specified head boundary with the same pressure distribution along surface water (SW) sediment interface as *Hester et al.* [2013], originally from *Fehlman* [1985]. This pressure distribution simulated form drag across the dune which caused flow into and out of the sediment. The lower boundary was specified as a constant flow boundary to represent upward GW discharge, same as *Hester et al.* [2013]. Lower boundary GW flux was varied for the final sensitivity analysis only (Table 2-2). Porosity and anisotropy were the same in all basecases, were not varied and were the same as *Hester et al.* [2013].

Hydraulic conductivity (K) was homogeneous in all basecase models, and set to 84.4 m/d, as in *Hester et al.* [2013]. K was varied in all four sensitivity analyses (Table 2-1, 2-2); however heterogeneity of K was only varied for the final sensitivity analysis (Table 2-2). Heterogeneity of K was varied in the final sensitivity analysis as in *Hester et al.* [2013], where K was a lognormally spatially correlated random field, where the degree of heterogeneity was expressed as the variance of lnK, and the spatial structure was described as the spatial covariance of lnK in each direction [*Salehin et al.*, 2004]. We generated the heterogeneous K fields using the turning band method of [*Tompson et al.*, 1989] which created a single realization of second-order stationary, lognormally correlated, multi-dimensional random K field with user specified correlation scales, mean conductivity, and standard deviation. All inputs used to create the heterogeneous K fields were the same as *Hester et al.* [2013]. Our fine model grid size was used to minimize numerical dispersion; however it also resulted in long run times (~24 hours). Long run times are the key reason why we chose not to do Monte-Carlo simulations and instead conducted sensitivity analyses where controlling factors were varied one at a time relative to a basecase. This allowed us to minimize numerical dispersion as required for this kind of study. Yet we acknowledge that varying parameters one at a time reduced our ability to explore parameter interaction.

2.2.3 Transport and Reaction Kinetic Model Boundary Conditions and Parameters

In each model run, the transport and reaction kinetic model (i.e., SEAM3D) was run until it reached steady state (i.e., the concentration field no longer changed with time). We used the same longitudinal and transverse dispersivities as *Hester et al.* [2013] (α_L = 0.01 m and α_T = 0.001 m) to model local dispersion rather than macrodispersion. This is critical in order to obtain accurate mixing between solutes originating from GW and SW. We used 1E-09 m^2/s for molecular diffusion (same as *Hester et al.* [2013]), which is in the middle of the range for organic compounds in water [*Schwarzenbach et al.*, 1993]. SEAM3D requires a series of inputs for Monod kinetics of aerobic respiration and denitrification (Table 2-3) as shown by equations (5-9). Few studies quantify these values for hyporheic sediments, however *Zarnetske et al.* [2012] does an excellent job of summarizing what literature values do exist. We

adopted most of their values for our model (Table 2-3) because their study was the most similar model to our own that we could find.

Table 2-3: Summary table of Monod kinetic inputs for all basecases

Parameter	Abbreviation	Unit	Value
Maximum specific oxygen reaction rate	v_{O2}	h^{-1}	1.97
Maximum specific denitrification rate	v_{NO3-}	h^{-1}	3.98
Inhibition constant for the denitrification reaction	K_I	mg/L	0.24
Half saturation constant for DOC	K_{DOC}	mg/L	8.68
Half saturation constant for DO	K_{DO}	mg/L	5.28
Half saturation constant for NO_3^-	K_{NO3-}	mg/L	1.64
Use coefficient for biodegradation of DO from aerobic respiration	$\gamma_{AR,DO}$	-	1.07
Use coefficient for biodegradation of NO_3^- from denitrification	$\gamma_{DN,NO3-}$	-	1.65
Biomass concentration of aerobes	M_{AR}	mg/L	5.0
Biomass concentration of denitrifiers	M_{DN}	mg/L	4.9

Inputs to the Monod kinetic reaction model were not varied in preliminary or final sensitivity analyses. Initially we did vary the maximum specific reaction rates, yet because it was obvious that higher rates yielded increased reaction products, we omitted such rates from the sensitivity analyses. We also originally varied the half saturation constants and the inhibition constant, but found that they have little effect on results trends consistent with *Zarnetske et al.* [2012]. As a result, we did not vary these parameters in later sensitivity analyses either. Biomasses of the functional microbial groups facilitating the reactions (M_n) are implicitly included as lumped parameters in the model. The lumped parameter is the product of the biomasses with their respective microbial maximum specific reaction rate V_n [*Gu et al.*, 2007; *Zarnetske et al.*, 2012]. Little concrete guidance is available in the literature for hyporheic zone microbial biomass. *Zarnetske et al.* [2012] assumes the biomass concentration for aerobes is equal to the influent (SW) DO concentration (8.3 mg/L in their study) and that the biomass value for denitrifiers is equal to the influent (SW) NO_3^- concentration (0.32 mg/L in their study). In another study, [*Widdowson et al.*, 1988] develops a model to simulate aerobic respiration and denitrification in groundwater using Monod kinetics, and assumes that the biomass concentration for aerobics and denitrifiers is equal to 0.565 mg/L. The hyporheic zone would be expected to have denser microbial populations than deeper GW [*Febria et al.*, 2011]. For this parameter, we therefore made the same assumptions as *Zarnetske et al.* [2012] resulting in a biomass value for aerobes equal to 5.0 mg/L and a biomass value for denitrifiers equal to 4.9 mg/L. The biomass values were not varied with changing biogeochemical boundary

conditions and remained constant throughout the sensitivity analysis. Additional conceptual model assumptions include:

1. Multiple Monod kinetics is appropriate for modeling biodegradation reactions in the hyporheic zone [*Zarnetske et al.*, 2012]
2. Biomass is in equilibrium with equal rates of growth and decay [*Marzadri et al.*, 2011; *Zarnetske et al.*, 2012]
3. POC dissolution is not modeled
4. Top boundary influent DO, NO_3^- and DOC are equal to their SW stream concentrations [*Zarnetske et al.*, 2011a; *Zarnetske et al.*, 2012]
5. DOC modeled represents labile DOC that can be readily used for biodegradation reactions [*Gu et al.*, 2007; *Zarnetske et al.*, 2012]
6. Retardation from sorption is negligible because the model will be solved to steady state [*Marzadri et al.*, 2011; *Zarnetske et al.*, 2012]
7. Nitrification is not modeled [*Gu et al.*, 2012]. Nitrification produces NO_3^- from DO and NH_4^+. It is reasonable to neglect nitrification because we do vary DO and NO_3^- in both the SW and GW boundary conditions. Additionally, although the net production or consumption of NO_3^- depends on the relative balance between nitrification and denitrification in a system [*Maggi et al.*, 2008], we are more interested in controls on mixing and non-mixing dependent reactions than net production or consumption of NO_3^-.
8. Dissimilatory NO_3^- reduction to ammonium (DNRA) and anaerobic ammonium oxidation (ANAMMOX) are not modeled [*Marzadri et al.*, 2011; *Zarnetske et al.*, 2012]

Run times were very long (~24 hours) for the fine grid model and significantly shorter (<6 hours) for the coarse grid models. However, the coarse grid models had the risk of increased numerical dispersion and therefore decreased accuracy. Because we had a large number of simulations to run, we first did preliminary sensitivity analyses for the three coarse grid basecases (Table 2-1) to determine basic trends, and then picked a single basecase (i.e., set of biogeochemical boundary conditions) for the fine grid (Table 2-2). We chose three coarse grid basecases with different biogeochemical boundary conditions for the preliminary sensitivity analyses (Table 2-1). Coarse grid basecase 1 and 2 represented GW that was derived from watersheds affected by agriculture, which are associated with large amounts of fertilizer and/or manure applications, and coarse grid basecase 3 represented water that was contaminated by septic systems. The only difference between basecase 1 and 2 was that in basecase 2, SW contained no NO_3^-. In coarse grid basecase 3 there was also no SW NO_3^-. The basecases without SW NO_3^- allowed

us to focus on mixing dependent denitrification. When NO_3^- is present in both SW and GW, it is difficult to accurately differentiate between mixing and non-mixing dependent processes. Although a stream or river without NO_3^- (especially in a watershed affected by fertilizer application) is not necessarily realistic, we tested the effect of this assumption for both coarse grid basecase 2 and 3. We left SW NO_3^- in coarse grid basecase 1 so that we could determine how much this assumption affected the results. The only difference between basecase 2 and 3 was that basecase 3 had no GW DO. As explained in the introduction, septic system plumes typically have high NO_3^-, depleted DO, and low DOC. The selection of one particular basecase for the final sensitivity analysis (fine grid) occurred after we had results for the preliminary sensitivity analyses (coarse grid), and hence the rationale for that decision is discussed below in section 2.3.1 of the Results.

2.3.3 Calculation of Sensitivity Coefficients

In order to determine the relative sensitivity of the model to the various input parameters, we calculated sensitivity coefficients for all parameters varied in the fine grid model. The sensitivity coefficients were calculated as [*Zheng and Bennett*, 2002]:

$$X_{m,n} = \frac{\partial \hat{y}_m}{\partial a_n / a_n} \approx \frac{\hat{y}_m(a_n + \Delta a_n)}{\Delta a_n / a_n} \qquad (10)$$

where $X_{m,n}$ is the sensitivity coefficient of the model dependent variable $\hat{y}$ with respect to the mth parameter at the nth observation point (either amount of NO_3^- or percent of NO_3^- consumed in the entire model domain), a_n is the parameter value for the basecase and Δa_n is a change in the parameter, and $\hat{y}(a_n)$ and $\hat{y}(a_n + \Delta a_n)$ are the values of the model dependent variable obtained for the basecase and for the varied-parameter case, respectively. In calculating the sensitivity coefficients, we use both amount and percent of NO_3^- consumed as the model dependent variable ($\hat{y}$). For each varied parameter (e.g., SW DOC, SW DO, K, etc.), at least 5 sensitivity coefficients were calculated using 5 different Δa_n values that scaled the full range in the sensitivity analysis. The maximum sensitivity coefficient calculated from each parameter varied was then used to compare and contrast sensitivity coefficients for other input parameters varied in the sensitivity analysis.

2.3 Results

2.3.1 Preliminary Sensitivity Analysis (Coarse Grid) Results and Choice of Basecase for Final Sensitivity Analysis (Fine Grid)

In this section we compare the results from the three coarse grid runs (basecases 1-3). We first discuss relative magnitudes of denitrification among the basecases and show how they relate to where and

when mixing dependent versus non-mixing dependent reactions are occurring. Next we show how similarities among the basecases allow us to pick a basecase that is in some ways representative of all mixing dependent denitrification processes. Such similarities are primarily in terms of trends of denitrification and other chemical reactions versus controlling factors rather than absolute magnitudes of reactions due to uncertainty of the input parameters as mentioned in section 2.2.3.

70.7 mg/d, 24.5 mg/d and 42.8 mg/d nitrate (NO_3^-) was consumed by denitrification for basecase 1, 2 and 3 respectively (Table 2-4). These amounts translate to 19%, 9.9% and 17% of total NO_3^- entering the model consumed by denitrification for basecase 1, 2 and 3 respectively (Table 2-4). Because basecase 1 had surface water (SW) NO_3^- of 4.9 mg/L, in total more NO_3^- entered the model for basecase 1 than for basecase 2 and 3. Additionally, basecase 1 had NO_3^- consumed via non-mixing dependent and mixing dependent denitrification, whereas basecase 2 and 3 only had NO_3^- consumed via mixing dependent denitrification.

Basecase 1 had 46.2 mg/d more NO_3^- consumed compared to basecase 2 (Table 2-4). Since basecase 1 and basecase 2 had all of the same boundary conditions except for SW NO_3^-, if we make the assumption that the same amount of mixing dependent denitrification occurred in both basecase 1 and 2 (i.e., 24.5 mg/d), we find that 46.2 mg/d NO_3^- was consumed via non-mixing dependent denitrification in basecase 1. It should be noted that there is some error in this assumption, in that solute concentrations (i.e., dissolved organic carbon (DOC) and NO_3^-) in the model domain are different between basecase 1 and 2, and therefore it is impossible to know exactly how much NO_3^- was consumed by mixing versus non-mixing denitrification. However, we are confident that these values for mixing dependent and non-mixing dependent denitrification are close, because in the model simulation when groundwater (GW) NO_3^- equaled 0 mg/L for basecase 1, we found that 47.6 mg/d NO_3^- was consumed from non-mixing denitrification, which is only about a 3% error.

Table 2-4: Amount of DOC, DO and NO_3^- consumed (and percent) for each of the 3 basecases for the coarse grid, and for basecase 2 for the fine grid.

Basecase	Amount of Solute Consumed (mg/d) [%]		
	DOC	DO	NO_3^-
Coarse Grid			
1	104.6 [8.8%]	66.6 [45%]	70.7 [19%]
2	76.8 [6.5%]	66.6 [45%]	24.5 [9.9%]
3	84.2 [7.1%]	62.5 [53%]	42.8 [17%]
Fine Grid			
2	76.6 [6.8%]	65.6 [46%]	24.2 [9.7%]

Overall, the results from the coarse grid sensitivity analyses showed that all trends for reactions versus controlling parameters (and even most magnitudes) changed little among basecases. For example, when comparing basecase 1 with basecase 2, the presence or absence of SW NO_3^- did not affect trends of

DOC, dissolved oxygen (DO), or NO_3^- consumption within the model domain versus any parameter varied (see Table 2-1 for list of varied parameters), although magnitudes were altered somewhat in some cases. In particular, DOC and NO_3^- consumption was higher for basecase 1 than for basecase 2 for all parameters varied, due to an increase in non-mixing dependent denitrification of SW NO_3^- within the hyporheic flow cell. By contrast, neither trends nor magnitudes of DO consumption within the model were altered by the presence of SW NO_3^- for any parameter varied. We show an example case of varying SW DOC in Figure 2-2.

Similarly, when comparing basecase 2 with basecase 3, the presence or absence of GW DO did not affect trends of DOC, DO or NO_3^- consumption within the model domain versus any parameter varied, although again magnitudes were altered somewhat in some cases. In particular, DO consumption was higher for basecase 2 than for basecase 3 for all parameters varied, due to an increase in mixing dependent aerobic respiration. By contrast, DOC and NO_3^- consumption was lower for basecase 2 than for basecase 3 for all parameters varied, due to a decrease in mixing dependent denitrification caused by inhibition from oxygen. Although the presence of GW DO increased mixing dependent aerobic respiration which increased DOC consumption, denitrification had a higher reaction rate, resulting in overall less DOC consumed when DO was present. An example case of varying SW DOC is again shown in Figure 2-2.

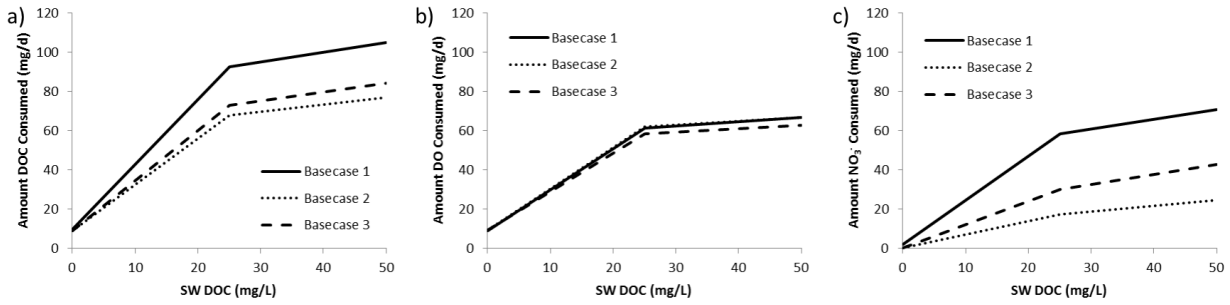

Figure 2-2: Amount of a) DOC consumed, b) DO consumed and c) $NO3^-$ consumed versus SW DOC for basecases 1, 2 and 3 (coarse grid). Basecase 1 and basecase 2 have all the same boundary conditions except basecase 1 has SW $NO3^-$ of 4.9 mg/L and basecase 2 has SW $NO3^-$ of 0 mg/L. Basecase 2 and basecase 3 have all the same boundary conditions except basecase 3 has GW DO of 3 mg/L and basecase 3 has GW DO of 0 mg/L.

Since the trends between solute consumption and various controlling parameters were identical and the magnitudes of results were similar between the three coarse grid basecases, we only ran the sensitivity analysis on the fine grid using one set of biogeochemical boundary conditions. We chose to run the final (fine grid) sensitivity analysis using the biogeochemical boundary conditions from coarse grid basecase 2 for two reasons. First, basecase 2 represented GW affected by agriculture which is a more

common situation than GW affected by septic systems (basecase 3) [*Howarth et al.*, 2002]. Second, SW NO_3^- was absent in basecase 2, unlike basecase 1. Although this situation is generally not realistic, for most of the sensitivity analysis runs, it allowed us to calculate and isolate the mixing dependent portion of denitrification. If there had been SW NO_3^- in all of the runs, it would have been much more difficult to accurately separate mixing dependent and non-mixing dependent denitrification. Finally, in comparing results from the coarse and fine grids for basecase 2, we found that the consumption rates for DOC, DO, and NO_3^- were almost identical (e.g., Table 2-4 for unmodified basecase scenarios). This confirms that results from the coarse grid are fairly accurate, and therefore our process for selecting which basecase to run on the fine grid (e.g., using Figure 2-2) is well justified.

2.3.2 Final Sensitivity Analysis (Fine Grid) Results

Basecase 2 included DOC from SW, DO from SW and GW, and NO_3^- from GW. This allowed for both mixing and non-mixing dependent aerobic respiration, but only mixing dependent denitrification. Non-mixing dependent reactions occur within the hyporheic flow cell induced by the dunes and mixing dependent reactions occur in the mixing zone between the hyporheic flow cell and upwelling GW as shown in the steady state SEAM3D concentration maps (Figure 2-3). To create the "conservative tracer" concentration maps (top row of plots in Figure 2-3b), we duplicated the boundary condition concentrations for each of the reactive solutes (DOC, DO, NO_3^-) using conservative tracers instead of reactive solutes. In other words, the conservative tracers have the same boundary conditions as the solute they represent, but do not undergo reaction. The conservative tracer concentration maps can be compared with the reactive solute concentration maps to help see where consumption is occurring. For example, from comparison of reactive solute and conservative tracer maps for DOC and DO (Figure 2-3b), it is clear that much of the consumption of these solutes is occurring in the hyporheic flow cell, and thus is by definition non-mixing dependent. This is shown for DOC by the color change of red (conservative tracer) to orange (reactive solute) and for DO by the color change of red (conservative tracer) to many colors including blue (reactive solute) in the hyporheic flow cell. For NO_3^-, consumption is mixing dependent, and is only occurring in the mixing zone, which is difficult to see in Figure 2-3b. However, if one compares the depth that the color blue (representing lack of NO_3^-) that penetrates vertically down into the dune in the conservative tracer map to the same depth in the reactive solute map, one can see that the depth is greater in the reactive solute map. The hydraulics are identical for both the reactive solute and conservative tracer maps, and therefore this change in depth shows that some mixing dependent denitrification is occurring.

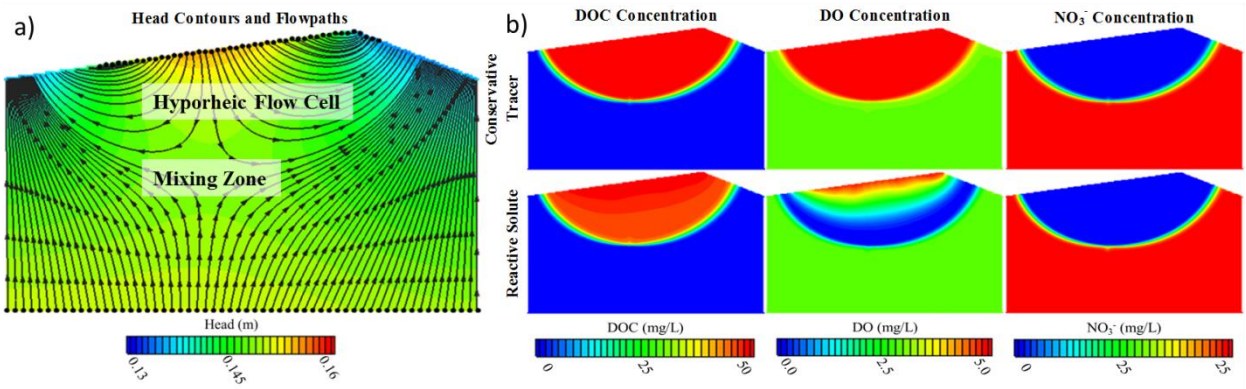

Figure 2-3: Results from fine grid basecase 2, including a) MODFLOW head contours and MODPATH particle tracking (each arrow represents ~14.4 min) and b) concentration maps showing each reactive solute and conservative tracer concentration in the model domain at steady state. Conservative tracer plots had the same boundary conditions as the solute they represent and are provided so that they can be compared with the solute plot to see where consumption is occurring.

2.3.2.1 Varying Biogeochemical Boundary Conditions

Figure 2-4 presents the results of the biogeochemical boundary condition portion of the sensitivity analysis. As SW DOC increased (Figure 2-4a), consumption of DOC, DO and NO_3^- all increased. This is also shown in Figure 2-5a, which shows reactive solute and conservative tracer concentration maps for varying SW DOC. When there was no SW DOC, there was no consumption of any of the reactive solutes because there was no electron donor available. As SW DOC increased from 0 to 5 mg/L, DO and DOC consumption increased very quickly due to an increase in non-mixing (and possibly mixing) dependent aerobic respiration. At higher DOC concentrations, DO consumption continued to increase but at a much slower rate. At SW DOC concentrations between 0 and 5 mg/L, almost no NO_3^- was consumed. This was because almost all DOC was consumed via non-mixing dependent aerobic respiration in SW derived hyporheic water before the DOC could mix with the upwelling GW. These results show that for our model conditions, mixing dependent denitrification was SW DOC limited.

As SW DO increased (Figure 2-4b), consumption of DO via non-mixing dependent aerobic respiration increased. Additionally, as SW DO increased, consumption of NO_3^- via mixing dependent denitrification decreased very slightly. The slight decrease in NO_3^- consumption could be from decreased DOC availability and/or from inhibition from DO. As SW NO_3^- increased (Figures 2-4c, 2-5b), DO consumption via aerobic respiration remained about the same, but NO_3^- and DOC consumption increased. This increase was due to an increase in non-mixing dependent denitrification of SW derived NO_3^- in the hyporheic flow cell.

GW DO and DOC were varied simultaneously such that as GW DO increased, GW DOC decreased [*Chapelle et al.*, 2012]. For the basecase (GW DOC = 0 mg/L, GW DO = 3 mg/L, Table 2-2),

NO_3^- was consumed only via mixing dependent denitrification because NO_3^- and DOC came from different source waters (GW and SW, respectively). The results (Figure 2-4d) show that as GW DOC increased and GW DO decreased, consumption of NO_3^- and DOC increased substantially and then leveled off. The significant initial increase was due to non-mixing dependent denitrification in upgradient GW, and the leveling off at higher GW DOC levels was likely because all NO_3^- had been consumed. DOC consumption then leveled off for this reason. The strongly nonlinear trends (i.e., sharp corners) in Figures 2-4d, e are due to the relationship between GW DOC and GW DO (i.e., when GW DOC is high, GW DO is very low and vice versa).

As GW NO_3^- increased (Figure 2-4f), the amount of DO consumed stayed constant, however the amount of NO_3^- and DOC consumed increased. The increase in DOC and NO_3^- consumption was due to an increase in mixing dependent denitrification.

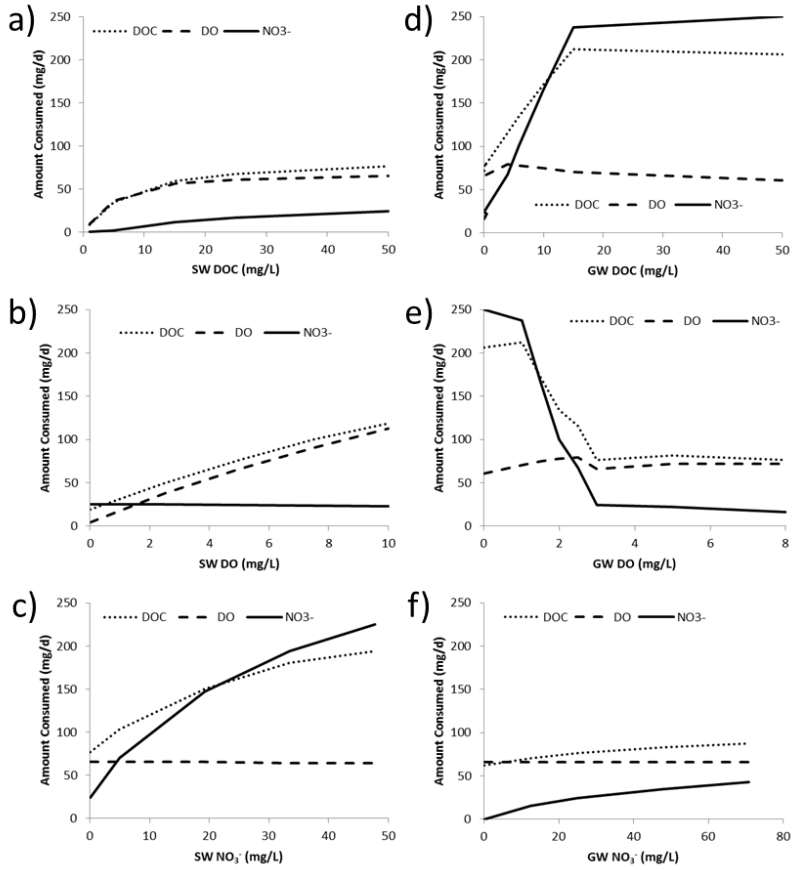

Figure 2-4: Amount of each solute consumed versus a) SW DOC, b) SW DO, c) SW NO_3^-, d) GW DOC, e) GW DO and f) SW NO_3^-. GW DOC and GW DO were varied simultaneously such that GW DOC decreased as GW DO increased; for this reason the consumption data in d and e are the same but plotted on different x-axes. Amount consumed was plotted on the y-axis instead of percent consumed because when varying biogeochemical boundary conditions (e.g., SW DOC) the amount of the solute entering the model for the varied parameters changes. Percent consumed would be confusing because the each

percent of solute consumed is not always normalized to the same value (i.e., amount of solute entering the model).

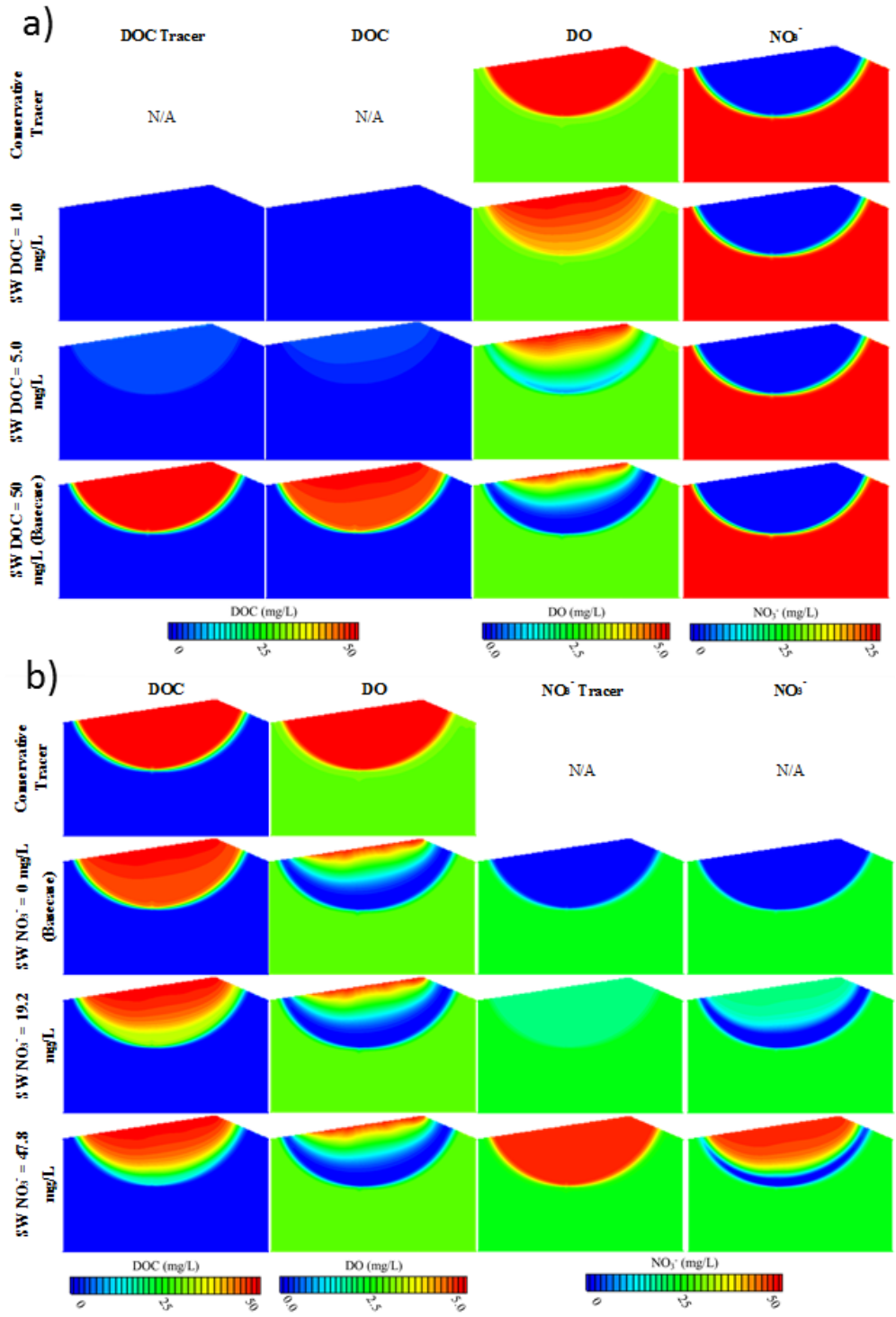

Figure 2-5: Concentration maps showing reactive solute and conservative tracer concentration in the model domain at steady state for fine grid basecase 2 and for varying a) SW DOC and b) SW NO_3^-. Conservative tracer plots had the same boundary conditions as the solute they represent and are provided so that they can be compared with the solute plot to see where consumption is occurring.

Figures 2-4a and 2-4f show that increasing SW DOC or increasing GW NO_3^- increased the amount of mixing dependent denitrification. Additionally, Figures 2-4c-e, show that increasing SW NO_3^- or increasing GW DOC (which simultaneously decreased GW DO), increased the amount of non-mixing dependent denitrification. When comparing the magnitude of changes in NO_3^- consumption, one can see that parameters affecting non-mixing dependent denitrification can increase NO_3^- consumption much more than parameters effecting mixing dependent denitrification can increase NO_3^- consumption. The described trends are also shown in Figures 2-5a, b. As SW DOC increased (Figure 2-5a), mixing dependent denitrification increased (shown in Figure 2-4a), however the increase is very slight and difficult to see (similar to Figure 2-3). However as SW NO_3^- increased (Figure 2-5b) it is much clearer that non-mixing dependent denitrification increased greatly. This is seen in the substantial differences between the NO_3^- tracer and NO_3^- concentration maps in the hyporheic flow cell.

Non-mixing dependent denitrification was generally greater than mixing dependent denitrification for basecase 2 (Figure 2-6). For example, when varying SW NO_3^-, non-mixing dependent denitrification exceeded mixing dependent denitrification for SW NO_3^- > 2.6 mg/L. When SW NO_3^- and GW NO_3^- are about equal (~24.8 mg/L), NO_3^- consumed from non-mixing dependent denitrification is about 5 times higher than NO_3^- consumed from mixing dependent denitrification.

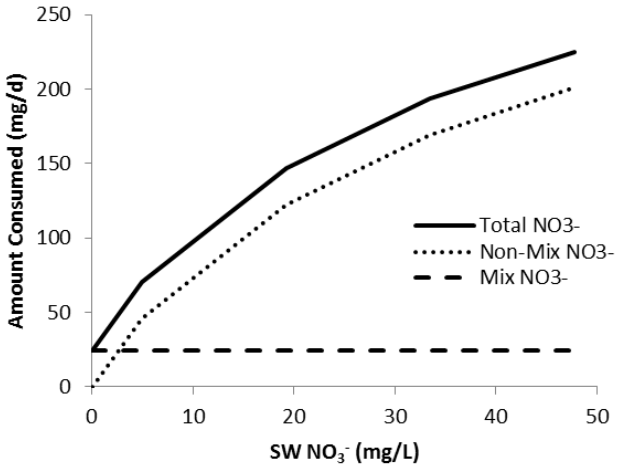

Figure 2-6: Total NO_3^-, non-mixing dependent NO_3^- and mixing dependent NO_3^- consumed with increasing SW NO_3^-. Mixing and non-mixing dependent denitrification were determined as described in Section 2.3.1. For all SW NO_3^- values, about 24 mg/d NO_3^- is consumed via mixing dependent denitrification, and the total NO_3^- consumed minus 24 mg/d is equal to the amount of NO_3^- consumed via non-mixing dependent denitrification.

2.3.2.2 Varying Hydraulic Parameters and Boundary Conditions

As homogeneous hydraulic conductivity (K) increased, hyporheic flow cell and GW residence times decreased (e.g., Figure 9 in *Hester et al.* [2013]), resulting in decreased time available for all reactions. However, as K increased, the amount of solutes entering the model domain from SW increased (Figure 2-7a) which increased all reactions (equations (5-7)). Ultimately, the increase in SW DOC outweighed the decrease in residence times for an overall increasing trend (for all reactions) with K (Figure 2-7d). The higher increase in DOC and DO consumption relative to NO_3^- is likely due to increased non-mixing dependent aerobic respiration promoted by increases in the SW solute inflows. However, the percent of DOC consumed decreased with increasing K, and the percent of DO consumed increased and then decreased with increasing K (Figure 2-7g). This is likely due to the decreased residence times and increased SW DOC and DO entering the model. Unlike DOC, the percent NO_3^- consumed increased with increasing K (Figure 2-7g), showing that for mixing dependent reactions, the amount of DOC entering the model outweighed decreased residence times more than for non-mixing dependent reactions.

As the lower boundary flux increased, hyporheic flow cell and GW residence times decreased (Figures 2-8a, b), resulting in decreased time available for all reactions. Additionally, as lower boundary flux increased, GW NO_3^- flowing into the model increased, but SW DOC entering the model simultaneously decreased (Figure 2-7b). Decreased DOC decreases denitrification and increased NO_3^- increases denitrification (equation (8)). The decrease in DOC and residence times outweighed the increase in NO_3^-, except for very low lower boundary fluxes, for an overall declining trend of amount and percent consumed with bottom flowrate (Figure 2-7e, h). Additionally, consumption of DO decreased with increased lower boundary flux, also due to a decrease in SW DOC and DO entering the model and a decrease in residence times.

As the variance of the heterogeneous K field increased, the amount of DOC and DO entering from SW increased and the amount of DO and NO_3^- coming from GW stayed about the same (Figure 2-7c). Despite the increase in SW DOC and DO, non-mixing dependent aerobic respiration of DOC and DO (amount and percent consumed) actually decreased with increasing variance (Figure 2-7f, i), unlike when homogeneous K was varied (Figure 2-4d). This can be explained by flow focusing and the stair-stepping of the upper boundary. As variance of K increases, flow paths become bunched together in certain areas leaving more empty space in other areas (see *Hester et al.* [2013] Figure 6a). This creates preferential flow paths via flow focusing in higher K areas throughout the model domain. Such flow focusing causes more solutes to enter from the SW boundary, yet these flow paths have shorter residence times (Figure 2-8c) and therefore less biodegradation. This may be accentuated at the SW boundary by the stair-stepping required to represent an angled dune face in a finite difference model, because it gives

the flow paths even more opportunities to enter and then leave the model quickly. By contrast, the same increase in shorter residence times with increasing K variance does not occur with flow paths originating at the lower (GW) boundary (Figure 2-8d) because such flow primarily crosses the boundary perpendicularly and the border is not stair-stepped.

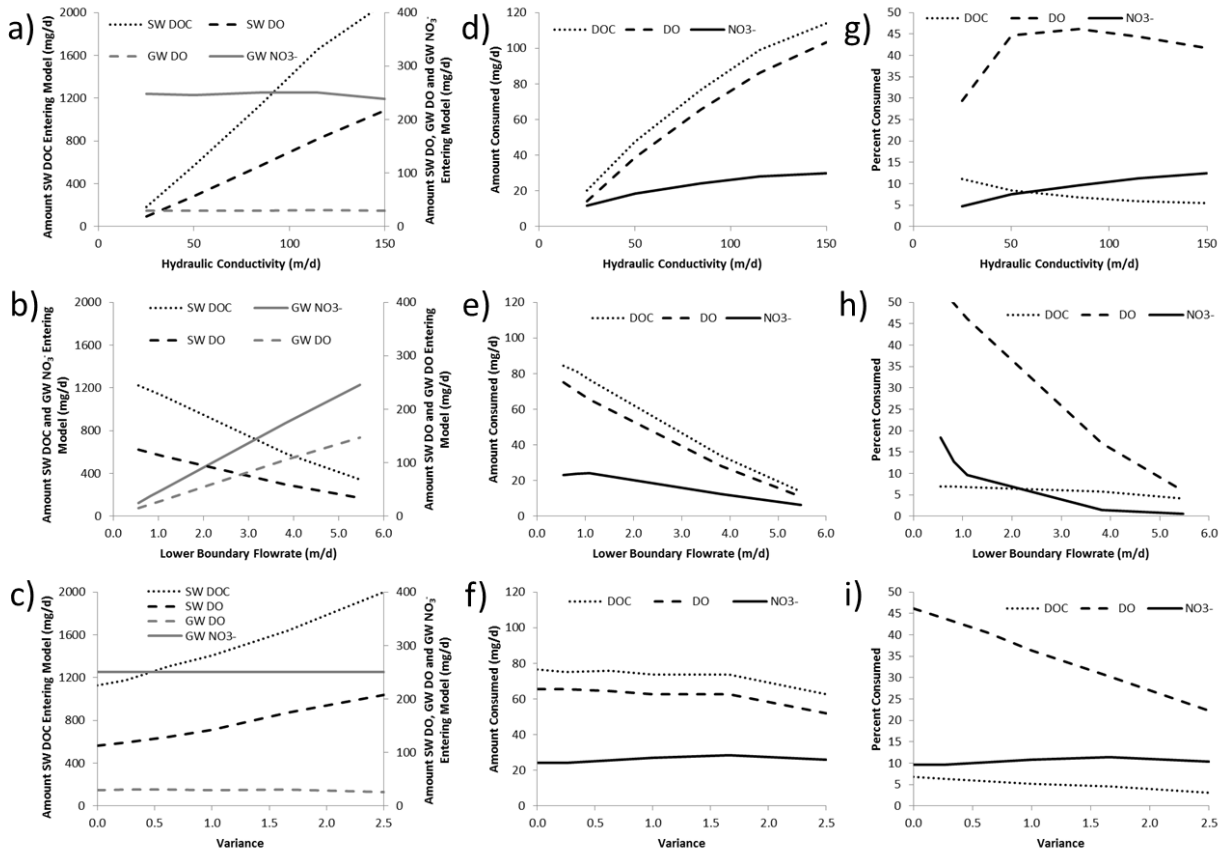

Figure 2-7: Amount of each solute entering the model from SW and GW versus a) homogeneous K, b) lower boundary flowrate and c) variance of heterogeneous K field. Amount of each solute consumed versus d) homogeneous K, e) lower boundary flowrate and f) variance of heterogeneous K field. Percent of each solute consumed versus g) homogeneous K, h) lower boundary flowrate and i) variance of heterogeneous K field. Percent of each solute consumed was determined by dividing the amount of each solute consumed by the total amount of each solute entering the model and multiplying by 100.

As variance increased, mixing dependent denitrification increased slightly and then decreased (Figure 2-7i). *Hester et al.* [2013] shows that an increase in variance increases mixing between the hyporheic flow cell and GW. This is probably why denitrification increased initially. However, an increase in variance also decreased non-mixing dependent aerobic respiration leaving more DO in the model, which probably inhibited mixing dependent denitrification at higher variances.

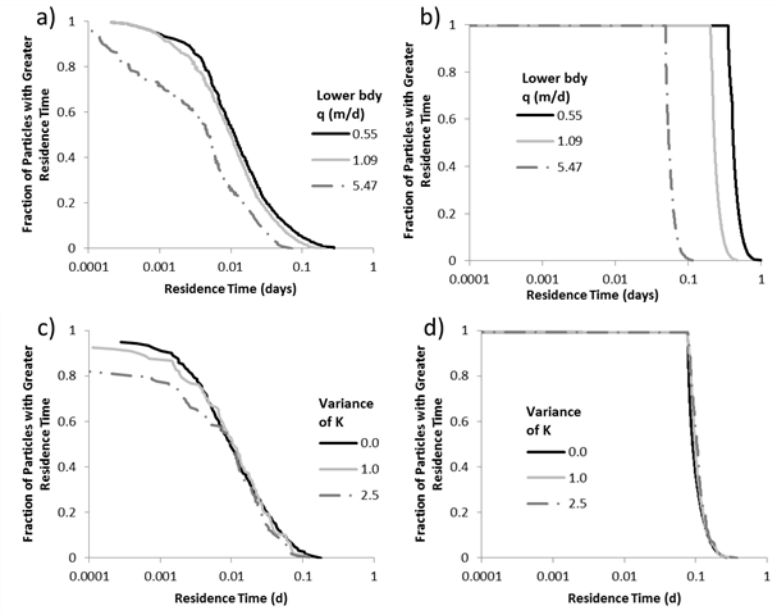

Figure 2-8: Cumulative residence time distributions within model domain for a, c) particles released at upper model boundary with SW (i.e., residence times within hyporheic flow cells) and b, d) at the lower model boundary (i.e., upwelling groundwater). Results for a series of lower boundary fluxes (a-b) and for a series of variances of K (c-d) are shown.

2.3.2.3 Sensitivity Coefficients

Figure 2-9 presents the maximum sensitivity coefficients for varying all parameters in the fine grid sensitivity analysis. Sensitivity coefficients were calculated based on the amount of NO_3^- consumed (Figure 2-9a, c) and based on the percent of NO_3^- consumed (Figure 2-9b, d).

Varying GW DOC and GW DO simultaneously (Figure 2-9a, b) was the most sensitive parameter whether the sensitivity coefficients were determined using amount or percent NO_3^- consumed. This is because when GW DOC was added to the model and GW DO was decreased from the model, non-mixing dependent denitrification could occur in the upwelling GW. The upwelling GW had longer residence times than the hyporheic flow cells, and therefore there was more time for the reactions to occur.

Varying SW NO_3^- (Figure 2-9a) was the second most sensitive parameter when the sensitivity coefficients were calculated based on the amount of NO_3^- consumed. However, when the sensitivity coefficients were calculated based on the percent of NO_3^- consumed (Figure 2-9b), SW NO_3^- was the 6th most sensitive parameter. When SW NO_3^- was introduced into the model, consumption of NO_3^- increased significantly due to an increase in non-mixing dependent denitrification, which explains the high sensitivity to SW NO_3^- when the sensitivity coefficients were calculated based upon the amount of NO_3^- consumed. However when SW NO_3^- was introduced into the model, the amount of SW NO_3^- entering the model also increased, which explains why the model is not very sensitive to SW NO_3^- when the sensitivity coefficients were calculated based on the percent of NO_3^- consumed.

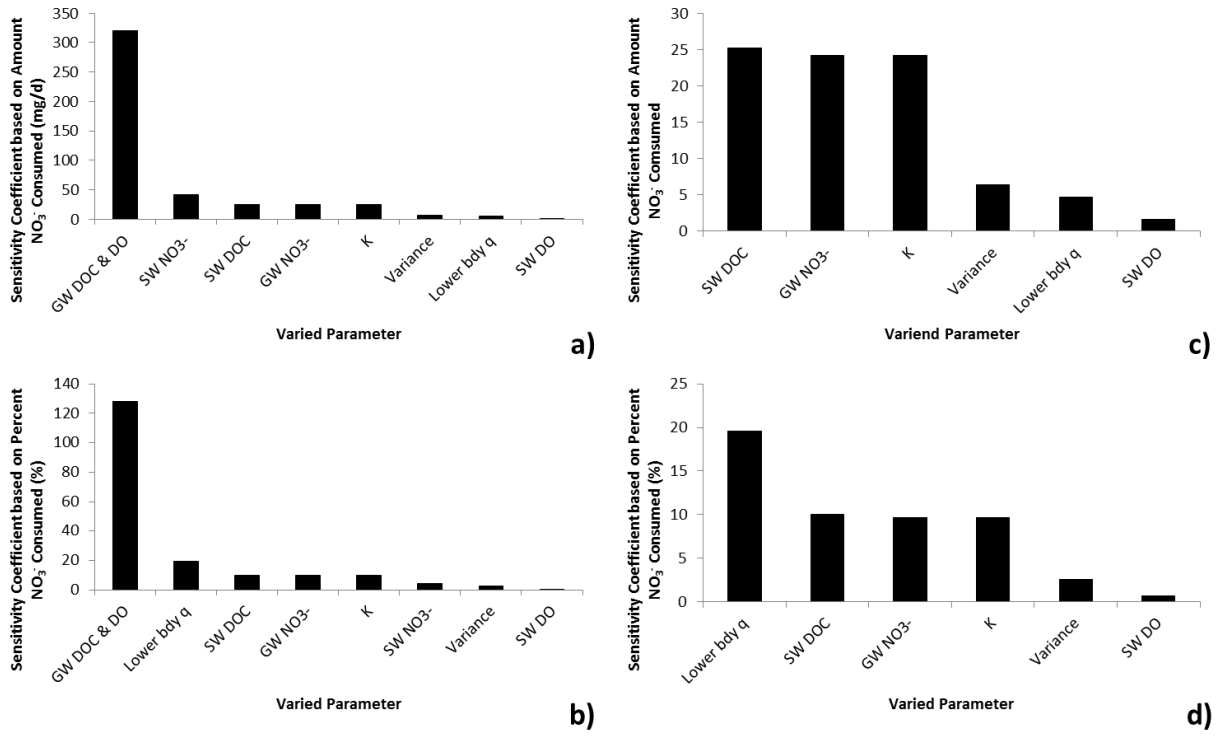

Figure 2-9: Maximum sensitivity coefficients for all points within the model for varying each parameter from the fine grid sensitivity analysis based on a) the amount of NO_3^- consumed and b) the percent of NO_3^- consumed. Maximum sensitivity coefficients for varying parameters only affecting mixing dependent denitrification from the fine grid sensitivity analysis based on c) the amount of NO_3^- consumed and d) the percent of NO_3^- consumed.

SW DOC, GW NO_3^- and K had approximately the same values for sensitivity coefficients whether calculated using the amount (Figure 2-9a, c) or percent (Figure 2-9b, d) of NO_3^- consumed. When only including parameters affecting mixing dependent denitrification, SW DOC, GW NO_3^- and K were the most sensitive parameters when the sensitivity coefficients were calculated based upon the amount of NO_3^- consumed (Figure 2-9c), yet where less sensitive than lower boundary flux when the sensitivity coefficients were calculated based upon the percent of NO_3^- (Figure 2-9d) consumed.

Similar to SW NO_3^-, the sensitivity of the lower boundary flux changed depending on how it was calculated. As lower boundary flux increased, the amount of NO_3^- entering the model increased, and the amount of NO_3^- consumed decreased. This explains why this parameter was more sensitive when calculated based upon percent NO_3^- (Figure 2-9b, d) consumed than when calculated based upon amount NO_3^- (Figure 2-9a, c) consumed.

Finally, SW DO was the least sensitive parameter whether the sensitivity coefficients were calculated using the amount (Figure 2-9a, c) or percent (Figure 2-9b, d) of NO_3^- consumed.

2.4 Discussion

2.4.1 Disentangling Mixing Dependent and Non-Mixing Dependent Contaminant Reactions in the Hyporheic Zone

Previous studies have examined the interaction of upwelling contaminants with hyporheic zones [*Moser et al.*, 2003; *Conant et al.*, 2004; *Gu et al.*, 2007; *Kennedy et al.*, 2009a; b; *Krause et al.*, 2009; *Landmeyer et al.*, 2010; *Stelzer and Bartsch*, 2012; *Krause et al.*, 2013], but to our knowledge, no previous studies have rigorously distinguished mixing dependent reactions from other related processes that affect contaminant concentrations and fluxes in riverbed sediments. Here we distinguish three key processes: mixing dependent reactions of contaminants from groundwater (GW), non-mixing dependent reactions of contaminants from either surface water (SW) or GW, and dilution of contaminants from GW by SW advecting through hyporheic flow cells. Prior studies can be categorized based on which of these processes they distinguish, including non-mixing dependent reactions of SW contaminants and all three types of transformations of GW contaminants. Here we generally focus more broadly than just denitrification, as our results have implications for many environmental contaminants.

2.4.1.1 Non-Mixing Dependent Reactions of SW Contaminants in Hyporheic Zones

Studies of non-mixing dependent reactions of contaminants from SW in the hyporheic zone are very common [*Kim et al.*, 1995; *Williams and Fulthorpe*, 2003; *Hoehn et al.*, 2007; *Cardenas et al.*, 2008b; *Boano et al.*, 2010; *Marzadri et al.*, 2011; *Zarnetske et al.*, 2011a; *Bardini et al.*, 2012; *Marzadri et al.*, 2012; *Zarnetske et al.*, 2012], so here we focus on non-mixing dependent denitrification. In a wide-ranging numerical modeling study of hyporheic exchange and nitrogen transformations across a gravel bar, *Zarnetske et al.* [2012] found that from a transport perspective, the residence times were one of the most important factors in determining the fate of nitrate (NO_3^-) in hyporheic zones with non-mixing dependent reactions. This is in agreement with other modeling studies of reactive NO_3^- transport in the hyporheic zone [*Gu et al.*, 2007; *Cardenas et al.*, 2008a; *Boano et al.*, 2010; *Marzadri et al.*, 2011; *Zarnetske et al.*, 2011a; *Bardini et al.*, 2012].

We see the importance of residence times when varying hydraulic conductivity (K) (Figures 2-7a, d and g) and varying lower boundary flux (Figures 2-7b, e and h). When K was higher, residence times were shorter throughout the model domain, resulting in a decreased percentage of dissolved organic carbon (DOC) consumed in the hyporheic flow cell due a decrease in aerobic respiration. An increase in lower boundary flux had the same effect. Finally, the importance of residence times can be seen within

the hyporheic flow cell itself for non-mixing dependent reactions. Figure 2-9 shows the concentration of NO_3^- at steady state for the case of high SW NO_3^-. Areas with longer residence times are more depleted in NO_3^- compared to areas with shorter residence times. This is because flow paths with longer residence times have more time to deplete dissolved oxygen (DO) from SW, and have more time for denitrification to occur.

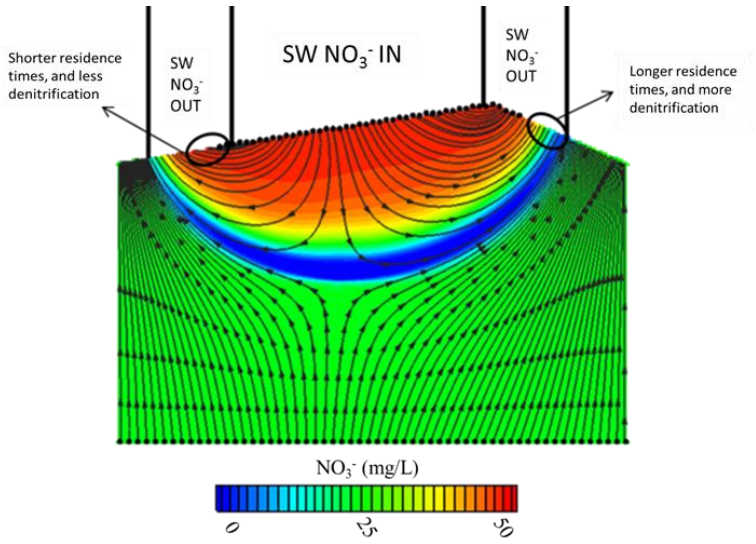

Figure 2-10: NO_3^- concentration map at steady state for basecase 2 when SW NO_3^- = 47.8 mg/L (Table 2-2). Straight black lines on top delineate zones where SW flows into and out of the model, and where deeper GW flows out of the model. MODPATH particle tracks have arrows each ~14.4 minutes. The red area represents water with hyporheic residence times < ~22 minutes, the area shaded green represents residences times > ~22 minutes and <~36 minutes, and the area shaded blue represents residences times > ~36 minutes.

In an example from field data, *Zarnetske et al.* [2011a] observed hyporheic nitrogen transformations in the same gravel bar mentioned above, and found net nitrification occurred for residence times of less than 6.9 hours and net denitrification occurred thereafter. This threshold residence time is controlled by a combination of hyporheic zone water temperature, DO concentration, DOC supply and quality, and NO_3^- supply. Residence times calculated for our model domain (~1 hour) were much shorter than this threshold, yet we still saw denitrification. This is likely because we had significantly higher SW DOC concentrations (50 vs ~ 3 mg/L), which increased the rate at which DO was consumed (equation (7)) and therefore reduced inhibition by DO.

2.4.1.2 Transformations of Upwelling GW Contaminants in Hyporheic Zones

Another important group of prior studies involve field investigations of upwelling contaminants where mixing dependent reactions may be occurring in the hyporheic zone. None of these studies

identify the reactions taking place as mixing dependent even though that is often the most likely explanation. Some studies do not even fully distinguish upwelling contaminant concentration reduction in the hyporheic zone due to mixing dependent reactions from that due to dilution with uncontaminated water from SW. For example, *Kennedy et al.* [2009a] studied GW NO_3^- upwelling into streambeds, however their experimental setup did not include the shallowest sediments where mixing of SW and GW is most likely. It was therefore impossible to tell if observed NO_3^- reduction was due to mixing dependent denitrification or dilution with lower concentration SW. Similarly, *Krause et al.* [2013] investigated how NO_3^- rich GW is affected by upwelling across heterogeneous streambed sediments, and presented very detailed data of NO_3^- concentrations in the top sediments of a streambed. They found that NO_3^- concentrations in the upwelling GW varied by up to 68 mg/L within the top 15 cm of streambed sediments, however it was unclear why this was occurring and where water at these depths originated.

Conant et al. [2004] similarly showed another anaerobic process, reductive dehalogenation of upwelling perchloroethene (PCE), occurring in shallow riverbed sediments unlike in the upgradient plume. It is possible that the higher rates of dehalogenation occurring in the shallow sediments were due to advection of DOC from SW, depletion of DO in hyporheic flow cells due to non-mixing dependent aerobic respiration, mixing of SW derived DOC with upwelling GW flow paths, mixing dependent aerobic respiration depleting any GW derived DO, and finally mixing dependent dehalogenation. Dilution with SW in the shallowest sediments is also possible. Nevertheless, the spatial resolution of their sampling grid was too coarse to determine the relative magnitudes of these processes.

Landmeyer et al. [2010] studied petroleum hydrocarbons and fuel oxygenates in GW as they upwelled to a river, and they found that concentrations decreased significantly in shallow sediments, unlike in the upgradient aquifer. Consumption of the hydrocarbons occurred as only a few percent of the upwelling contaminant mass flux, and seems likely to be mixing dependent reaction because these contaminants degrade aerobically and likely required DO supplied from SW. By contrast, dilution with SW was reported as the main reason for the observed reduction, yet they did not rigorously characterize the mixing processes that cause such dilution. Future research that better distinguishes among mixing dependent reactions, non-mixing dependent reactions, and dilution in hyporheic zones is needed.

In our model and as shown in *Hester et al.* [2013], dilution of upwelling contaminants with SW can be very small due to thin mixing zones. It is possible that the high levels of dilution observed by *Landmeyer et al.* [2010] may be due to variable river stages which can cause additional mixing. In addition, if they sampled from sufficiently long well screens, they might be drawing water from both above and below the thin mixing zone, resulting in water samples with intermediate concentrations. *Landmeyer et al.* [2010] also found the highest rates of consumption when GW discharge was the lowest (Table 4 in [*Landmeyer et al.*, 2010]). The low GW flux possibly allowed more oxygen to enter the bed

with longer flow paths and residence times, allowing for more consumption. We found the same response of oxygen entry, flow path lengths and residence times in our study, which allowed more mixing and non-mixing dependent consumption.

Based on our work and the previously discussed studies, an important conclusion appears to be that for mixing dependent reactions to occur in the hyporheic zone, residence times in hyporheic flow cells must exceed the time needed for the reaction of interest to occur *plus* the time needed for any necessary precursor reactions to occur. This can also be said for reactions in general, but the new twist for mixing dependent reactions in the hyporheic zone is that the precursor reactions can occur either in the hyporheic flow cell or the mixing zone between the hyporheic flow cell and upwelling GW, while the reaction of interest by definition only occurs in the mixing zone. This should favor aerobic over anaerobic mixing dependent reactions. Regardless, sufficient reactants for both mixing dependent and precursor reactions then must also be present (e.g., SW DOC for our study). Hydraulic conditions in turn affect both residence times and reactant supplies. For example, when our lower boundary flowrate was high, much less DO was consumed in the hyporheic flow cell due to insufficient residence times, and leftover DO inhibited mixing dependent denitrification. Additionally, when SW DOC levels were low, all DOC was consumed by aerobic respiration, leaving none for mixing dependent denitrification.

A key distinction with non-mixing dependent reactions is that mixing dependent reactions will only occur in hydrologically gaining or neutral rivers where hyporheic flow cells form. The degree of gaining varies with the seasons, such that mixing dependent reactions also likely vary with seasons. For example, in wet climates or in steeper mountain valleys where stronger gaining conditions exist, mixing dependent reactions may only occur in summer when the water table and degree of gaining is at its lowest.

As stated in the Results section, non-mixing dependent reactions may be more prevalent than mixing dependent reactions, due to insufficient mixing flux compared to the total flux of SW or GW. This is consistent with *Hester et al.* [2013] who found that mixing is only a few percent of total SW and GW flux, and only occurs in a thin zone. Nevertheless, mixing dependent reactions can still be important, and in fact could be greater than mixing dependent reactions if neither SW nor GW contain all the necessary reactants. For denitrification, this could be the case when there is a NO_3^- plume upwelling to a stream that has low SW NO_3^-. This could occur for example where a relatively pristine stream flows into an area with septic systems, which may be quite common in rural areas. By contrast, this is unlikely to happen in an agriculture watershed, because if GW is contaminated with NO_3^- from fertilizers, SW likely will also be contaminated. Even though mixing dependent reactions may be of lesser magnitude overall than non-mixing dependent reactions, such mixing dependent reactions provide potentially important functions that non-mixing dependent reactions cannot. Plumes of contaminants in deeper GW that upwell

towards rivers may only encounter suitable redox conditions or reactants once they encounter the hyporheic zone. As such, mixing dependent reactions can be the "last line of defense" before a contaminant enters a potentially ecologically sensitive SW body.

2.4.2 Applications to Increase Contaminant Reactions in the Hyporheic Zone

For mixing dependent denitrification, it is necessary to have enough time for aerobic respiration to deplete SW and GW DO and consume NO_3^-. Depending on parameters such as K and actual reaction rates, dunes may or may not create sufficient residence times. Residence time will scale with dune size which scales with river size, so dunes in large rivers such as the Columbia River which can have dunes 10m long [*Peterson and Johnson*, 1992; *Geist et al.*, 1994; *Moser et al.*, 2003], may have more potential for mixing dependent reactions. Hyporheic flow cells can also be induced by submerged bars, riffles and debris dams [*Thibodeaux and Boyle*, 1987; *Gooseff et al.*, 2006; *Hester and Doyle*, 2008; *Sawyer et al.*, 2011], all of which will frequently have longer flow paths than the dunes we modeled. Stream and river restoration efforts that create such bedforms could increase both non-mixing dependent reactions such as denitrification (of SW contaminants in hyporheic flow cells) and mixing dependent reactions (of GW contaminants in mixing zones) by increasing flow path length and residence times. Stream, river, or watershed restoration can similarly promote natural and more sustainable creation of such bedforms, for example by riparian reforestation which can ultimately provide a source of large wood to the channel that enhances formation of bedforms such as debris dams [*Lautz et al.*, 2006; *Groffman et al.*, 2009].

Anaerobic conditions are necessary for reactions such as denitrification and Cr(VI) reduction. *Zarnetske et al.* [2011b] showed that injection of labile DOC (AcO^-) at the start of hyporheic flow paths increased metabolic processing rates down gradient such that the injected DOC was utilized and removed rapidly. Utilization of labile DOC stimulated additional aerobic respiration, and consequently increased anaerobic conditions which led to signification increases in denitrification rates. Such carbon injections as a remedial measure could help reduce NO_3^- levels by enabling mixing and non-mixing dependent denitrification. In this case as well, natural and ultimately more sustainable practices may be preferred. Riparian forest planting may help in this way as well, because it can contribute natural DOC and POC to the riverbed [*Vannote et al.*, 1980; *Hester and Gooseff*, 2010].

Ultimately, although mixing dependent reactions may often have less mass consumed than non-mixing dependent reactions, mixing dependent reactions can provide important functions that non-mixing dependent reactions cannot. By taking advantage of additional sources of carbon not present in GW, mixing dependent reactions may prove decisive in addressing lingering GW contamination which makes it past more active GW remediation technologies such as permeable reactive barriers or upgradient

aquifer monitored natural attenuation before it exits to SW. As such, mixing dependent reactions may be the "last line of defense" before contaminants enter potentially ecologically sensitive SW.

2.4.3 Implications of Model Assumptions

In our modeling we assumed all organic carbon was in the form of labile DOC. In real rivers, organic carbon sources are much more diverse. For example, buried POC, as it decomposes, can provide additional sources of electron donors for both mixing and non-mixing dependent reactions [*Moser et al.*, 2003; *Stelzer and Bartsch*, 2012].

We ran the model in steady state, such that that residence times do not change with time. Under real field conditions, residence times could likely change due to time-varying hydraulic boundary conditions such as variable GW upwelling rates, storm events, hydropeaking of reservoirs upstream, snowmelt, and daily evapotranspiration cycles [*Wondzell and Swanson*, 1996; *Peterson and Connelly*, 2001; *Loheide and Lundquist*, 2009]. Such unsteady hydraulics may increase mixing [*Hester et al.*, 2013] and therefore could affect the prevalence of mixing dependent reactions. Biogeochemical boundary conditions could also vary with time (i.e., DO with temperature). These are key areas for future research.

Finally, many assumptions were necessary when picking reaction rates. We used the best data available [*Zarnetske et al.*, 2012], but there remains considerable uncertainty in the literature. Actual reaction rates may be higher or lower than what we used and may vary spatially and/or temporally in the field. To partially test the effect of this type of variability, we reran all model runs (Table 2-2) with a lower rate (on the coarse grid), and the trends in Figures 2-4 and 2-7 remained the same although consumption was significantly less. Regardless, this points to the critical need to better characterize reaction rates and microbial communities in hyporheic settings to better parameterize models of microbially-mediated reactions in the hyporheic zone.

2.5 Conclusions

We numerically modeled upwelling groundwater (GW) interacting with riverbed dune-induced hyporheic flow. We quantified denitrification due to mixing dependent and non-mixing dependent reactions in the hyporheic zone, and varied both biogeochemical and hydraulic conditions (Table 3). Overall, we found that non-mixing dependent reactions consume more mass than mixing dependent reactions.

We first varied biogeochemical boundary conditions. As GW and surface water (SW) nitrate (NO_3^-) concentrations increased, mixing dependent and non-mixing dependent denitrification increased, respectively. Additionally, as GW dissolved organic carbon (DOC) concentrations increased and GW dissolved oxygen (DO) concentrations simultaneously decreased, non-mixing dependent denitrification

increased in GW. We also found that as SW DOC inputs increased, either by increasing SW DOC concentrations or by increasing hydraulic conductivity (K), mixing dependent denitrification increased after aerobic DOC respiration needs were satisfied. It is clear that the amount of DOC entering the model is a key biogeochemical control on mixing and non-mixing dependent denitrification.

Next we varied hydraulic boundary conditions and parameters. As the lower boundary flux decreased, an increase in SW DOC entering the model outweighed the decrease in GW NO_3^- resulting in a net increase in mixing dependent denitrification. Similarly, as K increased, the increase in SW DOC outweighed the decrease in residence times resulting overall in increased mixing dependent denitrification. When we used a heterogeneous K field, and we found that as variance of K increased, mixing dependent denitrification initially increased due to increased mixing between hyporheic water and GW. However, non-mixing dependent aerobic respiration in the hyporheic flow cell simultaneously declined, allowing more DO to make it to the mixing zone, which inhibited denitrification at higher variances.

GW DOC and GW DO were the most sensitive parameters overall, and SW DO was the least sensitive parameter. SW DOC, GW NO_3^- and K all had about the same sensitivity to the model, and were most sensitive parameters affecting mixing dependent denitrification when the sensitivity coefficients were calculated using the amount of NO_3^-. These three parameters were also of similar sensitivity when coefficients were calculated using percent of NO_3^- consumed, but were also less sensitive than lower boundary flux.

Mixing dependent reactions in the hyporheic zone have likely been observed in a number of prior studies, but these studies did not fully distinguish such reactions from non-mixing dependent hyporheic reactions or dilution of upwelling solute with water advecting through hyporheic flow cells in shallow sediments. We distinguish these two types of reactions in our modeling, as well as demonstrate that dilution is minimal due to a thin mixing zone between hyporheic flow cell and upwelling GW.

Mixing dependent reactions will only occur in circum-neutral to moderately gaining rivers, and will be maximized with higher residence times in hyporheic flow cells. Residence times in mixing zones would be maximized by larger hyporheic flow cells, such as those created by larger dunes in large rivers, or pool-riffle sequences in smaller systems.

Even though mixing dependent reactions may be of lesser magnitude overall than non-mixing dependent reactions, mixing dependent reactions provide potentially important functions that non-mixing dependent reactions cannot. Plumes of contaminants in deeper GW that upwell towards rivers may only encounter suitable redox conditions or reactants to allow for attenuation once they encounter the hyporheic zone. As such, mixing dependent reactions can be the “last line of defense” before a contaminant enters a potentially ecologically sensitive SW body. Mixing dependent reactions may prove

decisive in addressing lingering GW contamination which makes it past more active GW remediation technologies such as permeable reactive barriers or monitored natural attenuation in upgradient aquifers.

2.6 References

Barbaro, J. W., Donald; LeBlanc, Denis (2013), Transport of Nitrogen in a Treated-Wastewater Plume to Coastal Dischargee Areas, Ashumet Valley, Cape Cod, Massachusetts*Rep.*, U.S. Geological Survey Scientific Investigations Report.

Bardini, L., F. Boano, M. Cardenas, R. Revelli, and L. Ridolfi (2012), Nutrient cycling in bedform induced hyporheic zones, *Geochimica et Cosmochimica Acta*, *84*, 47-61.

Boano, F., A. Demaria, R. Revelli, and L. Ridolfi (2010), Biogeochemical zonation due to intrameander hyporheic flow, *Water Resources Research*, *46*(2).

Braun, E. (2007), *Reactive Nitrogen in the Environment: Too Much Or Too Little of a Good Thing*, United Nations Publications.

Brunke, M., and T. Gonser (1997), The ecological significance of exchange processes between rivers and groundwater, *Freshwater Biology*, *37*(1), 1-33.

Cardenas, M. B., and J. Wilson (2006), The influence of ambient groundwater discharge on exchange zones induced by current–bedform interactions, *Journal of Hydrology*, *331*(1), 103-109.

Cardenas, M. B., and J. L. Wilson (2007), Dunes, turbulent eddies, and interfacial exchange with permeable sediments, *Water Resources Research*, *43*(8).

Cardenas, M. B., J. L. Wilson, and R. Haggerty (2008a), Residence time of bedform-driven hyporheic exchange, *Advances in Water Resources*, *31*(10), 1382-1386.

Cardenas, M. B., P. L. Cook, H. Jiang, and P. Traykovski (2008b), Constraining denitrification in permeable wave-influenced marine sediment using linked hydrodynamic and biogeochemical modeling, *Earth and Planetary Science Letters*, *275*(1), 127-137.

Cey, E. E., D. L. Rudolph, R. Aravena, and G. Parkin (1999), Role of the riparian zone in controlling the distribution and fate of agricultural nitrogen near a small stream in southern Ontario, *Journal of Contaminant Hydrology*, *37*(1), 45-67.

Chapelle, F. H., P. M. Bradley, P. B. McMahon, K. Kaiser, and R. Benner (2012), Dissolved Oxygen as an Indicator of Bioavailable Dissolved Organic Carbon in Groundwater, *Ground Water*, *50*(2), 230-241.

Cirpka, O. A., E. O. Frind, and R. Helmig (1999), Numerical simulation of biodegradation controlled by transverse mixing, *Journal of Contaminant Hydrology*, *40*(2), 159-182.

Cirpka, O. A., Å. Olsson, Q. Ju, M. Rahman, and P. Grathwohl (2006), Determination of transverse dispersion coefficients from reactive plume lengths, *Ground Water*, *44*(2), 212-221.

Conant, B., J. A. Cherry, and R. W. Gillham (2004), A PCE groundwater plume discharging to a river: influence of the streambed and near-river zone on contaminant distributions, *Journal of Contaminant Hydrology*, *73*(1), 249-279.

Corsi, S. R., R. D. Klaper, D. N. Weber, and R. T. Bannerman (2011), Water-and sediment-quality effects on Pimephales promelas spawning vary along an agriculture-to-urban land-use gradient, *Science of the Total Environment*, *409*(22), 4847-4857.

DeSimone, L. A., and B. L. Howes (1998), Nitrogen transport and transformations in a shallow aquifer receiving wastewater discharge: A mass balance approach, *Water Resources Research*, *34*(2), 271-285.

Diaz, R. J., and R. Rosenberg (2008), Spreading dead zones and consequences for marine ecosystems, *Science*, *321*(5891), 926-929.

Dubrovsky, N. M., K. R. Burow, G. M. Clark, J. Gronberg, P. A. Hamilton, K. J. Hitt, D. K. Mueller, M. D. Munn, B. T. Nolan, and L. J. Puckett (2010), *The Quality of Our Nation's Water: Nutrients in the Nation's Streams and Groundwater, 1992-2004*, US Department of the Interior, US Geological Survey.

Duff, J. H., and F. J. Triska (1990), Denitrifications in sediments from the hyporheic zone adjacent to a small forested stream, *Canadian Journal of Fisheries and Aquatic Sciences*, *47*(6), 1140-1147.

Elliott, A. H., and N. H. Brooks (1997), Transfer of nonsorbing solutes to a streambed with bed forms: Theory, *Water Resources Research*, *33*(1), 123-136.

Febria, C. M., P. Beddoes, R. R. Fulthorpe, and D. D. Williams (2011), Bacterial community dynamics in the hyporheic zone of an intermittent stream, *The ISME journal*, *6*(5), 1078-1088.

Fehlman, H. M. (1985), Resistance components and velocity distributions of open channel flows over bedforms, Colorado State University, Fort Collins, CO.

Galloway, J. N., W. H. Schlesinger, H. Levy, A. Michaels, and J. L. Schnoor (1995), Nitrogen fixation: Anthropogenic enhancement-environmental response, *Global Biogeochemical Cycles*, *9*(2), 235-252.

Galloway, J. N., J. D. Aber, J. W. Erisman, S. P. Seitzinger, R. W. Howarth, E. B. Cowling, and B. J. Cosby (2003), The nitrogen cascade, *BioScience*, *53*(4), 341-356.

Garcia, M. H. (2008), Sediment transport and morphodynamics, *Sedimentation engineering: processes, management, modeling, and practice*, 21-163.

Geist, D. R., T. Poston, and D. D. Dauble (1994), Assessment of potential impacts of major groundwater contaminants to fall Chinook salmon (Oncorhynchus tshawytscha) in the Hanford Reach, Columbia River*Rep.*, Battelle Pacific Northwest Lab., Richland, WA (United States).

Gooseff, M. N., J. K. Anderson, S. M. Wondzell, J. LaNier, and R. Haggerty (2006), A modelling study of hyporheic exchange pattern and the sequence, size, and spacing of stream bedforms in mountain stream networks, Oregon, USA, *Hydrological Processes*, *20*(11), 2443-2457.

Groffman, P. M., A. M. Dorsey, and P. M. Mayer (2009), N processing within geomorphic structures in urban streams.

Gu, C., W. Anderson, and F. Maggi (2012), Riparian biogeochemical hot moments induced by stream fluctuations, *Water Resources Research*, *48*(9).

Gu, C., G. M. Hornberger, A. L. Mills, J. S. Herman, and S. A. Flewelling (2007), Nitrate reduction in streambed sediments: Effects of flow and biogeochemical kinetics, *Water Resources Research*, *43*(12).

Harbaugh, A. W. (2005), *MODFLOW-2005, the US Geological Survey modular ground-water model: The ground-water flow process*, US Geological Survey Reston, Virginia.

Harvey, J. W., and B. Wagner (2000), Quantifying hydrologic interactions between streams and their subsurface hyporheic zones, *Streams and Ground Waters*, *344*.

Hedin, L. O., J. C. von Fischer, N. E. Ostrom, B. P. Kennedy, M. G. Brown, and G. P. Robertson (1998), Thermodynamic Constraints on Nitrogen Transformations and Other Biogeochemical Processes at Soil-Stream Interfaces, *Ecology*, *79*(2), 684-703.

Hester, E. T., and M. W. Doyle (2008), In-stream geomorphic structures as drivers of hyporheic exchange, *Water Resources Research*, *44*(3).

Hester, E. T., and M. N. Gooseff (2010), Moving beyond the banks: Hyporheic restoration is fundamental to restoring ecological services and functions of streams, *Environmental Science & Technology*, *44*(5), 1521-1525.

Hester, E. T., K. I. Young, and M. A. Widdowson (2013), Mixing of Surface and Groundwater Induced by Riverbed Dunes: Implications for Hyporheic Zone Definitions and Pollutant Reactions, *Water Resources Research*.

Hill, A. R., and D. J. Lymburner (1998), Hyporheic zone chemistry and stream-subsurface exchange in two groundwater-fed streams, *Canadian Journal of Fisheries and Aquatic Sciences*, *55*(2), 495-506.

Hoehn, E., M. Plumlee, and M. Reinhard (2007), Natural attenuation potential of downwelling streams for perfluorochemicals and other emerging contaminants, *Water Science & Technology*, *56*(11), 59-64.

Howarth, R. W., E. W. Boyer, W. J. Pabich, and J. N. Galloway (2002), Nitrogen use in the United States from 1961-2000 and potential future trends, *AMBIO: A Journal of the Human Environment*, *31*(2), 88-96.

Howden, N. J., T. P. Burt, F. Worrall, S. Mathias, and M. J. Whelan (2011), Nitrate pollution in intensively farmed regions: What are the prospects for sustaining high-quality groundwater?, *Water Resources Research*, *47*(6).

Hunter, K. S., Y. Wang, and P. Van Cappellen (1998), Kinetic modeling of microbially-driven redox chemistry of subsurface environments: coupling transport, microbial metabolism and geochemistry, *Journal of Hydrology*, *209*(1), 53-80.

Kennedy, C. D., D. P. Genereux, D. R. Corbett, and H. Mitasova (2009a), Spatial and temporal dynamics of coupled groundwater and nitrogen fluxes through a streambed in an agricultural watershed, *Water Resources Research*, *45*(9).

Kennedy, C. D., D. P. Genereux, D. R. Corbett, and H. Mitasova (2009b), Relationships among groundwater age, denitrification, and the coupled groundwater and nitrogen fluxes through a streambed, *Water Resources Research*, *45*(9), W09402.

Kessler, A. J., R. N. Glud, M. Bayani Cardenas, M. Larsen, M. F. Bourke, and P. L. Cook (2012), Quantifying denitrification in rippled permeable sands through combined flume experiments and modeling, *Limnology and Oceanography*, *57*(4), 1217.

Kim, H., H. F. Hemond, L. R. Krumholz, and B. A. Cohen (1995), In-Situ Biodegradation of Toluene in a Contaminated Stream. Part 1. Field Studies, *Environmental Science & Technology*, *29*(1), 108-116.

Krause, S., L. Heathwaite, A. Binley, and P. Keenan (2009), Nitrate concentration changes at the groundwater-surface water interface of a small Cumbrian river, *Hydrological Processes*, *23*(15), 2195-2211.

Krause, S., C. Tecklenburg, M. Munz, and E. Naden (2013), Streambed nitrogen cycling beyond the hyporheic zone: Flow controls on horizontal patterns and depth distribution of nitrate and dissolved oxygen in the upwelling groundwater of a lowland river, *Journal of Geophysical Research: Biogeosciences*.

Landmeyer, J. E., P. M. Bradley, D. A. Trego, K. G. Hale, and J. E. Haas (2010), MTBE, TBA, and TAME attenuation in diverse hyporheic zones, *Ground Water*, *48*(1), 30-41.

Lautz, L. K., and D. I. Siegel (2006), Modeling surface and ground water mixing in the hyporheic zone using MODFLOW and MT3D, *Advances in Water Resources*, *29*(11), 1618-1633.

Lautz, L. K., D. I. Siegel, and R. L. Bauer (2006), Impact of debris dams on hyporheic interaction along a semi-arid stream, *Hydrological Processes*, *20*(1), 183-196.

Loheide, S. P., and J. D. Lundquist (2009), Snowmelt-induced diel fluxes through the hyporheic zone, *Water Resources Research*, *45*(7).

Maggi, F., C. Gu, W. Riley, G. Hornberger, R. Venterea, T. Xu, N. Spycher, C. Steefel, N. Miller, and C. Oldenburg (2008), A mechanistic treatment of the dominant soil nitrogen cycling processes: Model development, testing, and application, *Journal of Geophysical Research: Biogeosciences (2005–2012)*, *113*(G2).

Marzadri, A., D. Tonina, and A. Bellin (2011), A semianalytical three-dimensional process-based model for hyporheic nitrogen dynamics in gravel bed rivers, *Water Resources Research*, *47*(11).

Marzadri, A., D. Tonina, and A. Bellin (2012), Morphodynamic controls on redox conditions and on nitrogen dynamics within the hyporheic zone: Application to gravel bed rivers with alternate-bar morphology, *Journal of Geophysical Research: Biogeosciences (2005–2012)*, *117*(G3).

Moser, D. P., J. K. Fredrickson, D. R. Geist, E. V. Arntzen, A. D. Peacock, S.-M. W. Li, T. Spadoni, and J. P. McKinley (2003), Biogeochemical processes and microbial characteristics across groundwater-surface water boundaries of the Hanford Reach of the Columbia River, *Environmental Science & Technology*, *37*(22), 5127-5134.

Peterson, R. E., and V. Johnson (1992), Riverbank seepage of groundwater along the Hanford Reach of the Columbia River, Washington*Rep.*, WHC-EP-0609.

Peterson, R. E., and M. P. Connelly (2001), Zone of Interaction Between Hanford Site Groundwater and Adjacent Columbia River, *PNNL-13674, Richland, WA*.

Puckett, L. J., and W. B. Hughes (2005), Transport and fate of nitrate and pesticides, *Journal of Environmental Quality*, *34*(6), 2278-2292.

Robertson, W., and J. Cherry (1992), Hydrogeology of an unconfined sand aquifer and its effect on the behavior of nitrogen from a large-flux septic system, *Applied Hydrogeology*, 32-44.

Robertson, W., J. Cherry, and E. Sudicky (1991), Ground-water contamination from two small septic systems on sand aquifers, *Ground Water*, *29*(1), 82-92.

Sala, O. E., F. S. Chapin, J. J. Armesto, E. Berlow, J. Bloomfield, R. Dirzo, E. Huber-Sanwald, L. F. Huenneke, R. B. Jackson, and A. Kinzig (2000), Global biodiversity scenarios for the year 2100, *Science*, *287*(5459), 1770-1774.

Salehin, M., A. I. Packman, and M. Paradis (2004), Hyporheic exchange with heterogeneous streambeds: Laboratory experiments and modeling, *Water Resources Research*, *40*(11).

Savant, S. A., D. D. Reible, and L. J. Thibodeaux (1987), Convective transport within stable river sediments, *Water Resources Research*, *23*(9), 1763-1768.

Sawyer, A. H., and M. B. Cardenas (2009), Hyporheic flow and residence time distributions in heterogeneous cross-bedded sediment, *Water Resources Research*, *45*(8).

Sawyer, A. H., M. Bayani Cardenas, and J. Buttles (2011), Hyporheic exchange due to channel-spanning logs, *Water Resources Research*, *47*(8).

Schwartz, A. F. (2010), *Housing policy in the United States*, Routledge.

Schwarzenbach, R. P., P. M. Gschwend, and D. M. Imboden (1993), Environmental organic chemistry.

Spencer, R. G., K. D. Butler, and G. R. Aiken (2012), Dissolved organic carbon and chromophoric dissolved organic matter properties of rivers in the USA, *Journal of Geophysical Research: Biogeosciences (2005–2012)*, *117*(G3).

Stelzer, R. S., and L. A. Bartsch (2012), Nitrate removal in deep sediments of a nitrogen-rich river network: A test of a conceptual model, *Journal of Geophysical Research: Biogeosciences (2005–2012)*, *117*(G2).

Storey, R. G., K. W. Howard, and D. D. Williams (2003), Factors controlling riffle-scale hyporheic exchange flows and their seasonal changes in a gaining stream: A three-dimensional groundwater flow model, *Water Resources Research*, *39*(2), 1034.

Thibodeaux, L. J., and J. D. Boyle (1987), Bedform-generated convective transport in bottom sediment.

Tian, Y. Q., Q. Yu, A. D. Feig, C. Ye, and A. Blunden (2013), Effects of climate and land-surface processes on terrestrial dissolved organic carbon export to major US coastal rivers, *Ecological Engineering*, *54*, 192-201.

Toetz, D. (2006), Nitrate in ground and surface waters in the vicinity of a concentrated animal feeding operation, *Archiv für Hydrobiologie*, *166*(1), 67-77.

Tompson, A. F. B., R. Ababou, and L. W. Gelhar (1989), IMPLEMENTATION OF THE 3-DIMENSIONAL TURNING BANDS RANDOM FIELD GENERATOR, *Water Resources Research*, *25*(10), 2227-2243.

Triska, F. J., V. C. Kennedy, R. J. Avanzino, G. W. Zellweger, and K. E. Bencala (1989), Retention and transport of nutrients in a third-order stream in northwestern California: hyporheic processes, *Ecology*, 1893-1905.

United States Census Bureau. (1993), 1990 Census Of Housing: Detained Housing Characteristics., edited, Housing and Economic Statistics Divisions, Bureau of the Census Washington, D.C.

USGS (2009), Redox Conditions in Selected Principal Aquifers of the United States, edited, Denver Publishing Service Center, Denver, Colorado.

Vannote, R. L., G. W. Minshall, K. W. Cummins, J. R. Sedell, and C. E. Cushing (1980), The river continuum concept, *Canadian Journal of Fisheries and Aquatic Sciences*, *37*(1), 130-137.

Vitousek, P. M., J. D. Aber, R. W. Howarth, G. E. Likens, P. A. Matson, D. W. Schindler, W. H. Schlesinger, and D. G. Tilman (1997), Human alteration of the global nitrogen cycle: sources and consequences, *Ecological Applications*, *7*(3), 737-750.

Werth, C. J., O. A. Cirpka, and P. Grathwohl (2006), Enhanced mixing and reaction through flow focusing in heterogeneous porous media, *Water Resources Research*, *42*(12).

Widdowson, M. A., F. J. Molz, and L. D. Benefield (1988), A numerical transport model for oxygen-and nitrate-based respiration linked to substrate and nutrient availability in porous media, *Water Resources Research*, *24*(9), 1553-1565.

Widdowson, M. A., D. Waddill, J. Brauner, F. Chapelle, and P. Bradley (2002), SEAM3D–A Numerical Model for Three-Dimensional Solute Transport Coupled to Sequential Electron Acceptor-Based Biological Reaction in Groundwater, *Blacksburg, Va.: The VA Department of Civil and Environmental Engineering, Virginia Polytechnic Institute and State University*.

Wilcock, R. J., J. W. Nagels, G. B. McBride, K. J. Collier, B. T. Wilson, and B. A. Huser (1998), Characterisation of lowland streams using a single-station diurnal curve analysis model with continuous monitoring data for dissolved oxygen and temperature, *New Zealand Journal of Marine and Freshwater Research*, *32*(1), 67-79.

Williams, D. D., and R. R. Fulthorpe (2003), Using invertebrate and microbial communities to assess the condition of the hyporheic zone of a river subject to 80 years of contamination by chlorobenzenes, *Canadian Journal of Zoology*, *81*(5), 789-802.

Wondzell, S. M., and F. J. Swanson (1996), Seasonal and storm dynamics of the hyporheic zone of a 4th-order mountain stream. I: Hydrologic processes, *Journal of the North American Benthological Society*, 3-19.

Zarnetske, J. P., R. Haggerty, S. M. Wondzell, and M. A. Baker (2011a), Dynamics of nitrate production and removal as a function of residence time in the hyporheic zone, *Journal of Geophysical Research: Biogeosciences (2005–2012)*, *116*(G1).

Zarnetske, J. P., R. Haggerty, S. M. Wondzell, and M. A. Baker (2011b), Labile dissolved organic carbon supply limits hyporheic denitrification, *Journal of Geophysical Research: Biogeosciences (2005–2012)*, *116*(G4).

Zarnetske, J. P., R. Haggerty, S. M. Wondzell, V. A. Bokil, and R. González-Pinzón (2012), Coupled transport and reaction kinetics control the nitrate source-sink function of hyporheic zones, *Water Resources Research*, *48*(11).

Zheng, C., and P. P. Wang (1999), MT3DMS: A modular three-dimensional multispecies transport model for simulation of advection, dispersion, and chemical reactions of contaminants in groundwater systems; documentation and user's guide*Rep.*, DTIC Document.

Zheng, C., and G. Bennett (2002), *Applied Contaminant Transport Modeling*, 2nd ed., Wiley Interscience, New York.

3 Engineering Applications

3.1 Applications to Increase Contaminant Reactions in the Hyporheic Zone

For mixing dependent denitrification, it is necessary to have enough time for aerobic respiration to deplete surface water (SW) dissolved oxygen (DO) and consume nitrate (NO_3^-). Depending on parameters such as hydraulic conductivity (K) and actual reaction rates, dunes may or may not create sufficient residence times. Residence time will scale with dune size which scales with river size, so dunes in large rivers such as the Columbia River which can have dunes 10m long [*Peterson and Johnson,* 1992; *Geist et al.*, 1994; *Moser et al.*, 2003], may have more potential for mixing dependent reactions. Hyporheic flow cells can also be induced by submerged bars, riffles and debris dams [*Thibodeaux and Boyle*, 1987; *Gooseff et al.*, 2006; *Hester and Doyle*, 2008; *Sawyer et al.*, 2011], all of which will frequently have longer flow paths than the dunes we modeled. Stream and river restoration efforts that create such bedforms could increase both non-mixing dependent reactions such as denitrification (of SW contaminants in hyporheic flow cells) and mixing dependent reactions (of groundwater (GW) contaminants in mixing zones) by increasing flow path length and residence times. Stream, river, or watershed restoration can similarly promote natural and more sustainable creation of such bedforms, for example by riparian reforestation which can ultimately provide a source of large wood to the channel that enhances formation of bedforms such as debris dams [*Lautz et al.*, 2006; *Groffman et al.*, 2009].

Anaerobic conditions are necessary for reactions such as denitrification and Cr(VI) reduction which require DO from SW to be depleted. *Zarnetske et al.* [2011b] showed that injection of labile DOC (AcO^-) at the start of hyporheic flow paths, increased metabolic processing rates down gradient such that the injected DOC was utilized and removed rapidly. Utilization of labile dissolved organic carbon (DOC) stimulated additional aerobic respiration, and consequently increased anaerobic conditions which led to signification increases in denitrification rates. Such carbon injections as a remedial measure could help reduce NO_3^- levels by enabling mixing and non-mixing dependent denitrification. In this case as well, natural and ultimately more sustainable practices may be preferred. Riparian forest planting may help in this way as well, because it can contribute natural DOC and POC to the riverbed [*Vannote et al.*, 1980; *Hester and Gooseff*, 2010].

Ultimately, although mixing dependent reactions may often have less mass consumed than non-mixing dependent reactions, mixing dependent reactions can provide important functions that non-mixing dependent reactions cannot. By taking advantage of additional sources of carbon not present in GW, mixing dependent reactions may prove decisive in addressing lingering GW contamination which makes it past more active GW remediation technologies such as permeable reactive barriers or upgradient aquifer monitored natural attenuation before it exits to SW. As such, mixing dependent reactions may be the “last line of defense” before contaminants enter potentially ecologically sensitive SW.

3.2 Broader Engineering Significance

It is clear that the hyporheic zone has the potential for attenuation of contaminants from both from SW and GW; however it is not clear if the hyporheic zone alone is enough to mitigate contaminants even with stream and river restoration and other enhancing efforts. It is important to better understand the hyporheic zone so that we can learn how much it can improve water quality and how that varies with space and time. This will lead to more focused and more effective ways to enhance the attenuation potential of hyporheic zones. Nevertheless, such efforts must be complemented by measures to reduce the amount of contaminants making it to SW and GW in the first place. More work needs to be done to better promote existing and invent new water quality BMPs in areas such as agriculture, urban stormwater, and industrial wastewater so that harmful pollutants can be reduced and treated before making it to SW and GW. Ultimately, the reduction of use of harmful compounds by consumers and industry in the first place may be required. On its own the hyporheic zone does not have the capability to cleanse all human impacts on water quality, yet is likely a valuable part of an environmentally sustainable landscape of holistic watershed management where ecosystem services and processes complement more active human treatment processes to provide clean water for both humans and other organisms.

3.3 References

Geist, D. R., T. Poston, and D. D. Dauble (1994), Assessment of potential impacts of major groundwater contaminants to fall Chinook salmon (Oncorhynchus tshawytscha) in the Hanford Reach, Columbia River*Rep.*, Battelle Pacific Northwest Lab., Richland, WA (United States).

Gooseff, M. N., J. K. Anderson, S. M. Wondzell, J. LaNier, and R. Haggerty (2006), A modelling study of hyporheic exchange pattern and the sequence, size, and spacing of stream bedforms in mountain stream networks, Oregon, USA, *Hydrological Processes*, *20*(11), 2443-2457.

Groffman, P. M., A. M. Dorsey, and P. M. Mayer (2009), N processing within geomorphic structures in urban streams.

Hester, E. T., and M. W. Doyle (2008), In-stream geomorphic structures as drivers of hyporheic exchange, *Water Resources Research*, *44*(3).

Hester, E. T., and M. N. Gooseff (2010), Moving beyond the banks: Hyporheic restoration is fundamental to restoring ecological services and functions of streams, *Environmental Science & Technology*, *44*(5), 1521-1525.

Lautz, L. K., D. I. Siegel, and R. L. Bauer (2006), Impact of debris dams on hyporheic interaction along a semi-arid stream, *Hydrological Processes*, *20*(1), 183-196.

Moser, D. P., J. K. Fredrickson, D. R. Geist, E. V. Arntzen, A. D. Peacock, S.-M. W. Li, T. Spadoni, and J. P. McKinley (2003), Biogeochemical processes and microbial characteristics across groundwater-surface water boundaries of the Hanford Reach of the Columbia River, *Environmental Science & Technology*, *37*(22), 5127-5134.

Peterson, R. E., and V. Johnson (1992), Riverbank seepage of groundwater along the Hanford Reach of the Columbia River, Washington*Rep.*, WHC-EP-0609.

Sawyer, A. H., M. Bayani Cardenas, and J. Buttles (2011), Hyporheic exchange due to channel-spanning logs, *Water Resources Research*, *47*(8).

Thibodeaux, L. J., and J. D. Boyle (1987), Bedform-generated convective transport in bottom sediment.

Vannote, R. L., G. W. Minshall, K. W. Cummins, J. R. Sedell, and C. E. Cushing (1980), The river continuum concept, *Canadian Journal of Fisheries and Aquatic Sciences*, *37*(1), 130-137.

Zarnetske, J. P., R. Haggerty, S. M. Wondzell, and M. A. Baker (2011), Labile dissolved organic carbon supply limits hyporheic denitrification, *Journal of Geophysical Research: Biogeosciences (2005–2012)*, *116*(G4).

Appendix A: How to use GMS Files

A.1 Files

- Homogeneous Basecase Files
    - HomoBASE.gpr – GMS project file for the homogeneous basecase
    - HomoBASE_MODFLOW – Folder with MODFLOW files for homogeneous basecase
    - HomoBASE_SEAM3D – Folder with SEAM3D files for homogeneous basecase
- Heterogeneous Basecase Files
    - HeteroBASE.grp
    - HeteroBASE_MODFLOW
    - HeteroBASE_SEAM3D

The files listed above can be obtained from either Erich Hester (**ehester@vt.edu**, (540) 231-9758) or Katherine Young (**kyoung1989@gmail.com**, (585) 355-5959). The files will be sent in a zip file that can be opened with any free zip futility, including:

- IZArc downloadable at **http://www.izarc.org/download.html**
- WinZip downloadable at **http://www.winzip.com/downwz.htm**

A.2 Hydraulic Boundary Conditions

- Hydraulic boundary conditions are specified in the "Map Data" which is located in the "Project Explorer"
- The top boundary is a specified head boundary. 21 nodes along the top boundary have specified Head-Stage values, and GMS interpolates these values along the boundary. To change these values one would need to change the Head-Stage values in the appropriate location.
- The bottom boundary is a constant flow boundary. To change the upwelling flux, one needs to change the value of the constant flow boundary.
- The sides are no flow boundaries
- If one changes the head values along the top, or the upwelling GW flux, you must "map" the conceptual model (Map Data) to MODFLOW. To do this, right click "new coverage", click "Map to" then click "MODFLOW/MODPATH"

A.3 MODFLOW

- Hydraulic conductivity and anisotropy can be changed in the "MODFLOW" section which is nested under "grid"
- To change hydraulic conductivity, double click "HK" and enter the desired values. For homogeneous HK, click "Constant Grid" then enter the desired HK. For heterogeneous HK, one can copy and paste the heterogeneous HK field into the grid.
- Similarly, anisotropy can be changed by double clicking "HANI"

A.4 SEAM3D

- The biogeochemical boundary conditions are entered by first navigating to "MT3D" -> "Source/Sink Mixing Package". The SW conditions are entered in the rows of type "conhead" (SW boundary is specified as constant head) and the GW conditions are entered in the rows of type "well" (GW boundary is specified as wells).
- Dispersivity values are entered by navigating to "MT3D: -> "Dispersion Package"
- All Monod Kinetic inputs are entered by navigating to "MT3D": -> "Biodegradation Package"

Appendix B: Turning Bands

B.1 Files

- **tb.pdf** – User Guide for Turning Bands Codes
- **turn2d.f** – Code used for Turning Bands
- **turn1.dat and turn2.dat** – data files that must be accompanied with the code
- **Base Inputs.ftn95p** – project file for Turning Bands Code, I used this with Silverfrost FTN95 (Plato 4.5.0)
- **HeteroHKField.m** – MATLAB script I used to get the Turning Bands output file into a form useable for inputting into GMS

The files listed above can be obtained from either Erich Hester (**ehester@vt.edu**, (540) 231-9758) or Katherine Young (**kyoung1989@gmail.com**, (585) 355-5959). The files will be sent in a zip file that can be opened with any free zip utility, including:

- IZArc downloadable at **http://www.izarc.org/download.html**
- WinZip downloadable at **http://www.winzip.com/downwz.htm**

B.2 Steps to Edit Data Files

The data files (turn2d1.day and turn2d2.dat) contain important information for running the code, like the grid spacing, correlation length, mean hydraulic conductivity, etc. To use the Turning Bands Code, one would need to change some numbers in the data files to get appropriate results. Below is a list of what numbers I used in these data files for my model, and what some of them mean. For more information on what all of these numbers mean, one can look in the User Guide. The inputs in the turn2d1.dat file were much more important for me to change than the ones in the turn2d2.dat file. Grid spacing and correlation length are in cm, and the mean permeability is in cm^2. They do not need to be in these units, that is just what I used.

- turn2d1.dat
  - idate: 210467 *current date*
  - irun: 1 *identification number*
  - nx: 188 *# of grid points in the x direction (up and down for my model)*
  - ny: 250 *# of grid points in the y direction (across for my model)*
  - nz: 1 *# of grid points in the z direction*
  - dx: 0.40 *grid spacing in the x direction*
  - dy: 0.40 *grid spacing in the y direction*
  - *dz: 0*
  - xl1: 0.40 *correlation length in x direction*
  - xl2: 4.0 *correlation length in y direction*
  - xl3: 0
  - condg: 0.000001 *mean permeability*
  - sig: 1 *standard deviation*
- turn2d2.dat
  - nline: 800
  - delzet: 0.1
  - nztest: 3000
  - bigk: 50
  - dk: 0.2
  - nmount: 1
  - iu: 1004579
  - n1: 161

- cmin: -3
- cmax: 3
- ndelt: 24
- ks(1): 1
- ks(2): 1
- ks(3): 1
- ilog: 1
- nfile: "no file" *Name of output file for normal z (I didn't use this)*
- tfile: "test2" *Name of output file for log z (I used this output file)*

B.3 Steps to Run Code

- Turning bands is written in Fortran, so you need to be able to compile the program on your computer
- Download Silverfrost FTN95 (Plato 4.5.0)… you can use other programs to run the code, this just worked for me
- Have code, project file and two data files in the same folder
- In Plato click File -> Open Project/Solution
- Then navigate to the project file Base Inputs.ftn95p
- Then click Build -> Build
- Then Build -> Run
- After the run is complete, the heterogeneous K field will be in the file labeled "test2" located in the same folder with the project file, two data files and code

B.4 Steps to get Output in Useable Format for GMS using MATLAB

The files I have included use the turning bands code to make a heterogeneous hydraulic conductivity field for a matrix that is 250 cells across and 188 cells up and down. However, the turning band codes output this data as permeability [L^2], as a list of 47000 numbers that is in a 6715x7 matrix. The data is in order, it just needs to be reshaped and converted to hydraulic conductivity [L/T]. To do this, I used a MATLAB script. One will definitely have to change inputs in the MATLAB script depending on the size of the matrix used (see details below).

- Import "test2" file to MATLAB
- Open the script "HeteroHKField.m"
- Change the numbers in lines 2-20 to correspond with the size of the test2 matrix being used.
    - For a 250x188 matrix, the test2 data was in a matrix of 6715x7, with the last numbers in columns 3-7 being "NaN". The numbers I use in this m file go through the test2 matrix, skip the "NaN" entries, and put the data in the correct spot of a useable 188x250 matrix.
- The rest of the MATLAB script converts the test2 permeability data (now in an appropriate sized matrix) to hydraulic conductivities.
- If one opens **list5**, they can directly copy and paste this data into the HK field in GMS.

Appendix C: How to Calculate Biodegradation Rates and Errors

C.1 Calculation for Biodegradation Rate using OUT file from GMS

1. The .OUT file from SEAM3D gives cumulative mass budgets at the end of each time step for total flow through constant head boundaries (top of model), total flow through wells (bottom of model), total biodegradation and for total mass storage in and out of the model
    - *Cumulative mass storage out refers to mass accumulating in the model. This occurs only during early times when the model is not at steady state. Once the model is at steady state, cumulative mass storage out stops increasing. Cumulative mass storage in would refer to mass from storage that acts as a source for the model. This could happen if I made the entire grid have an initial concentration of DOC of 100 mg/L and had boundary conditions of only 50 mg/L. The grid would act as a source of DOC for early times, until the model reached steady state. Nevertheless, mass storage doesn't matter for this model because we only care about steady state.*
2. By using the last two time steps (when model is already at steady state) one can calculate the biodegradation rate
3. For example, if the model prints cumulative mass budgets at 1.4 and 1.5 days, one can calculate the biodegradation rate by subtracting the mass biodegraded at 1.4 days from the mass biodegraded at 1.5 days and then divide by 0.1 days

- $Mass_{Bio\_n}$ [mg] = cumulative mass biodegraded for each solute at end of n days
- Bio [mg/d] = $(Mass_{Bio\_X} - Mass_{Bio\_Y})/(X - Y)$ = biodegradation rate for each solute

C.2 Error of Calculation for Biodegradation Rate using OUT file from GMS

1. Similar to the biodegradation rate calculation, one can calculate the mass rate in and out using the cumulative mass budgets
2. The error (sum of numerical errors in the model) rate from the .OUT file can then be calculated by subtracting the mass rate out and biodegradation rate from the mass rate in
3. The percent error is then just the error rate divided by the mass rate in times 100

- $Mass_{TopIN\_n}$ [mg] = cumulative mass entering the model at end of n days along the top boundary
- $Mass_{Well\_n}$ [mg] = cumulative mass entering the model at end of n days along bottom
- $Mass_{TopOUT\_n}$ [mg] = cumulative mass exiting the model at end of n days along top boundary
- M_{IN} [mg/d] = $(Mass_{TopIN\_X} - Mass_{TopIN\_Y})/(X - Y) + (Mass_{Well\_X} - Mass_{Well\_Y})/(X - Y)$ = total mass rate into model
- M_{OUT} [mg/d] = $(Mass_{TopOUT\_X} - Mass_{TopOUT\_Y})/(X - Y)$ = total mass rate out of model
- E [mg/d] = $M_{IN} - M_{OUT}$ – Bio = error rate for each solute
- %E = $(E/M_{IN})(100)$

C.3 Example Calculations

```
>>>>>>>>>>>>>>>>>>>>>>>>>>>>>>>>>>>>>>>>>>>>>>>>>>>>>>>>FOR COMPONENT NO. 04<<<<<<<<<<<<<<<<<<<<<<<<<<<<<<<<<<<<<<<<<<<<<<<<<<<<<<<<<<

                                             -------------------------------------------
                                                       TRANSPORT STEP NO.10486
                                             -------------------------------------------

TOTAL ELAPSED TIME SINCE BEGINNING OF SIMULATION =    1.400000        d
.....................................................................

                    CUMMULATIVE MASS BUDGETS AT END OF TRANSPORT STEP10486, TIME STEP   10, STRESS PERIOD    1
                    ------------------------------------------------------------------------------------------

                                                                IN                           OUT
                                                          ----------------             ----------------
                              CONSTANT CONCENTRATION:     0.000000                      0.000000
                                       CONSTANT HEAD:     1.565010                     -1.518219
                                               WELLS:     0.000000                      0.000000
                             DECAY OR BIODEGRADATION:     0.000000                     -0.1851108E-01
                               MASS STORAGE (SOLUTE):    0.3560329E-05                 -0.2311349E-01
                           ---------------------------------------------------------------------------
                                             [TOTAL]:     1.565014        g            -1.559843        g

                                                                 NET (IN - OUT):   0.5170941E-02
                                                          DISCREPANCY (PERCENT):   0.3309528
```

Figure C-1: Cumulative mass balance for carbon at 1.4 days

```
>>>>>>>>>>>>>>>>>>>>>>>>>>>>>>>>>>>>>>>>>>>>>>>>>>>>>>>>FOR COMPONENT NO. 04<<<<<<<<<<<<<<<<<<<<<<<<<<<<<<<<<<<<<<<<<<<<<<<<<<<<<<<<<<

                                             -------------------------------------------
                                                       TRANSPORT STEP NO.31458
                                             -------------------------------------------

TOTAL ELAPSED TIME SINCE BEGINNING OF SIMULATION =    1.500000        d
.....................................................................

                    CUMMULATIVE MASS BUDGETS AT END OF TRANSPORT STEP31458, TIME STEP   10, STRESS PERIOD    1
                    ------------------------------------------------------------------------------------------

                                                                IN                           OUT
                                                          ----------------             ----------------
                              CONSTANT CONCENTRATION:     0.000000                      0.000000
                                       CONSTANT HEAD:     1.677510                     -1.628218
                                               WELLS:     0.000000                      0.000000
                             DECAY OR BIODEGRADATION:     0.000000                     -0.1987826E-01
                               MASS STORAGE (SOLUTE):    0.3789844E-05                 -0.2311349E-01
                           ---------------------------------------------------------------------------
                                             [TOTAL]:     1.677514        g            -1.671210        g

                                                                 NET (IN - OUT):   0.6303906E-02
                                                          DISCREPANCY (PERCENT):   0.3764946
```

Figure C-2: Cumulative mass balance for carbon at 1.5 days

- M_{IN} [g/d] = total mass rate into model
- M_{IN} [g/d] = $(Mass_{TopIN\_X} – Mass_{TopIN\_Y})/(X – Y) + (Mass_{Well\_X} – Mass_{Well\_Y})/(X – Y)$
- M_{IN} = (1.677510 g – 1.565010 g)/(1.5 d – 1.4 d) + (0 g – 0 g)/(1.5 d – 1.4 d) = M_{IN} =1.125 g/d

- M_{OUT} [g/d] = total mass rate out of model
- M_{OUT} [g/d] = $(Mass_{TopOUT\_X} – Mass_{TopOUT\_Y})/(X – Y)$
- M_{OUT} = (1.628218 g – 1.518219 g)/(1.5 d – 1.4 d) = M_{OUT} = 1.100 g/d

- Bio [g/d] = biodegradation rate for each solute
- Bio [g/d] = $(Mass_{Bio\_X} – Mass_{Bio\_Y})/(X – Y)$
- Bio = (0.01987826 g – 0.01851108 g)/(1.5 d – 1.4 d) = Bio = 0.0136718 g/d

- E [g/d] = $M_{IN} – M_{OUT}$ – Bio = error rate for each solute
- E = 1.125 – 1.100 – 0.0134 = 0.012 g/d

- %E = $(E/M_{IN})(100)$ = (0.012/1.125)(100) = %E = 1.1

Appendix D: Additional (Complete) Data Not Included In Journal Article

D.1 Biogeochemical Boundary Conditions

- We chose 3 basecases with different biogeochemical boundary conditions for the sensitivity analysis (Figure 2). The basecases are identical except for NO3 in SW and DO in GW.

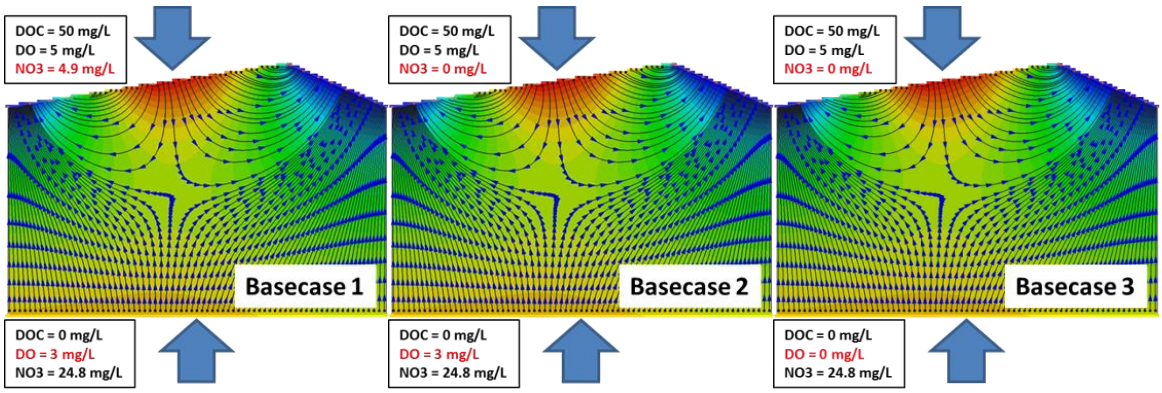

Figure D-1: Boundary conditions for basecase 1, 2 and 3

<u>Basecase 1 and 2 represent GW that is derived from watersheds affected by agriculture</u>

- GW DOC = 0 mg/L (vary from 0 to 50 mg/L)
  - *Chapelle et al.* [2012] presented a plot of DO versus DOC for 1552 wells sampled in 17 NAWQA study areas located throughout the US. The majority of these wells had GW DOC concentrations below 4 mg/L
  - *Puckett and Hughes* [2005] found GW DOC concentrations in a shallow aquifer near a dairy farm to be 0.25-0.99 mg/L (as CH_2O) at a depth of 3.1 meters below a creek
  - Chose basecase GW DOC concentration equal to 0 because of above references and we want to focus on mixing dependent reactions (higher DOC would increase non-mixing dependent denitrification)
  - Varied GW DOC up to 50 mg/L because the plot from *Chapelle et al.* [2012] does show GW DOC concentrations reaching 50 mg/L
- GW DO = 3 mg/L (vary from 0 to 8 mg/L)
  - GW DO concentrations vary a lot throughout the US [*USGS*, 2009; *Chapelle et al.*, 2012]
  - *Krause et al.* [2013] found a DO concentration of 3.79 mg/L in GW near a lowland river in a watershed affected by agriculture; *Puckett and Hughes* [2005] found GW DO of 4.1-6.9 mg/L 3.1 m below a creek in a shallow aquifer near a dairy farm; *Cey et al.* [1999] found GW DO concentrations ranging from 1-8 mg/L in a shallow aquifer 1-2 meters below the water table in a small agricultural watershed; and *Kennedy et al.* [2009b] found a mean streambed GW DO concentration of 0.64 mg/L (mean of 422 samples, range 0-7 mg/L) in an watershed affected by agriculture in NC.
  - An intermediate GW DO concentration was chosen for oxic aquifers because [*Dubrovsky et al.*, 2010] found that the redox status of an aquifer is a critical factor in its nitrate vulnerability. If aquifers are anoxic, there typically is almost no NO3 in the aquifer. Since we are interested in plumes containing NO3 contamination, we focus on oxic aquifers for this basecase.
  - We chose 3 mg/L as the basecase GW DO because it is an intermediate GW DO concentration for oxic aquifers and we chose a range of 0-8 mg/L.
- GW NO3 = 24.8 mg/L (vary from 0 to 70.9 mg/L)
  - *Gu et al.* [2007] found an average GW NO3 of 39.6 mg/L in 77 GW samples taken from monitoring wells at a field site near Oyster, VA; *Krause et al.* [2013] found GW NO3 of 25.9 mg/L near a lowland river in a watershed affected by agriculture; *Puckett and*

Hughes [2005] found NO3 concentrations of 12.5-20.8 mg/L at a depth of 3.1 m below a creek in a shallow aquifer near a dairy farm; *Cey et al.* [1999] found GW NO3 concentrations of 50 mg/L in a shallow aquifer 1-2 meters below the water table in a small agricultural watershed; *Kennedy et al.* [2009b] found an average GW NO3 concentration of 27 (422 samples, range 0.4-110) in a watershed affected by agriculture in NC

- 24.8 mg/L is the median GW NO3 concentration in the US in areas affected by agriculture with oxic GW aquifers (USGS Nutrients in SW and GW Report) so we used this as the basecase GW NO3
- 70.9 mg/L is the upper bound from the USGS Nutrients in SW and GW Report, so we use this for the upper range

<u>Basecase 3 represents GW that is contaminated by septic systems</u>

- GW DOC = 0 mg/L (vary from 0 to 50 mg/L)
  - *DeSimone and Howes* [1998] found GW DOC of 4.75 mg/L in a GW contaminant plume (contaminated by septic system discharge) in Cape Cod; *Robertson et al.* [1991] found GW DOC of 8.5 mg/L (as $CH2_2O$) in a GW contaminant plume from a single family home septic system
  - We chose 0 mg/L as the basecase because we want to focus on mixing dependent reactions (higher DOC would increase non-mixing dependent denitrification). Additionally, although the values found above are not consistent with zero, they are low compared to average SW DOC concentrations.
- GW DO = 0 mg/L (vary from 0 to 8 mg/L)
  - Septic system contaminant plumes typically have depleted DO [*Robertson et al.*, 1991; *DeSimone and Howes*, 1998]
- GW NO3 = 24.8 mg/L (vary from 0 to 70.9 mg/L)
  - Used the same GW NO3 concentration of 24.8 mg/L for basecase 2 because it falls within the range of NO3 concentrations found within wastewater plumes [*Barbaro*, 2013]

<u>Basecase 1 SW boundary conditions</u>

- SW DOC = 50 mg/L (vary from 0 to 50 mg/L)
  - Chose 50 mg/L as basecase so that DOC was not a limiting factor in reactions. This has been done in other papers [*Bardini et al.*, 2012].
  - The majority of US rivers have a mean SW DOC concentration (as CH_2O) ranging from 5 to 25 mg/L (Spencer et al., 2012)
  - Although 50 is above the average in the US, we address lower SW DOC's in the sensitivity analysis and 50 is within the observed levels we have seen [*Puckett and Hughes*, 2005; *Boano et al.*, 2010; *Bardini et al.*, 2012; *Tian et al.*, 2013]
- SW DO = 5 mg/L (vary from 0 to 10 mg/L)
  - We found SW DO concentrations ranging from 1.2 to 7.7 in streams and rivers affected by agriculture [*Wilcock et al.*, 1998; *Boano et al.*, 2010; *Corsi et al.*, 2011; *Krause et al.*, 2013]
  - Chose 5 mg/L as the basecase and varied from 0-10 mg/L because 10 mg/L is near saturation
- SW NO3 = 4.9 mg/L (vary from 0 to 47.8 mg/L)
  - The USGS Nutrient Report states that the median NO3 concentrations in streams affected by agriculture is 12.0 mg/L. 4.9 mg/L is the 25^{th} percentile of streams affected by agriculture. We chose this as the basecase so that we could focus on mixing dependent denitrification (higher NO3 would increase non-mixing dependent denitrification).
  - We varied SW NO3 from 0 to 47.8 mg/L because 47.8 mg/L is the USGS Nutrient Report's upper bound for NO3 in streams affected by agriculture

<u>Basecase 2 and 3 SW boundary conditions</u>

- SW DOC = 50 mg/L (vary from 0 to 50)
- SW DO = 5 mg/L (vary from 0 to 10)
- SW NO3 = 0 mg/L (vary from 0 to 47.8 mg/L)
    - We want the basecase SW NO3 to be 0 to so that we could focus on mixing dependent denitrification (higher NO3 would increase non-mixing dependent denitrification)
    - The addition of SW NO3 in the sensitivity analysis did not change result trends (in any cases)

D.2 Results for Coarse Grid Analysis

This section provides a complete set of all results from the coarse grid analysis. Section D.2.1, D.2.2 and D.2.3 contain data for basecase 1, 2 and 3 respectively. For each parameter varied, concentration maps for the conservative tracers and solutes are provided. The tracer concentration maps are plots of the tracer concentration over the model domain at steady state with the same boundary concentration as the solute they represent. Additionally, for each parameter varied in both sections, there are figures for the amount of each solute consumed, and the original bulleted text interpreting the results remains. Section D.2.4 contains a comparison of the three basecases. This section has plots for each parameter varied comparing the amount consumed for each basecases. This section also has the original bulleted text interpreting the results.

D.2.1 Basecase 1

D.2.1.1 Vary GW DOC and GW DO Simultaneously

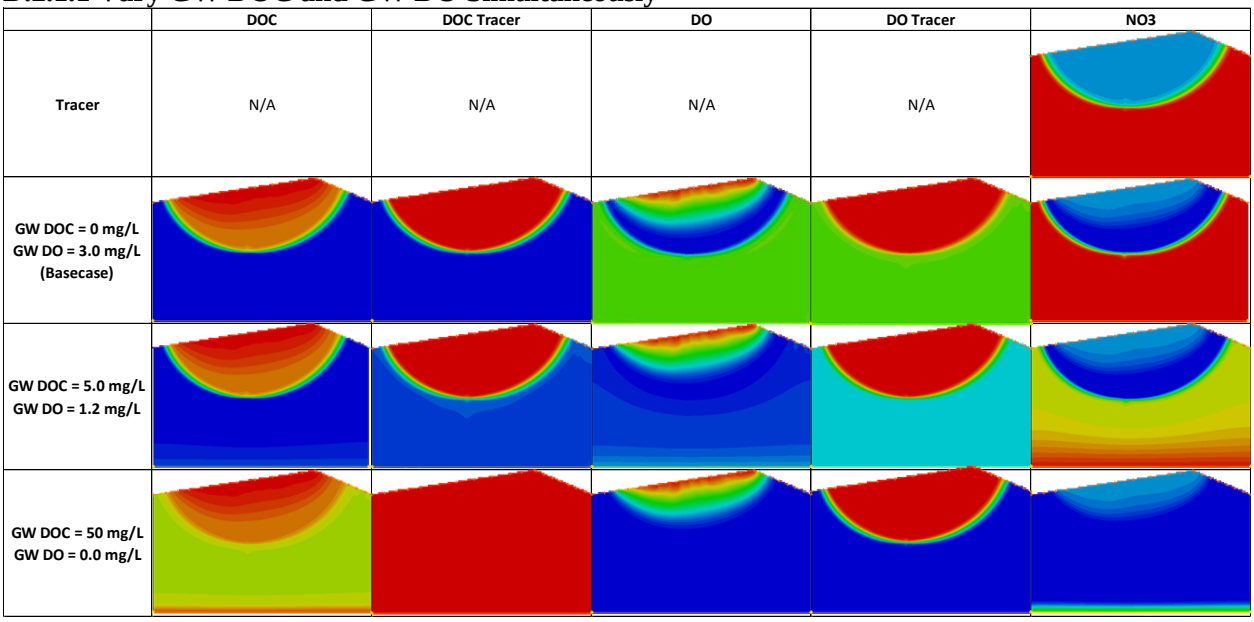

Figure D-2: DOC, DO, NO3 and tracer concentrations for varying GW DOC and GW DO simultaneously for the coarse grid for basecase 1.

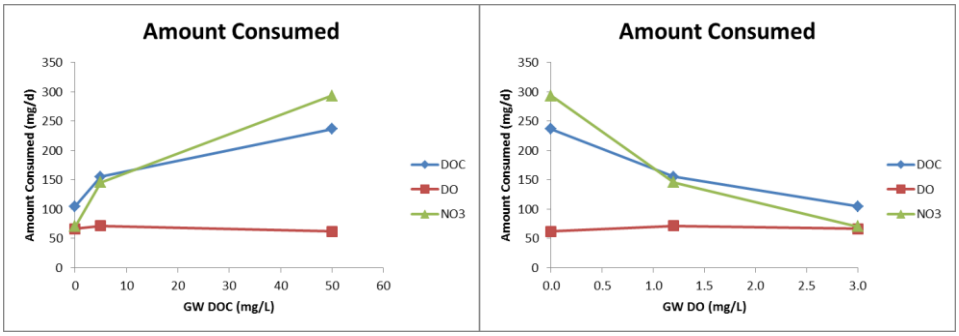

Figure D-3: Amount of each solute consumed for varying GW DOC and GW DO simultaneously for the coarse grid for basecase 1.

- GW DO and DOC are varied simultaneously such that as GW DO increases, GW DOC decreases
- The basecase has about 20% of nitrate consumed via denitrification. This occurs in both the mixing dependent and non-mixing dependent fashion. As GW DOC increases and GW DO decreases much more denitrification occurs. This is due to non-mixing dependent denitrification because the NO3 and DOC move together.
- As GW DOC increases and GW DO decreases, the consumption of DO via aerobic respiration remains about the same
- As GW DOC increases and GW DO decreases, the consumption of DOC increases. The increase in DOC consumption is mainly due to non-mixing dependent denitrification.

D.2.1.2 Vary SW DO

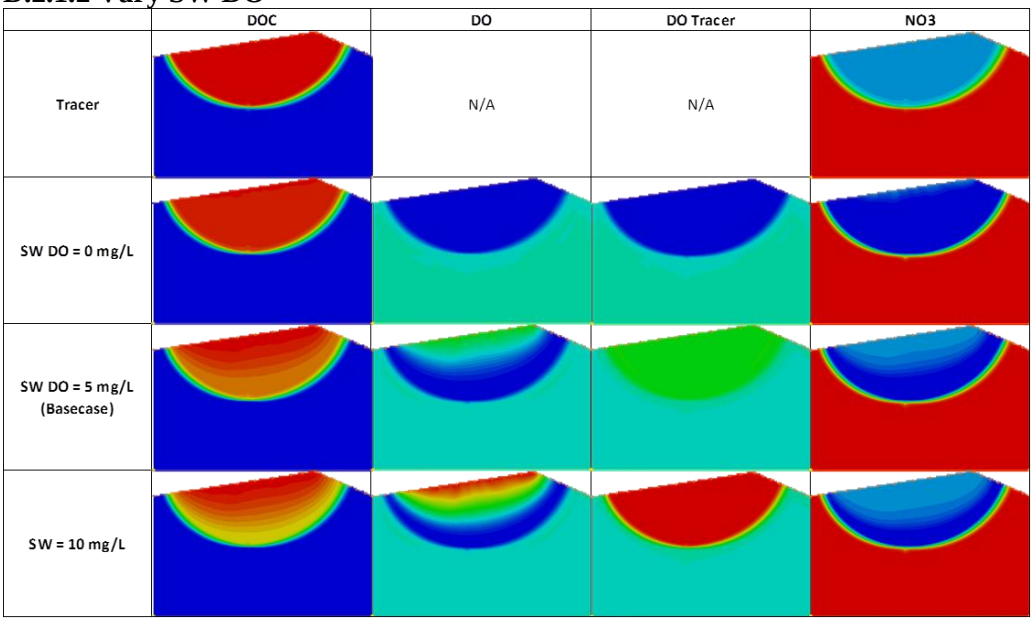

Figure D-4: DOC, DO, NO3 and tracer concentrations for varying SW DO for the coarse grid for basecase 1.

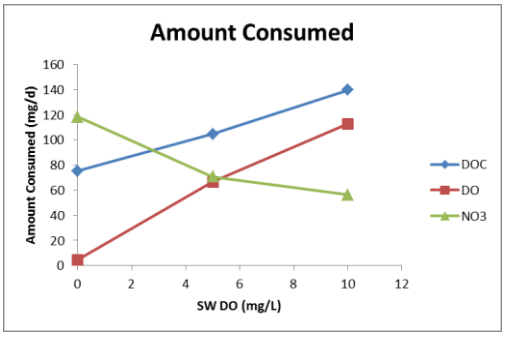

Figure D-5: Amount of each solute consumed for varying SW DO for the coarse grid for basecase 1.

- As SW DO increases, consumption of DO via non mixing dependent aerobic respiration increases
- As SW DO increases, consumption of DOC increases. The increase in DOC consumption is due to an increase in non-mixing dependent aerobic respiration
- As SW DO increase, consumption of NO3 decreases. DO inhibits denitrification and therefore higher DO concentrations will prevent more denitrification from occurring.

D.2.1.3 Vary SW DOC

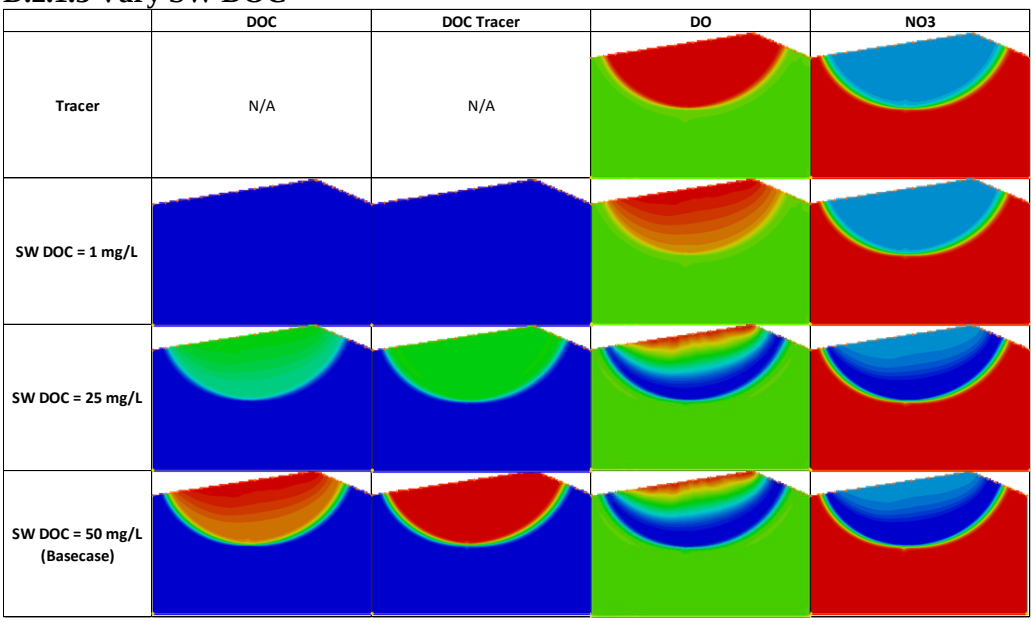

Figure D-6: DOC, DO, NO3 and tracer concentrations for varying SW DOC for the coarse grid for basecase 1.

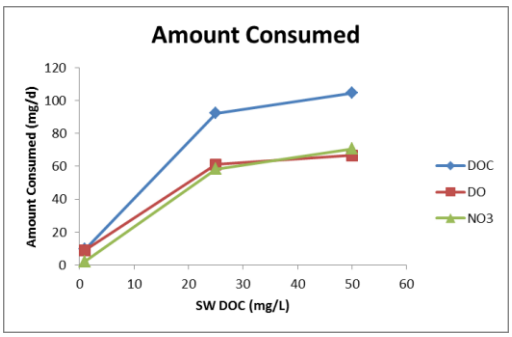

Figure D-7: Amount of each solute consumed for varying SW DOC for the coarse grid for basecase 1.

- As SW DOC increases, consumption of DOC, DO and NO3 increase

D.2.1.4 Vary GW NO_3^-

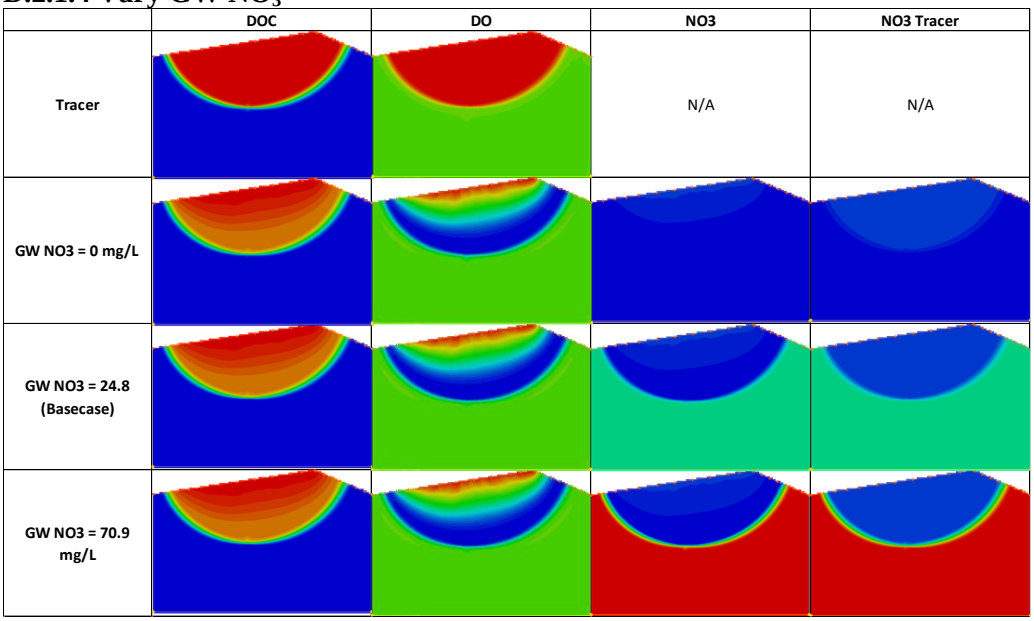

Figure D-8: DOC, DO, NO3 and tracer concentrations for varying GW NO_3^- for the coarse grid for basecase 1.

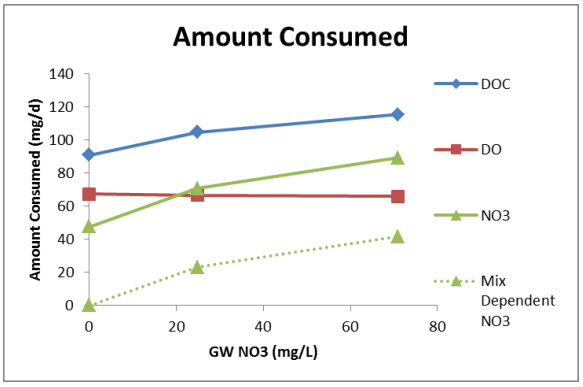

Figure D-9: Amount of each solute consumed for varying GW NO_3^- for the coarse grid for basecase 1.

- As GW NO3 increases, the amount of DO consumed stays constant
- As GW NO3 increases, the amount of NO3 consumed via mixing dependent denitrification increases
- As GW NO3 increases, the amount of DOC consumed increases. The increase in DOC consumption is due to an increase in mixing dependent denitrification

D.2.1.5 Vary SW NO_3^-

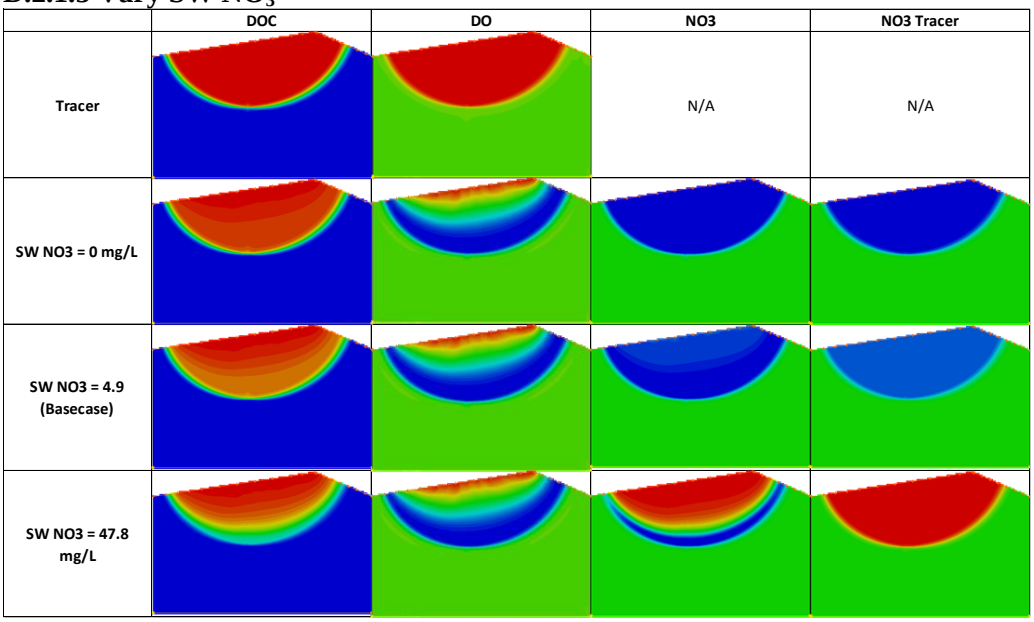

Figure D-10: DOC, DO, NO3 and tracer concentrations for varying SW NO_3^- for the coarse grid for basecase 1.

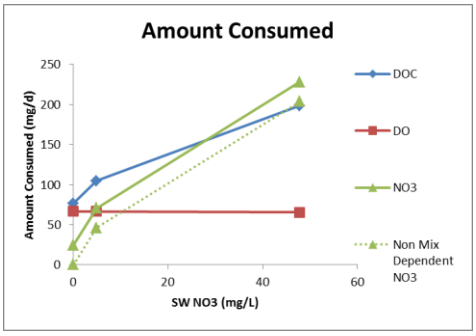

Figure D-11: Amount of each solute consumed for varying SW NO_3^- for the coarse grid for basecase 1.

- As SW NO3 increases, DO consumption via aerobic respiration remains about the same
- As SW NO3 increase, NO3 consumption via non-mixing dependent denitrification increases
- As SW NO3 increases, DOC consumption increases. The increase in DOC consumption is due to an increase in non-mixing dependent denitrification

D.2.1.6 Vary Hydraulic Conductivity

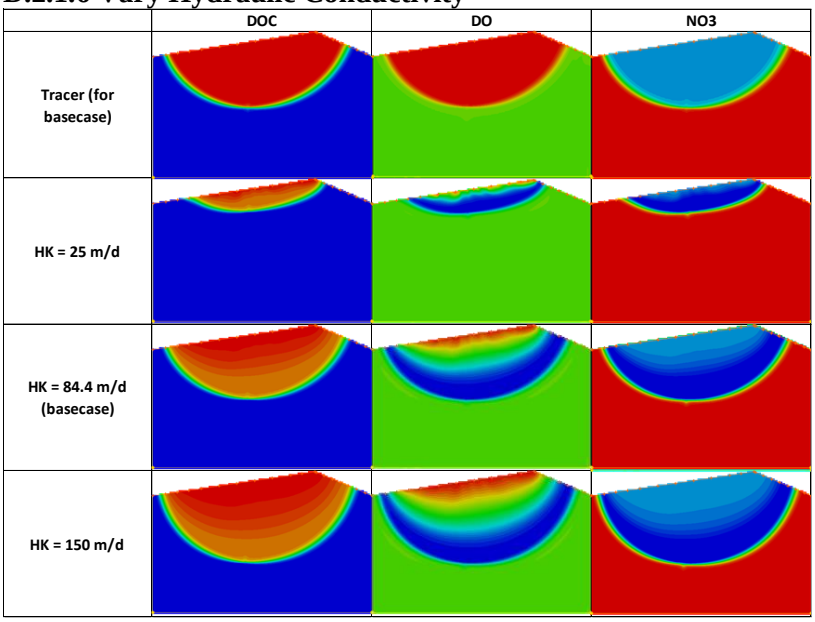

Figure D-12: DOC, DO, NO3 and tracer concentrations for varying hydraulic conductivity for the coarse grid for basecase 1.

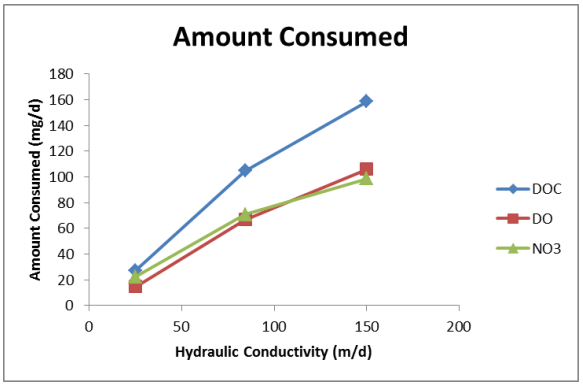

Figure D-13: Amount of each solute consumed for varying hydraulic conductivity for the coarse grid for basecase 1.

- As K increases, consumption of DOC, DO and NO3 increase. When K is higher, more solutes are able to enter the model and this is likely the reason why more biodegradation occurs with higher K's.

D.2.2 Basecase 2

D.2.2.1 Vary GW DOC and GW DO Simultaneously

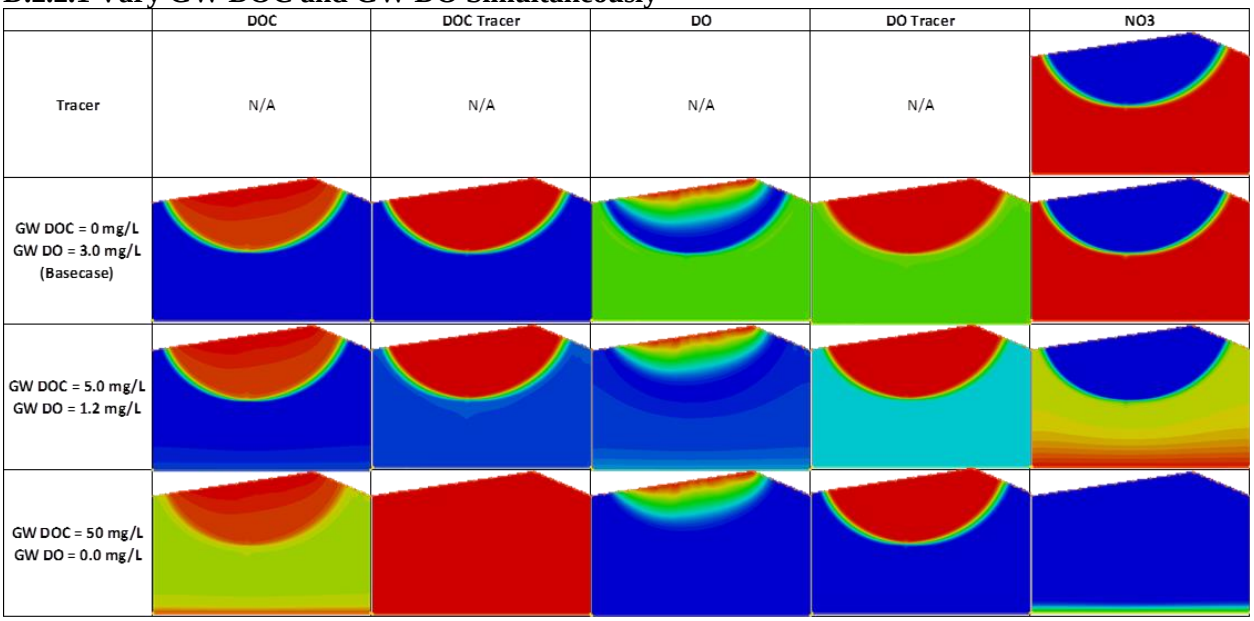

Figure D-14: DOC, DO, NO3 and tracer concentrations for varying GW DOC and GW DO simultaneously for the coarse grid for basecase 2.

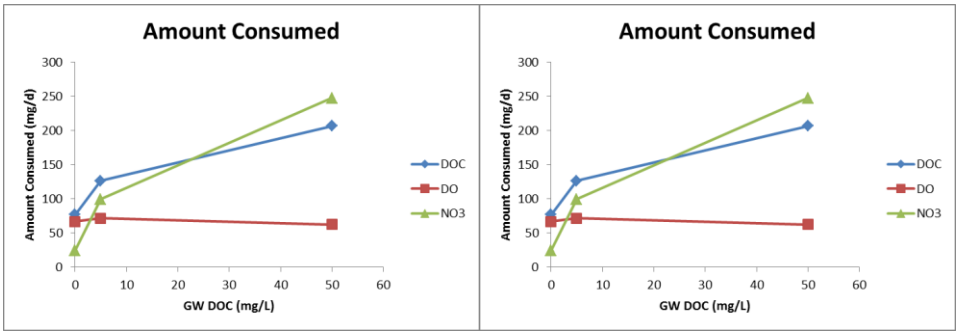

Figure D-15: Amount of each solute consumed for varying GW DOC and GW DO simultaneously for the coarse grid for basecase 2.

- GW DO and DOC are varied simultaneously such that as GW DO increases, GW DOC decreases
- The basecase has about 10% of nitrate consumed via denitrification. This occurs only in the mixing dependent fashion because the nitrate and DOC come from different source waters. As GW DOC increases and GW DO decreases NO3 consumption increases via non-mixing dependent denitrification.
- As GW DOC increases and GW DO decreases consumption of DO via aerobic respiration remains about the same
- As GW DOC increases and GW DO decreases, the consumption of DOC increases. The increase in DOC consumption is mainly due to non-mixing dependent denitrification.

D.2.2.2 Vary SW DO

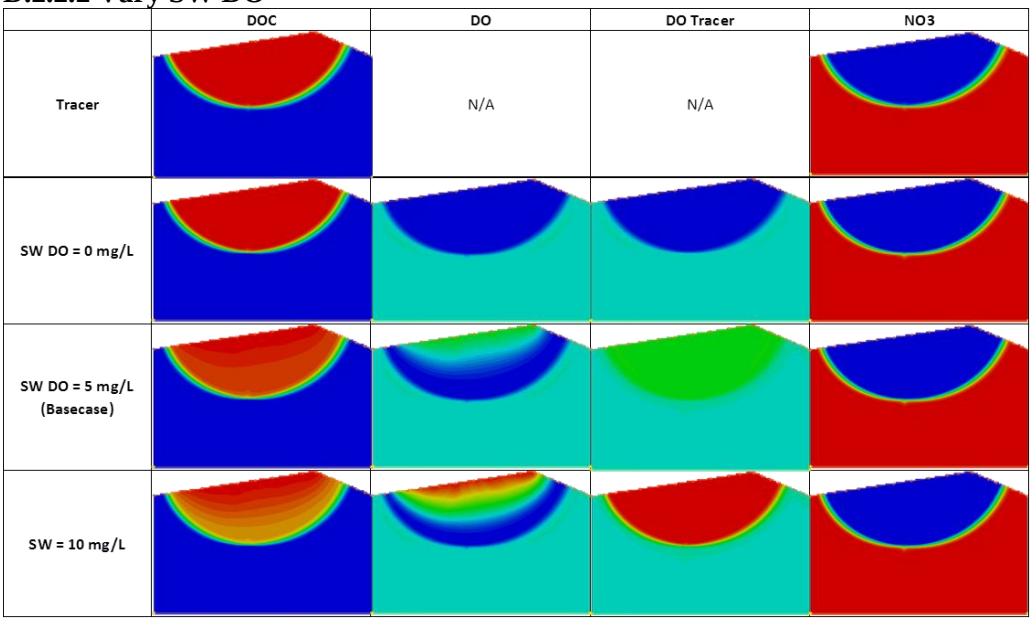

Figure D-16: DOC, DO, NO3 and tracer concentrations for varying SW DO for the coarse grid for basecase 2.

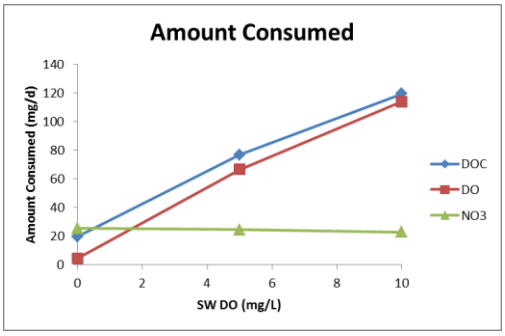

Figure D-17: Amount of each solute consumed for varying SW DO for the coarse grid for basecase 2.

- As SW DO increases, consumption of DO via non mixing dependent aerobic respiration increases
- As SW DO increases, consumption of DOC increases. The increase in DOC consumption is due to an increase in non-mixing dependent aerobic respiration
- As SW DO increases, consumption of NO3 via mixing dependent denitrification decreases slightly. The slight decrease in NO3 consumption could be from decreased DOC availability and/or inhibition from oxygen.

D.2.2.3 Vary SW DOC

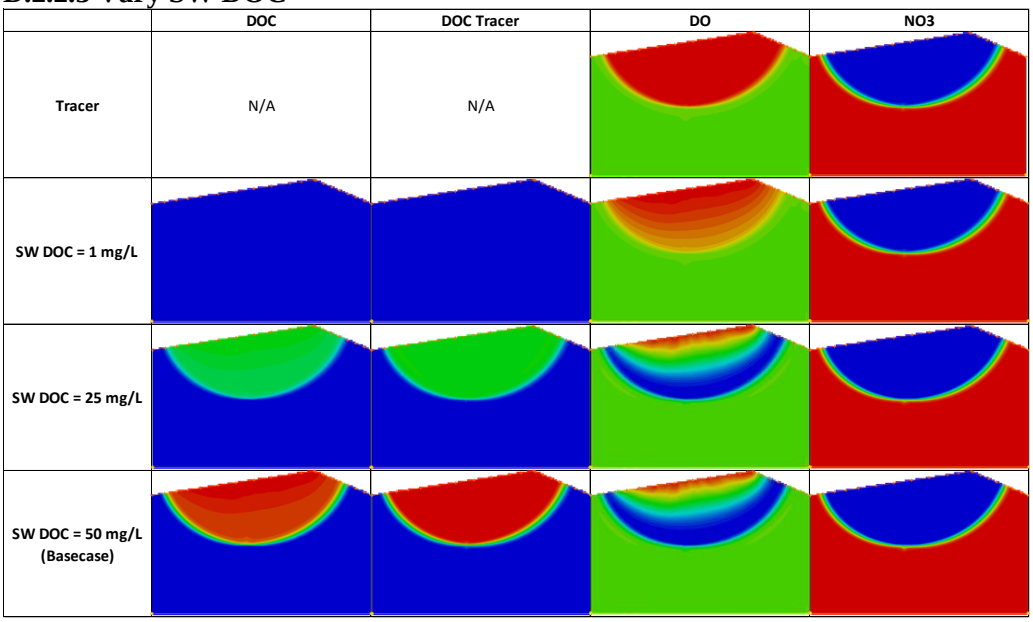

Figure D-18: DOC, DO, NO3 and tracer concentrations for varying SW DOC for the coarse grid for basecase 2.

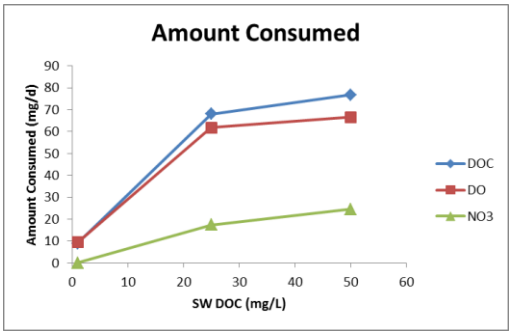

Figure D-19: Amount of each solute consumed for varying SW DOC for the coarse grid for basecase 2.

- As SW DOC increases, consumption of DOC, DO and NO3 increase

D.2.2.4 Vary GW NO_3^-

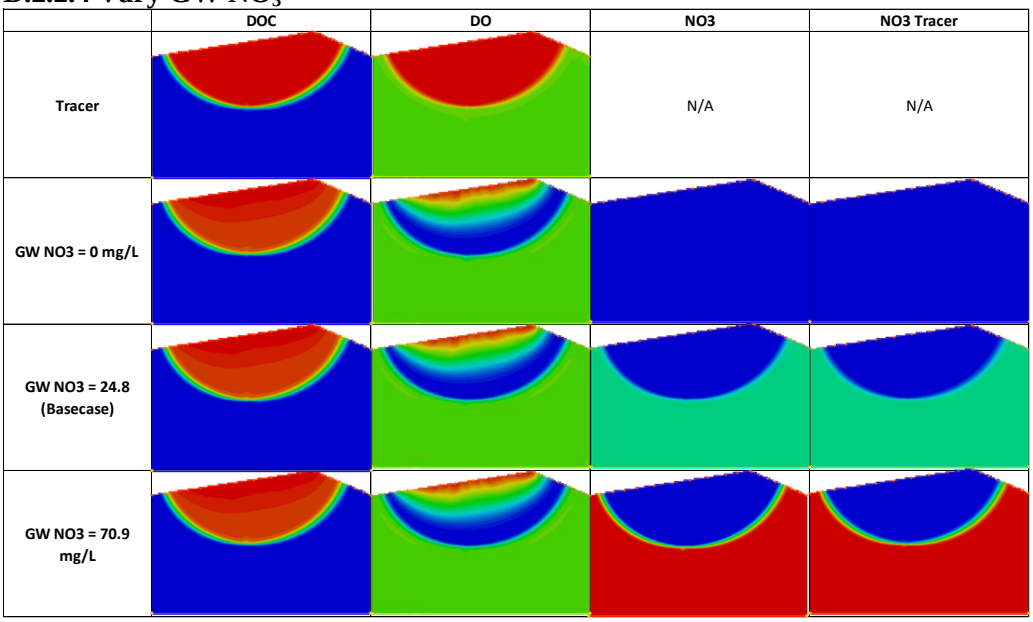

Figure D-20: DOC, DO, NO3 and tracer concentrations for varying GW NO_3^- for the coarse grid for basecase 2.

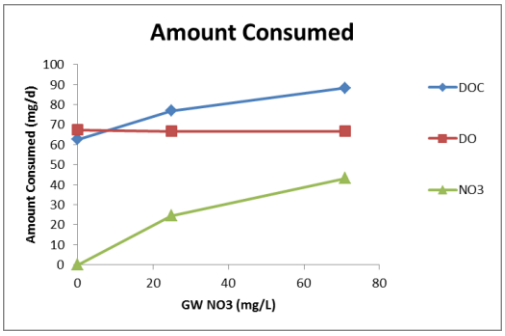

Figure D-21: Amount of each solute consumed for varying GW NO_3^- for the coarse grid for basecase 2.

- As GW NO3 increases, the amount of DO consumed stays constant
- As GW NO3 increases, the amount of NO3 consumed via mixing dependent denitrification increases
- As GW NO3 increases, the amount of DOC consumed increases. The increases in DOC consumption is due to an increase mixing dependent denitrification

D.2.2.5 Vary SW NO_3^-

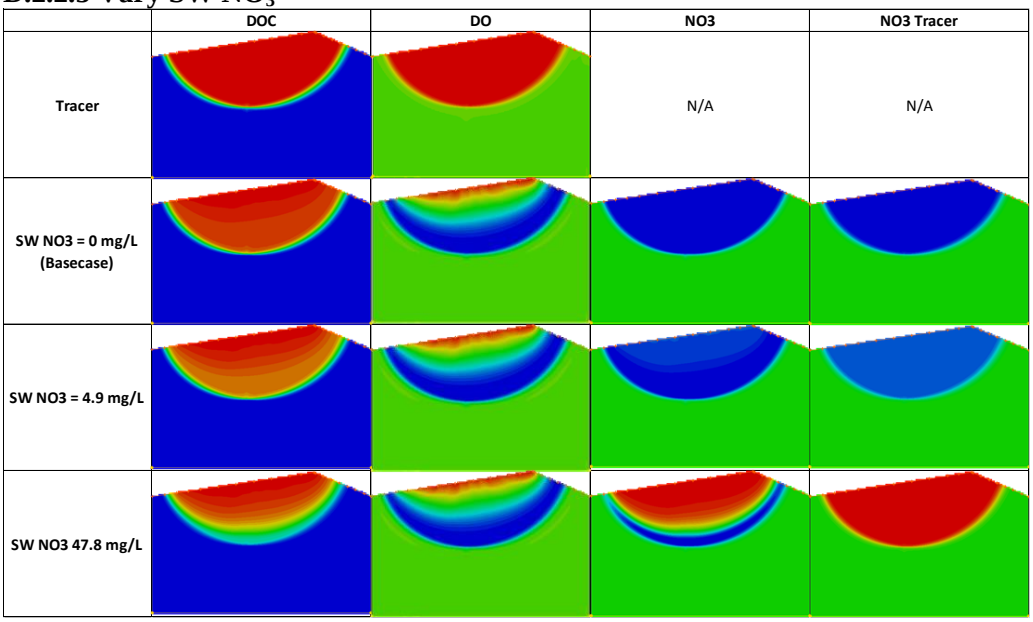

Figure D-22: DOC, DO, NO3 and tracer concentrations for varying SW NO_3^- for the coarse grid for basecase 2.

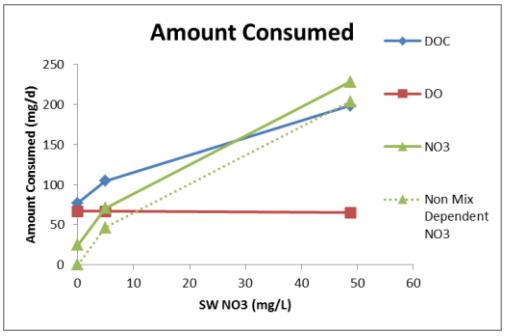

Figure D-23: Amount of each solute consumed for varying SW NO_3^- for the coarse grid for basecase 2.

- As SW NO3 increases, DO consumption via aerobic respiration remains about the same
- As SW NO3 increases, NO3 consumption via non-mixing dependent denitrification increases
- As SW NO3 increases DOC consumption increases. The increase in DOC consumption is due to an increase in non-mixing dependent denitrification

D.2.2.6 Vary Hydraulic Conductivity

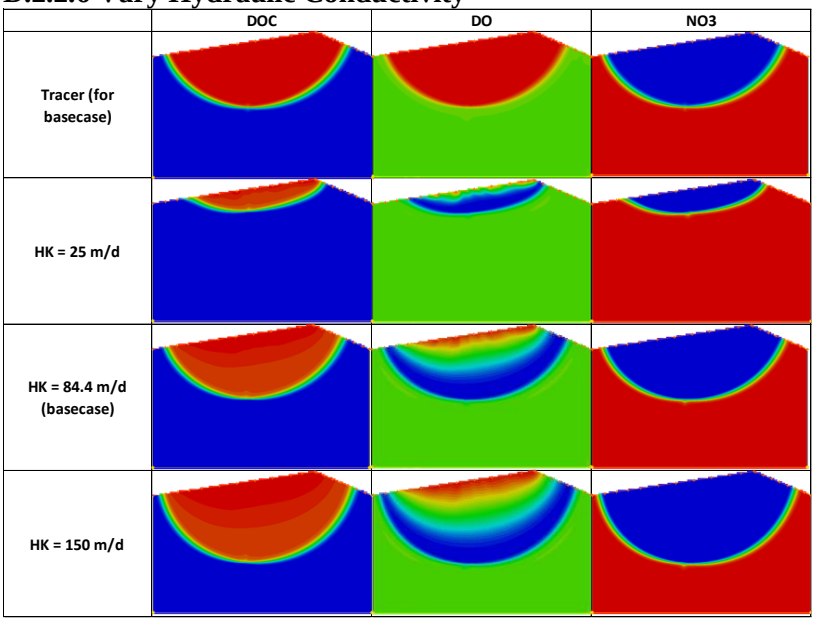

Figure D-24: DOC, DO, NO3 and tracer concentrations for varying hydraulic conductivity for the coarse grid for basecase 2.

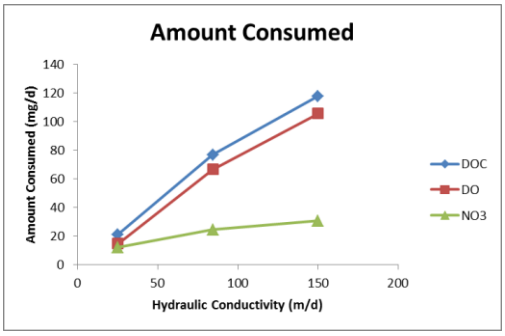

Figure D-25: Amount of each solute consumed for varying hydraulic conductivity for the coarse grid for basecase 2.

D.2.3 Basecase 3

D.2.3.1 Vary GW DOC and GW DO Simultaneously

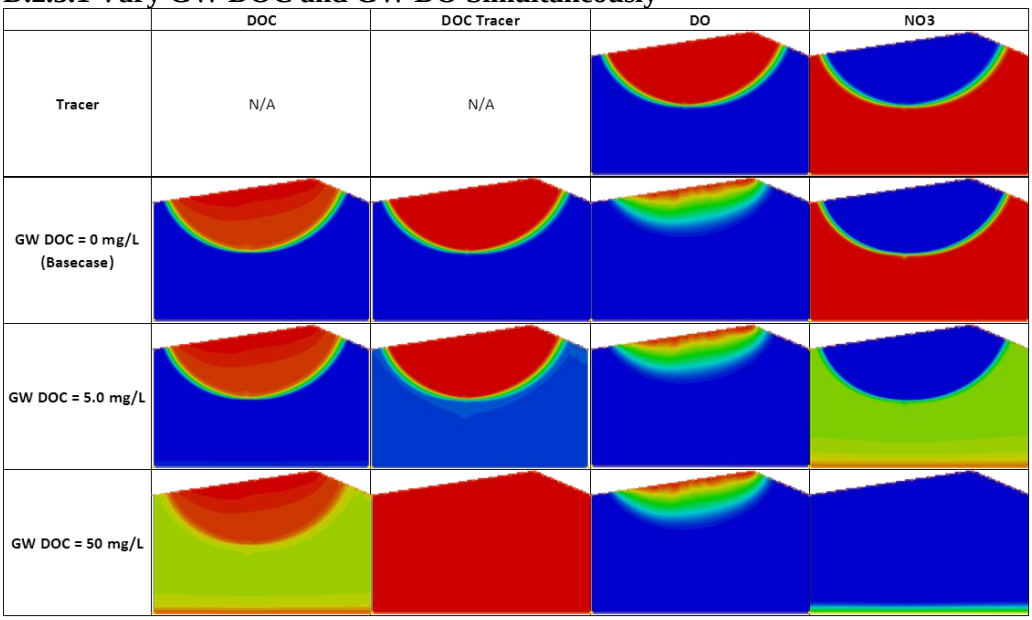

Figure D-26: DOC, DO, NO3 and tracer concentrations for varying GW DOC and GW DO simultaneously for the coarse grid for basecase 3.

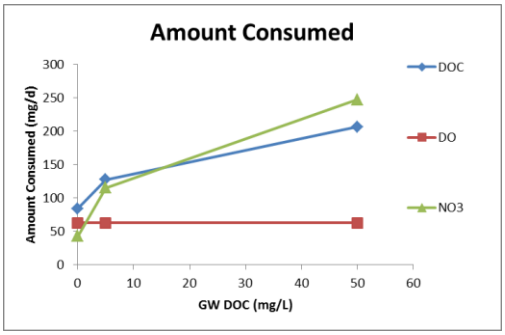

Figure D-27: Amount of each solute consumed for varying GW DOC and GW DO simultaneously for the coarse grid for basecase 3.

- The basecase has about 17% of nitrate consumed via denitrification. This occurs in the mixing dependent fashion because nitrate and DOC come from different source waters. As GW DOC increases, NO3 consumption increases via non-mixing dependent denitrification
- As GW DOC increases, consumption of DO via aerobic respiration remains about the same
- As GW DOC increases, consumption of DOC increases. The increase in DOC consumption is due to an increase in non-mixing dependent denitrification.

D.2.3.2 Vary SW DO

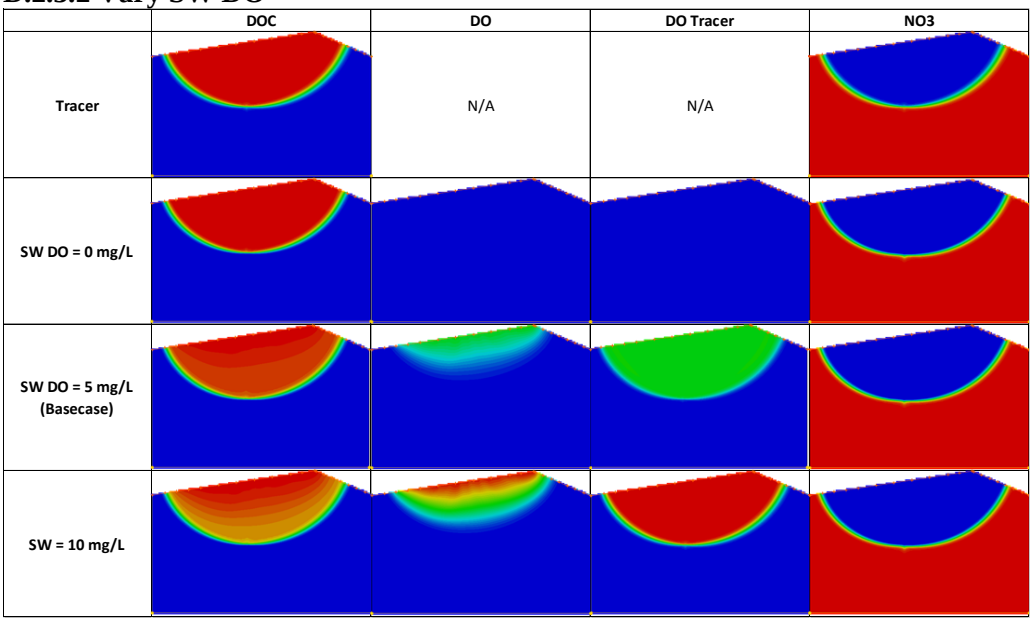

Figure D-28: DOC, DO, NO3 and tracer concentrations for varying SW DO for the coarse grid for basecase 3.

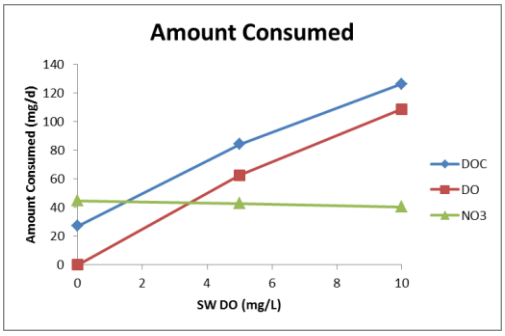

Figure D-29: Amount of each solute consumed for varying SW DO for the coarse grid for basecase 3.

- As SW DO increases, consumption of DO via non mixing dependent aerobic respiration increases
- As SW DO increases, consumption of DOC increases. The increase in DOC consumption is due to an increase in non-mixing dependent aerobic respiration
- As SW DO increases, consumption of NO3 via mixing dependent denitrification decreases slightly. The decrease in NO3 consumption could be from decreased DOC availability and/or inhibition from oxygen.

D.2.3.3 Vary SW DOC

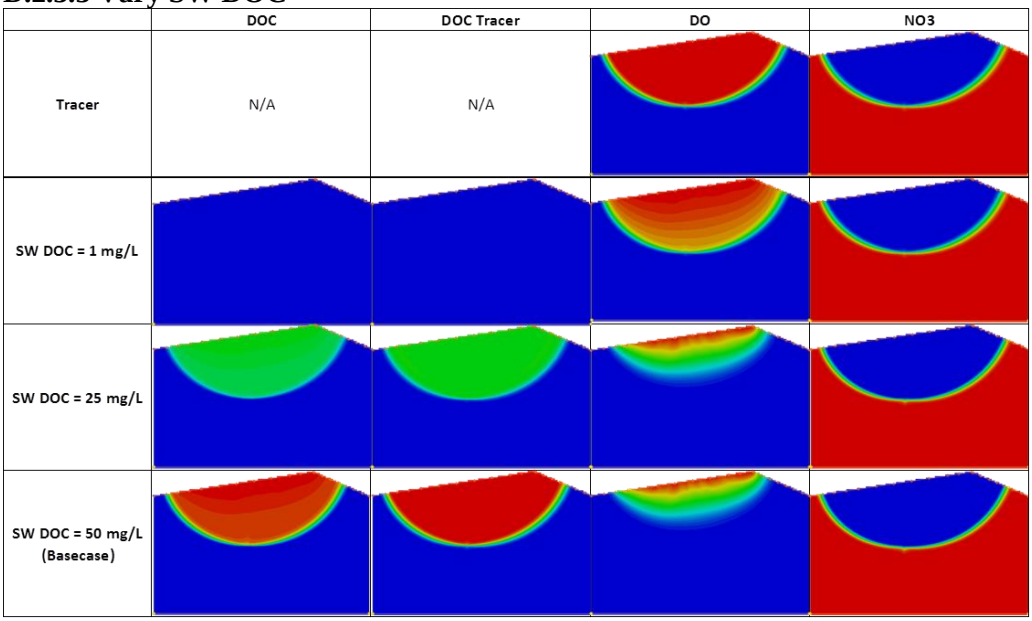

Figure D-30: DOC, DO, NO3 and tracer concentrations for varying SW DOC for the coarse grid for basecase 3.

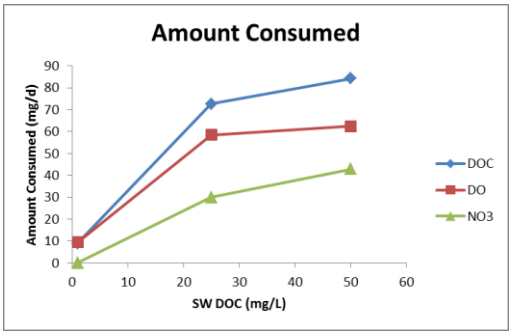

Figure D-31: Amount of each solute consumed for varying SW DOC for the coarse grid for basecase 3.

- As SW DOC increases, consumption of DOC, DO and NO3 increase

D.2.3.4 Vary GW NO_3^-

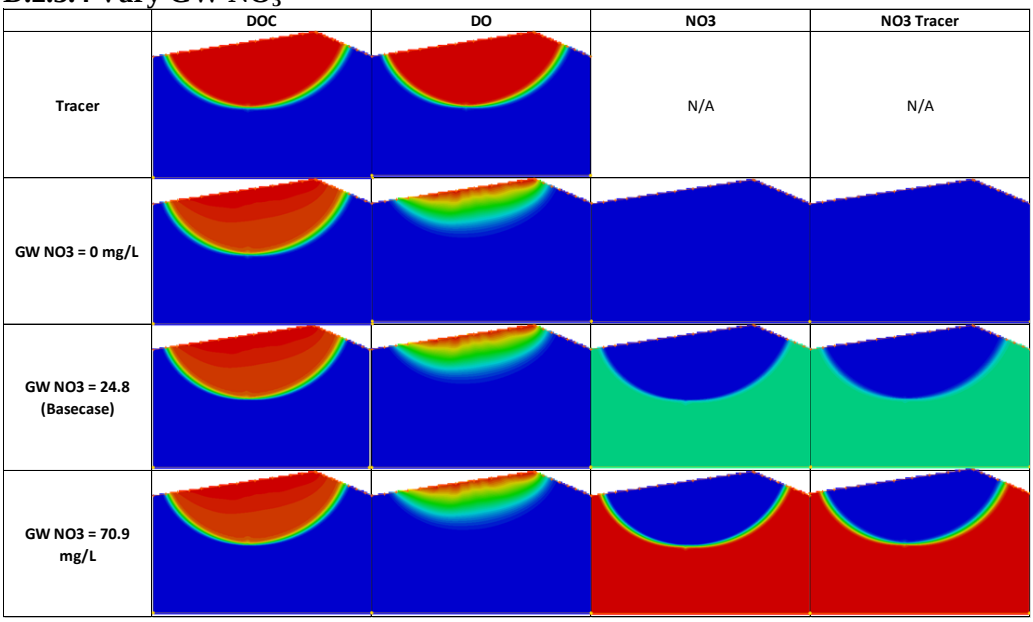

Figure D-32: DOC, DO, NO3 and tracer concentrations for varying GW NO_3^- for the coarse grid for basecase 3.

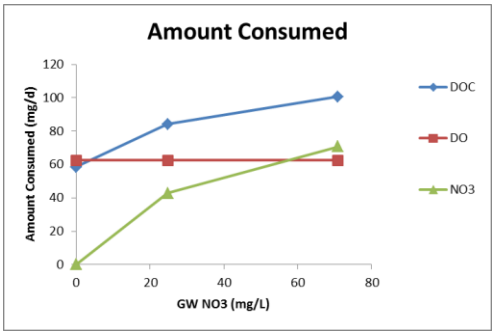

Figure D-33: Amount of each solute consumed for varying GW NO_3^- for the coarse grid for basecase 3.

- As GW NO3 increases, the amount of DO consumed stays constant
- As GW NO3 increases, the amount of NO3 consumed via mixing dependent denitrification increases
- As GW NO3 increases, the amount of DOC consumed increases. The increases in DOC consumption is due to an increase mixing dependent denitrification

D.2.3.5 Vary SW NO_3^-

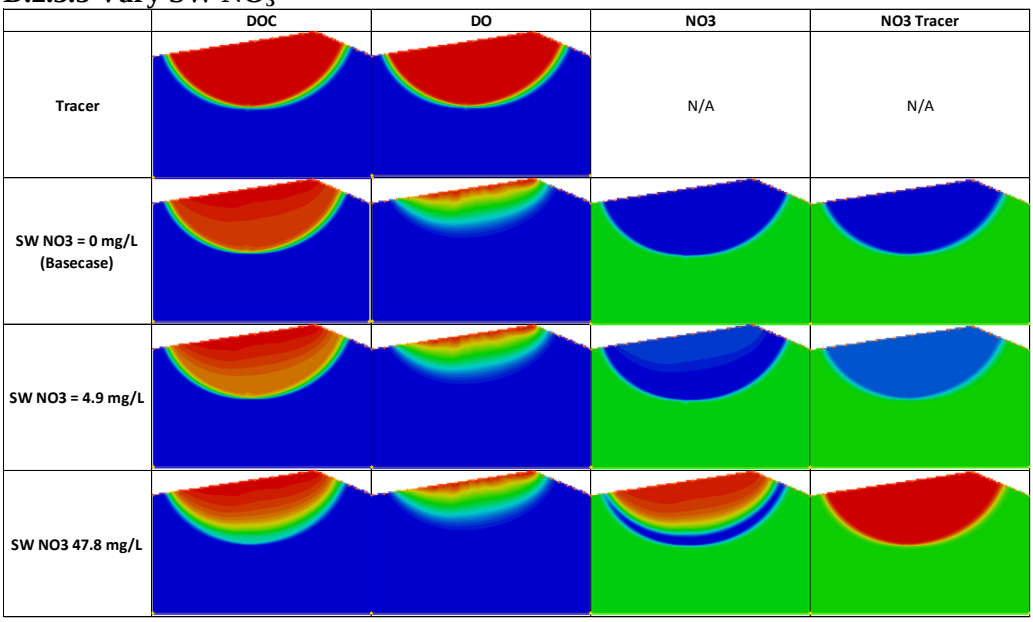

Figure D-34: DOC, DO, NO3 and tracer concentrations for varying SW NO_3^- for the coarse grid for basecase 3.

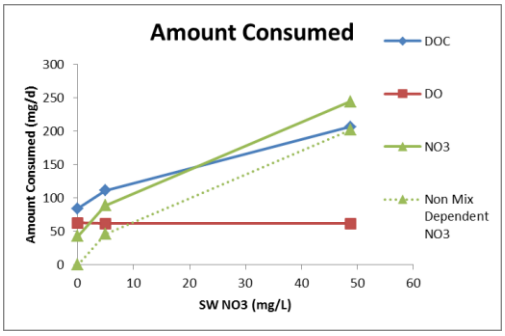

Figure D-35: Amount of each solute consumed for varying SW NO_3^- for the coarse grid for basecase 3.

- As SW NO3 increases, DO consumption via aerobic respiration remains about the same
- As SW NO3 increases, NO3 consumption via non-mixing dependent denitrification increases
- As SW NO3 increases, DOC consumption increases. The increase in DOC consumption is due to an increase in non-mixing dependent denitrification

D.2.3.6 Vary Hydraulic Conductivity

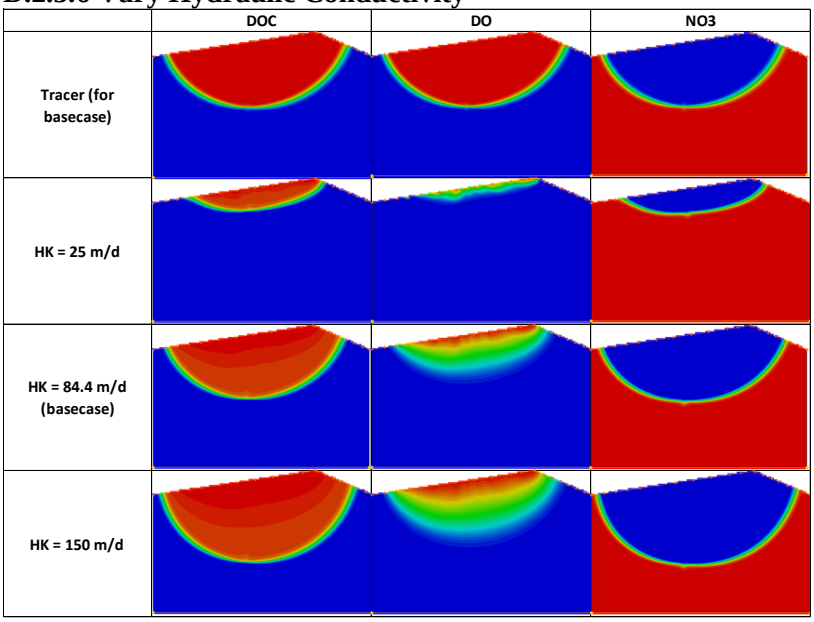

Figure D-36: DOC, DO, NO3 and tracer concentrations for varying hydraulic conductivity for the coarse grid for basecase 3.

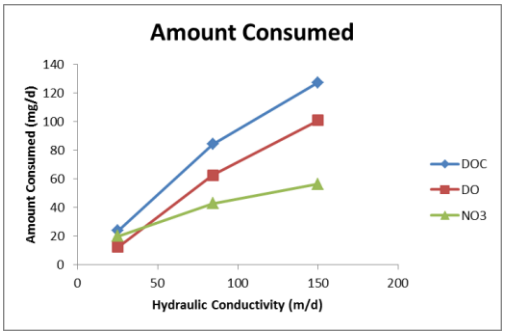

Figure D-37: Amount of each solute consumed for varying hydraulic conductivity for the coarse grid for basecase 3.

- As K increases, consumption of DOC, DO and NO3 increases. When K is higher, more solutes are able to enter the model and this is likely the reason why more biodegradation occurs with higher K's

D.2.4 Comparison of Basecases for Coarse Grid

D.2.4.1 Vary GW DOC and GW DO Simultaneously

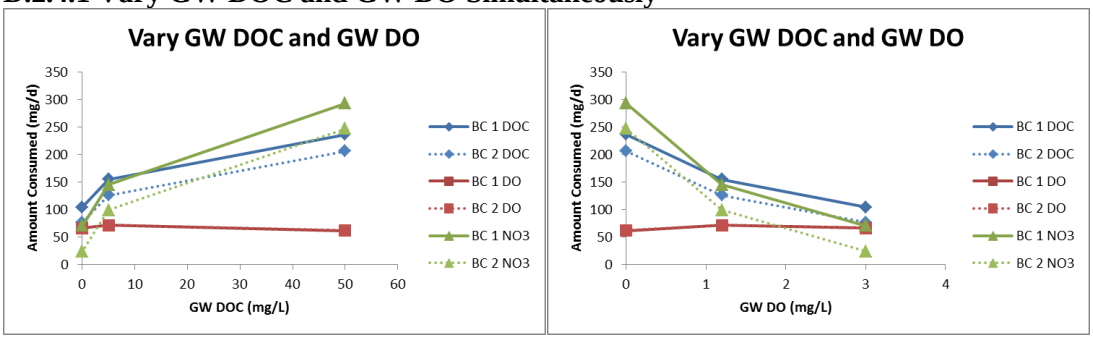

Figure D-38: Comparison of basecase 1, 2 and 3 for varying GW DOC and GW DO (simultaneously).

- GW DO and DOC are varied simultaneously such that as GW DO increases, GW DOC decreases
- BASECASE 1 has about 20% of NO3 consumed via denitrification. This occurs in both the mixing dependent and non-mixing dependent fashion.
- BASECASE 2 has about 10% of NO3 consumed via denitrification. This occurs in only the mixing dependent fashion because NO3 and DOC come from different source waters
- As GW DOC increases and GW DO decreases, for both BASECASE 1 and BASECASE 2, denitrification increases. This is due to non-mixing dependent denitrification because NO3 and DOC move together.
- As GW DOC increases and GW DO decreases, consumption of NO3 for BASECASE 1 and BASECASE 2 follow the same trend, except that consumption of NO3 for BASECASE 1 is slightly higher than for BASECASE 2. The additional NO3 consumed in BASECASE 1 is from non-mixing dependent denitrification.
- For all GW DOC and GW DO scenarios, consumption of DO is the same for BASECASE 1 and BASECASE 2
- As GW DOC increases and GW DO decreases, consumption of DO for BASECASE 1 and BASECASE 2 stays about constant
- As GW DOC increases and GW DO decrease, the consumption of DOC increases for both BASECASE 1 and BASECASE 2. The increase in DOC consumption is mainly due to an increase in non-mixing dependent denitrification
- As GW DOC increases and GW DO decreases, consumption of DOC for BASECASE 1 and BASECASE 2 follow the same trend, except that consumption of DOC for BASECASE 1 is slightly higher than for BASECASE 2. The additional DOC consumed in BASECASE 1 is from non-mixing dependent denitrification.

D.2.4.2 Vary SW DO

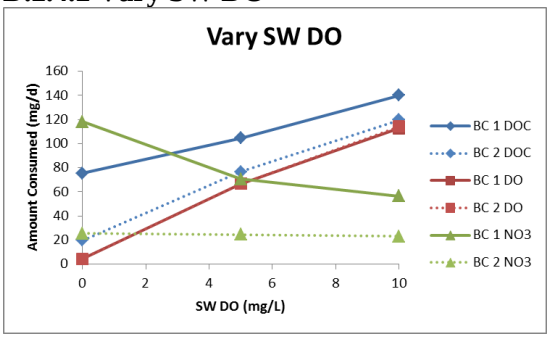

Figure D-39: Comparison of basecase 1 and 2 for varying SW DO.

- For all SW DO scenarios, consumption of DO is the same for BASECASE 1 and BASECASE 2
- As SW DO increases, consumption of DO via non-mixing dependent aerobic respiration increases for BASECASE 1 and BASECASE 2
- As SW DO increases, consumption of DOC increases for both BASECASE 1 and BASECASE 2. The increases in DOC consumption is due to an increase in non-mixing dependent aerobic respiration
- As SW DO increases, consumption of DOC for BASECASE 1 and BASECASE 2 follow about the same trend, except that consumption for BASECASE 1 is higher than for BASECASE 2. The additional DOC consumed in BASECASE 1 is from non-mixing dependent denitrification
- As SW DO increases, consumption of NO3 decreases a lot for BASECASE 1 and decreases very slightly for BASECASE 2. For BASECASE 1, DO greatly inhibits non-mixing dependent denitrification. For BASECASE 2, DO inhibits mixing dependent denitrification and/or a decreased availability of DOC slightly decreases the amount of NO3 consumed.
- A presence of SW DO more greatly inhibits non-mixing dependent denitrification than mixing dependent denitrification

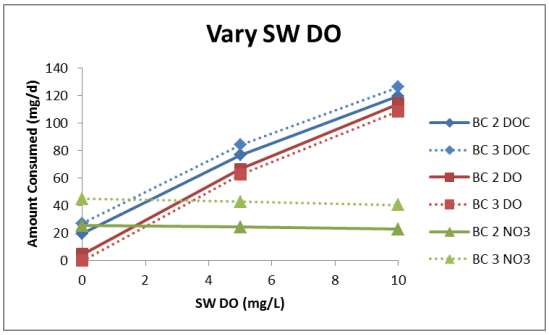

Figure D-40: Comparison of basecase 2 and 3 for varying SW DO.

- As SW DO increases, trends for DOC, DO and NO3 consumption are the same for BASECASE 2 and BASECASE 3, except that DOC and NO3 consumption for BASECASE 3 are slightly higher than for BASECASE 2, and DO consumption for BASECASE 2 is slightly higher than BASECASE 3.
- NO3 consumption is slightly higher for BASECASE 3 because there is no GW DO, and therefore GW DO does not inhibit mixing dependent denitrification.
- DO consumption is slightly higher for BASECASE 2 because there is GW DO, and therefore some mixing dependent aerobic respiration is occurring.

D.2.4.3 Vary SW DOC

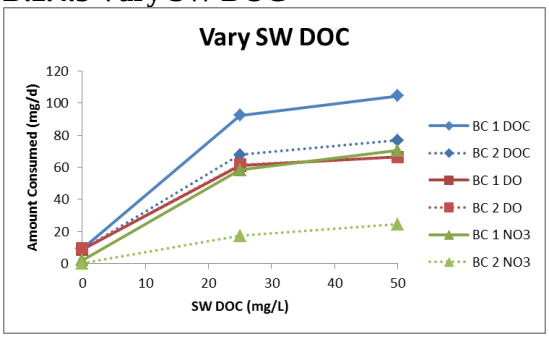

Figure D-41: Comparison of basecase 1 and 2 for varying SW DOC.

- As SW DOC increases, consumption of DOC, DO and NO3 increases for both BASECASE 1 and BASECASE 2
- As SW DOC increases, consumption of DOC for BASECASE 1 and BASECASE 2 follow about the same trend, except that consumption for BASECASE 1 is higher than for BASECASE 2. The additional DOC consumed in BASECASE 1 is from non-mixing dependent denitrification
- For all SW DOC scenarios, consumption of DO is the same for BASECASE 1 and BASECASE 2
- As SW DOC increases, consumption of DO via non-mixing dependent aerobic respiration increases for BASECASE 1 and BASECASE 2
- As SW DOC increases, consumption of NO3 for BASECASE 1 and BASECASE 2 follow the same trend, except that consumption of NO3 for BASECASE 1 is higher than for BASECASE 2. The additional NO3 consumed in BASECASE 1 is from non-mixing dependent denitrification. All NO3 consumed in BASECASE 2 is from mixing dependent denitrification.

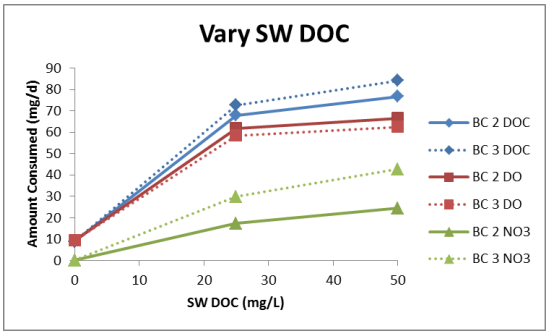

Figure D-42: Comparison of basecase 2 and 3 for varying SW DOC.

- As SW DOC increases, trends for DOC, DO and NO3 consumption are the same for BASECASE 2 and BASECASE 3, except that DOC and NO3 consumption for BASECASE 3 are slightly higher than for BASECASE 2, and DO consumption for BASECASE 2 is slightly higher than BASECASE 3.
- NO3 consumption is slightly higher for BASECASE 3 because there is no GW DO, and therefore GW DO does not inhibit mixing dependent denitrification.
- DO consumption is slightly higher for BASECASE 2 because there is GW DO, and therefore some mixing dependent aerobic respiration is occurring.

D.2.4.4 Vary GW NO_3^-

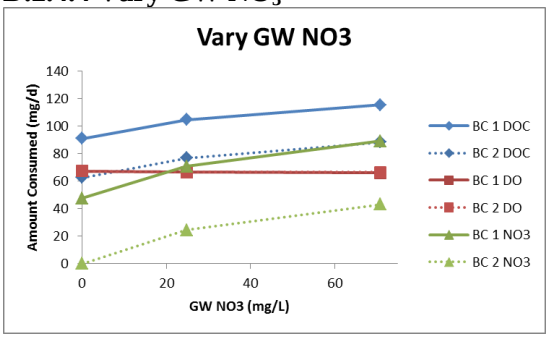

Figure D-43: Comparison of basecase 1 and 2 for varying GW NO_3^-.

- As GW NO3 increases, DOC consumption for both BASECASE 1 and BASECASE 2 increases. The increase in DOC consumed is from an increase in mixing dependent denitrification.

- As GW NO3 increases, consumption of DOC for BASECASE 1 and BASECASE 2 follow about the same trend, except that consumption for BASECASE 1 is higher than for BASECASE 2. The additional DOC consumed in BASECASE 1 is from non-mixing dependent denitrification
- For all GW NO3 scenarios, consumption of DO is the same for BASECASE 1 and BASECASE 2
- As GW NO3 increases, consumption of DO stays constant for BASECASE 1 and BASECASE 2
- As GW NO3 increases, NO3 consumption for both BASECASE 1 and BASECASE 2 increases. The increase in NO3 consumed is from an increase in mixing dependent denitrification.
- As GW NO3 increases, consumption of NO3 for BASECASE 1 and BASECASE 2 follow the same trend, except that consumption of NO3 for BASECASE 1 is higher than for BASECASE 2. The additional NO3 consumed in BASECASE 1 is from non-mixing dependent denitrification. All NO3 consumed in BASECASE 2 is from mixing dependent denitrification.

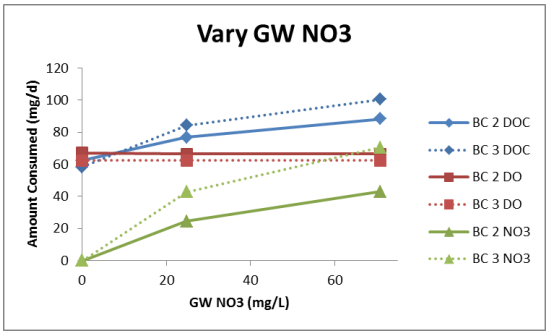

Figure D-44: Comparison of basecase 2 and 3 for varying GW NO_3^-.

- As GW NO3 increases, trends for DOC, DO and NO3 consumption are the same for BASECASE 2 and BASECASE 3, except that DOC and NO3 consumption for BASECASE 3 are slightly higher than for BASECASE 2, and DO consumption for BASECASE 2 is slightly higher than BASECASE 3.
- NO3 consumption is slightly higher for BASECASE 3 because there is no GW DO, and therefore GW DO does not inhibit mixing dependent denitrification.
- DO consumption is slightly higher for BASECASE 2 because there is GW DO, and therefore some mixing dependent aerobic respiration is occurring.

D.2.4.5 Vary SW NO_3^-

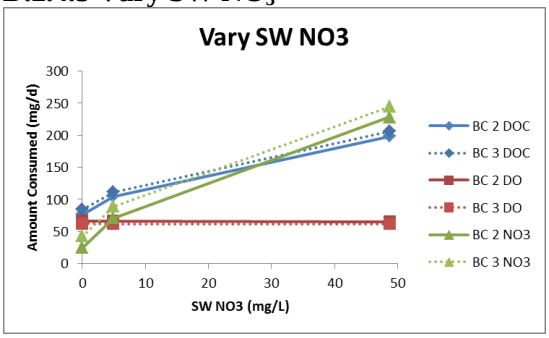

Figure D-45: Comparison of basecase 1 and 2 for varying SW NO_3^-.

- As SW NO3 increases, DOC and NO3 consumption for both BASECASE 2 and BASECASE 3 increase. The increase in DOC and NO3 consumption is due to an increase in non-mixing dependent denitrification
- As SW NO3 increases, DO consumption for both BASECASE 2 and B3 stays about constant

- As SW NO3 increases, trends for DOC, DO and NO3 consumption are the same for BASECASE 2 and BASECASE 3, except that DOC and NO3 consumption for BASECASE 3 are slightly higher than for BASECASE 2, and DO consumption for BASECASE 2 is slightly higher than BASECASE 3
- NO3 consumption is slightly higher for BASECASE 3 because there is no GW DO, and therefore GW DO does not inhibit mixing dependent denitrification.
- DO consumption is slightly higher for BASECASE 2 because there is GW DO, and therefore some mixing dependent aerobic respiration is occurring.

D.2.4.6 Vary Hydraulic Conductivity

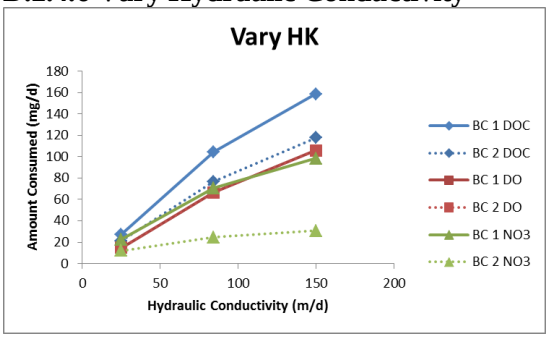

Figure D-46: Comparison of basecase 1 and 2 for varying hydraulic conductivity.

- As K increases, consumption of DOC, DO and NO3 for both BASECASE 1 and BASECASE 2 increase. When K is higher, more solutes are able to enter the model and this is likely the reason why more biodegradation occurs with higher K's.
- As K increases, consumption of DOC for BASECASE 1 and BASECASE 2 follow about the same trend, except that consumption for BASECASE 1 is higher than for BASECASE 2. The additional DOC consumed in BASECASE 1 is from non-mixing dependent denitrification
- For all K scenarios, consumption of DO is the same for BASECASE 1 and BASECASE 2
- As K increases, consumption of NO3 for BASECASE 1 and BASECASE 2 follow the same trend, except that consumption of NO3 for BASECASE 1 is higher than for BASECASE 2. The additional NO3 consumed in BASECASE 1 is from non-mixing dependent denitrification. All NO3 consumed in BASECASE 2 is from mixing dependent denitrification.

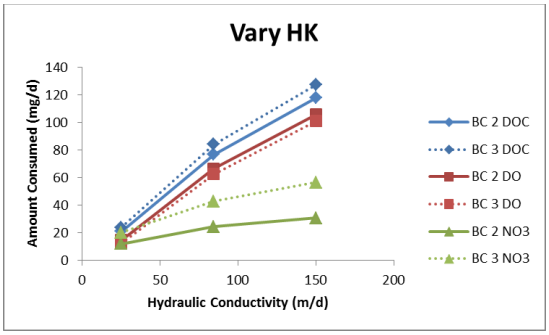

Figure D-47: Comparison of basecase 2 and 3 for varying hydraulic conductivity.

- As K increases, trends for DOC, DO and NO3 consumption are the same for BASECASE 2 and BASECASE 3, except that DOC and NO3 consumption for BASECASE 3 are slightly higher than for BASECASE 2, and DO consumption for BASECASE 2 is slightly higher than BASECASE 3.
- NO3 consumption is slightly higher for BASECASE 3 because there is no GW DO, and therefore GW DO does not inhibit mixing dependent denitrification.
- DO consumption is slightly higher for BASECASE 2 because there is GW DO, and therefore some mixing dependent aerobic respiration is occurring.

D.3 Complete Results for Fine Grid Analysis

This section provides a complete set of all results from the fine grid analysis. Section D.3.1 contains all results from varying the biogeochemical boundary conditions, and section D.3.2 contains all results from varying the hydraulic conditions. For each parameter varied in both sections, concentration maps for the conservative tracers and solutes are provided. The tracer concentration maps are plots of the tracer concentration over the model domain at steady state with the same boundary concentration as the solute they represent. Additionally, for each parameter varied in both sections, there are figures for the amount (and sometimes) percent of solute consumed, and tables showing how much of each solute is entering the model. Finally, for each parameter varied in both sections, the original bulleted text interpreting the results remains. Additionally, section D.3.2 contains some additional figures including residence time distributions, hydraulic conductivity and vector fields for the model domain and MODPATH particle tracking for some of the parameters varied.

D.3.1 Biogeochemical Boundary Conditions

D.3.1.1 Vary GW DOC and GW DO Simultaneously

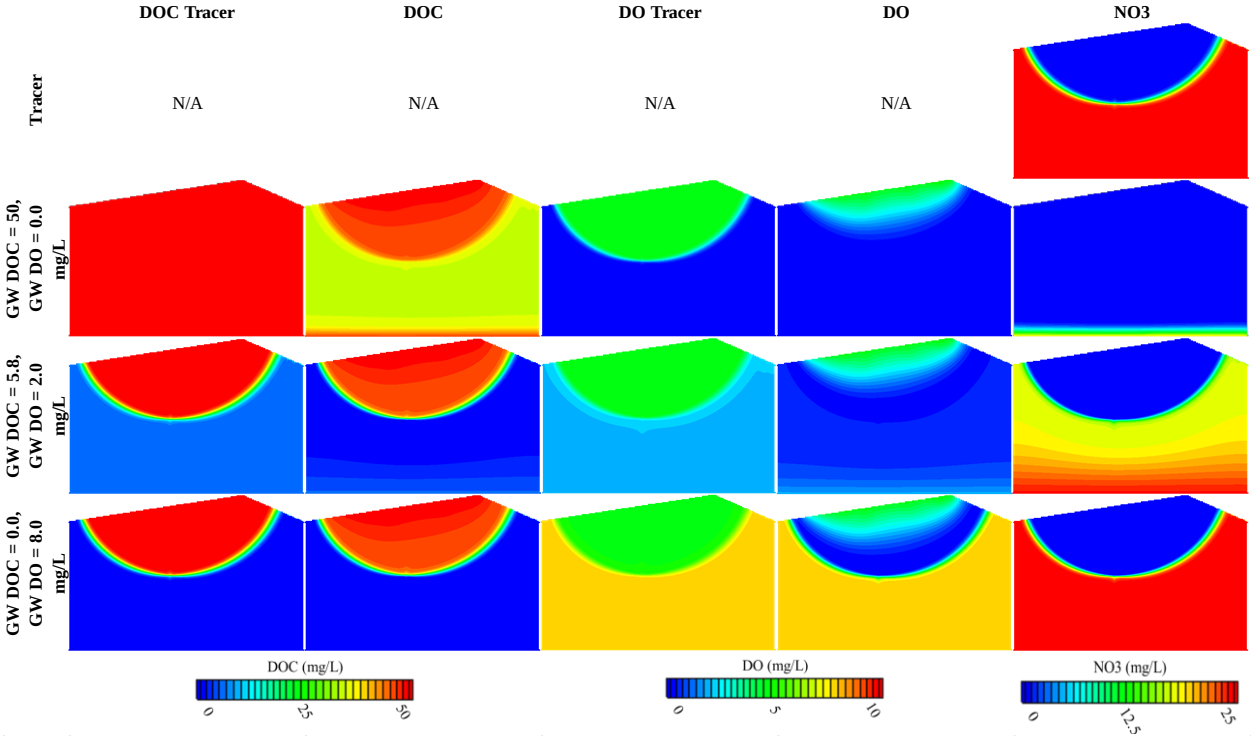

Figure D-48: DOC, DO, NO3 and tracer concentrations for varying GW DOC and GW DO simultaneously for the fine grid for basecase 2.

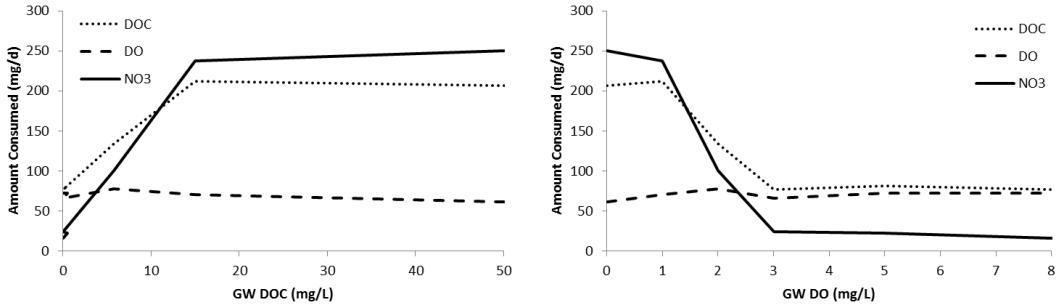

Figure D-49: Amount of each solute consumed for varying GW DOC and GW DO simultaneously for the fine grid for basecase 2.

Table D-1: Amount of each solute entering the model from SW and GW for varying GW DOC and GW DO for the fine grid for basecase 2.

GW DOC (mg/L)	GW DO (mg/L)	DOC IN (mg/d)		DO IN (mg/d)		NO3 IN (mg/d)	
		from SW	from GW	from SW	from GW	from SW	from GW
50.0	0.0	1125.0 (69.2%)	500.0 (30.8%)	112.5 (100%)	0	0	250.0 (100%)
15.0	1.0	1125.0 (88.2%)	150.0 (11.8%)	112.5 (91.9%)	10.0 (8.1%)	0	250.0 (100%)
5.8	2.0	1125.0 (95.1%)	57.8 (4.9%)	112.5 (85.0%)	19.9 (15.0%)	0	250.0 (100%)
0	3	1125.0 (100%)	0	112.5 (79.1%)	29.7 (20.9%)	0	250.0 (100%)
0.5	5.0	1125.0 (99.6%)	5.0 (0.4%)	112.5 (69.2%)	50.0 (30.8%)	0	250.0 (100%)
0.0	8.0	1125.0 (100%)	0	112.5 (58.5%)	79.7 (41.5%)	0	250.0 (100%)

- GW DO and DOC are varied simultaneously such that as GW DO increases, GW DOC decreases
- The basecase has nitrate consumed via mixing dependent denitrification because nitrate and DOC come from different source waters.
- As GW DOC increases and GW DO decreases, consumption of NO3 and DOC increase a lot and then level off due to non-mixing dependent denitrification in upgradient GW. NO3 consumption levels off at higher GW DOC levels because all NO3 has been consumed. DOC then levels off for this reason.
- As GW DOC increases and GW DO decreases consumption of DO via aerobic respiration remains about the same

D.3.1.2 Vary SW DO

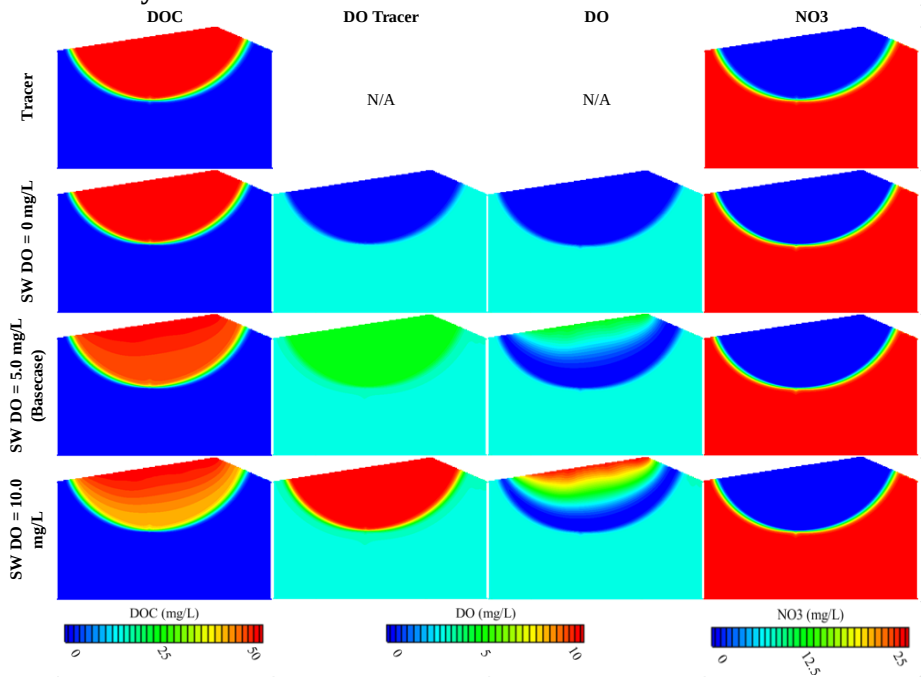

Figure D-50: DOC, DO, NO3 and tracer concentrations for varying SW DO for the fine grid for basecase 2.

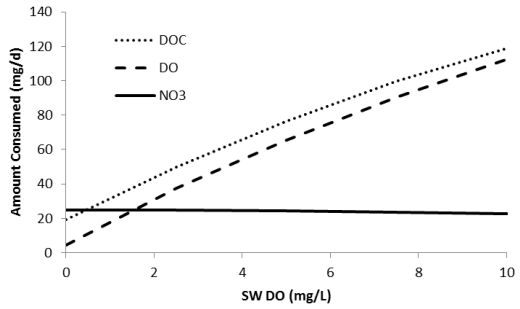

Figure D-51: Amount of each solute consumed for varying SW DO for the fine grid for basecase 2.

Table D-2: Amount of each solute entering the model from SW and GW for varying SW DO for the fine grid for basecase 2.

SW DO (mg/L)	DOC IN (mg/d)		DO IN (mg/d)		NO3 IN (mg/d)	
	from SW	from GW	from SW	from GW	from SW	from GW
0.0	1125.0 (100%)	0	0.0 (0%)	29.7 (100%)	0	250.0 (100%)
2.5	1125.0 (100%)	0	56.2 (65.5%)	29.7 (34.5%)	0	250.0 (100%)
5.0	1125.0 (100%)	0	112.5 (79.1%)	29.7 (20.9%)	0	250.0 (100%)
7.5	1125.0 (100%)	0	165.6 (84.8%)	29.7 (15.2%)	0	250.0 (100%)
10.0	1125.0 (100%)	0	225.0 (88.3%)	29.7 (11.7%)	0	250.0 (100%)

- As SW DO increases, consumption of DO via non-mixing dependent aerobic respiration increases
- As SW DO increases, consumption of NO3 via mixing dependent denitrification decreases slightly. The slight decreases in NO3 consumption could be from decreased DOC availability and/or inhibition from oxygen.

D.3.1.3 Vary SW DOC

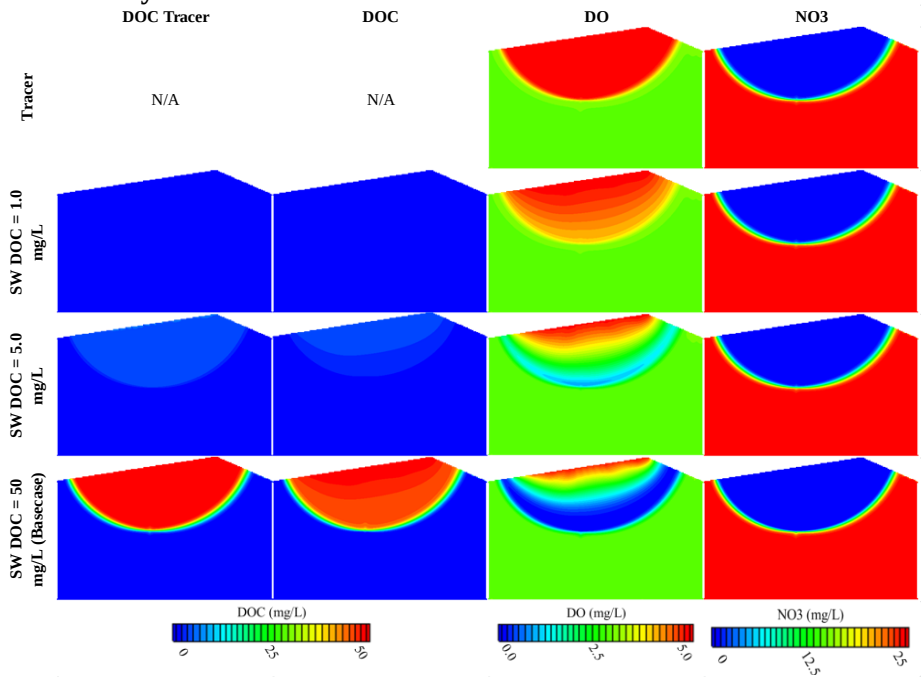

Figure D-52: DOC, DO, NO3 and tracer concentrations for varying SW DOC for the fine grid for basecase 2.

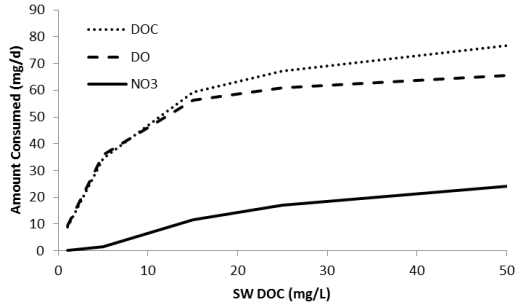

Figure D-53: Amount of each solute consumed for varying SW DOC for the fine grid for basecase 2.

Table D-3: Amount of each solute entering the model from SW and GW for varying SW DOC for the fine grid for basecase 2.

SW DOD (mg/L)	DOC IN (mg/d)		DO IN (mg/d)		NO3 IN (mg/d)	
	from SW	from GW	from SW	from GW	from SW	from GW
1.0	22.6 (100%)	0	112.5 (79.1%)	29.7 (20.9%)	0	250.0 (100%)
5.0	112.5 (100%)	0	112.5 (79.1%)	29.7 (20.9%)	0	250.0 (100%)
15.0	331.2 (100%)	0	112.5 (79.1%)	29.7 (20.9%)	0	250.0 (100%)
25.0	562.5 (100%)	0	112.5 (79.1%)	29.7 (20.9%)	0	250.0 (100%)
50.0	1125.0 (100%)	0	112.5 (79.1%)	29.7 (20.9%)	0	250.0 (100%)

- As SW DOC increases, consumption of DOC, DO and NO3 increase.
- As SW DOC increases from 0 to 5 mg/L, DO and DOC consumption increase very quickly. At higher DOC concentrations, DO consumption continues to increase but at a much slower rate.
- At DOC concentrations between 0 and 5 mg/L, almost no NO3 is consumed. This is because almost all DOC is consumed via non-mixing dependent aerobic respiration in SW derived water before the DOC can mix with the upwelling GW.
- Mixing dependent denitrification is SW DOC limited (the way we have the model set up)

D.3.1.4 Vary GW NO_3^-

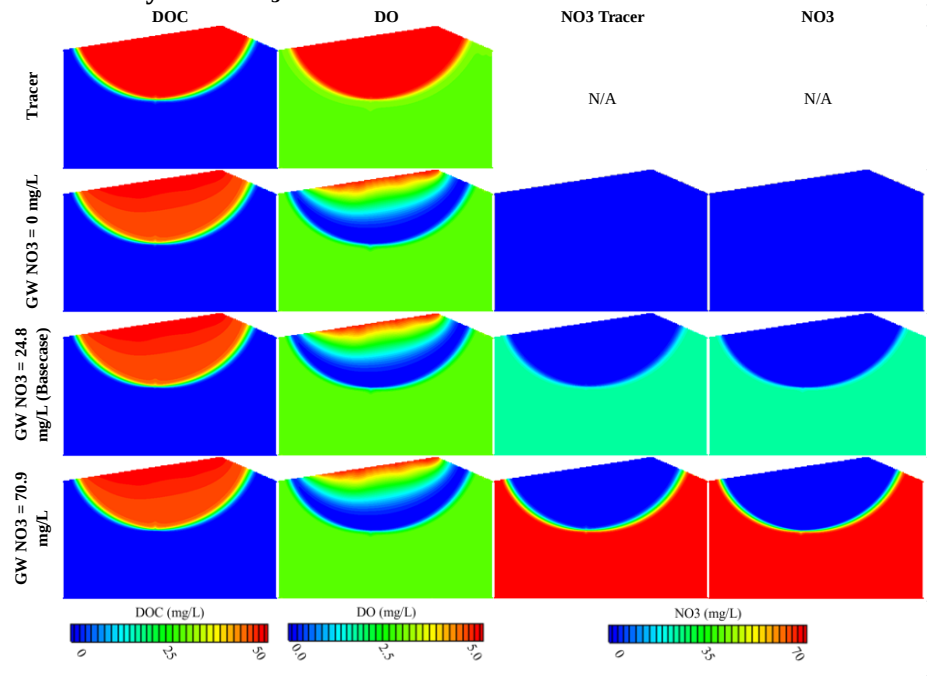

Figure D-54: DOC, DO, NO3 and tracer concentrations for varying GW NO3 for the fine grid for basecase 2.

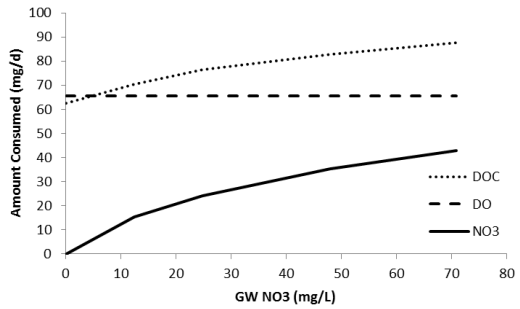

Figure D-55: Amount of each solute consumed for varying GW NO3 for the fine grid for basecase 2.

Table D-4: Amount of each solute entering the model from SW and GW for varying GW NO3 for the fine grid for basecase 2.

GW NO3 (mg/L)	DOC IN (mg/d)		DO IN (mg/d)		NO3 IN (mg/d)	
	from SW	from GW	from SW	from GW	from SW	from GW
0.0	1125.0 (100%)	0	112.5 (79.1%)	29.7 (20.9%)	0	0
12.4	1125.0 (100%)	0	112.5 (79.1%)	29.7 (20.9%)	0	125.0 (100%)
24.8	1125.0 (100%)	0	112.5 (79.1%)	29.7 (20.9%)	0	250.0 (100%)
47.9	1125.0 (100%)	0	112.5 (79.1%)	29.7 (20.9%)	0	475.0 (100%)
70.9	1125.0 (100%)	0	112.5 (79.1%)	29.7 (20.9%)	0	701.1 (100%)

- As GW NO3 increases, the amount of DO consumed stays constant
- As GW NO3 increases, the amount of NO3 consumed via mixing dependent denitrification increases
- As GW NO3 increases, the amount of DOC consumed increases. The increase in DOC consumption is due to an increase in mixing dependent denitrification.
- Mixing dependent denitrification is GW NO3 limited

D.3.1.5 Vary SW NO_3^-

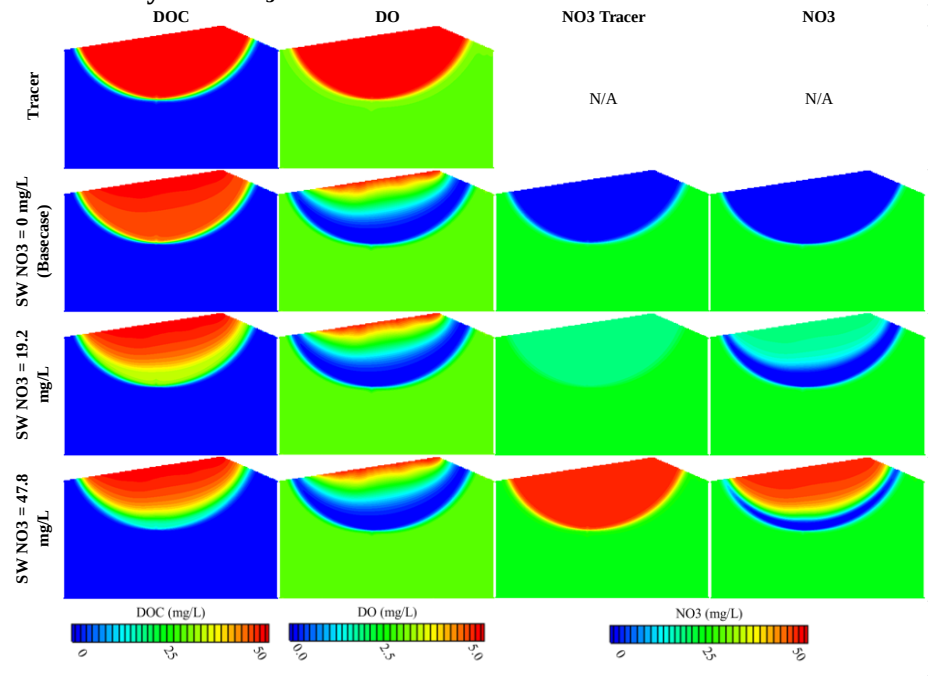

Figure D-56: DOC, DO, NO3 and tracer concentrations for varying SW NO3 for the fine grid for basecase 2.

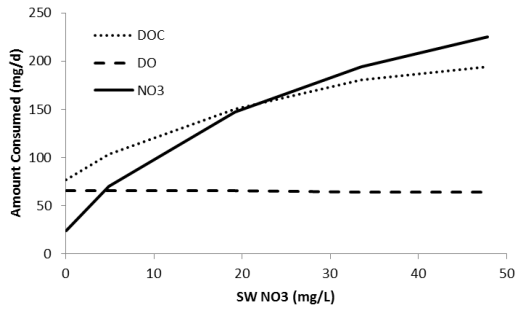

Figure D-57: Amount of each solute consumed for varying SW NO3 for the fine grid for basecase 2.

Table D-5: Amount of each solute entering the model from SW and GW for varying SW NO3 for the fine grid for basecase 2.

SW NO3 (mg/L)	DOC IN (mg/d)		DO IN (mg/d)		NO3 IN (mg/d)	
	from SW	from GW	from SW	from GW	from SW	from GW
0.0	1125.0 (100%)	0	112.5 (79.1%)	29.7 (20.9%)	0	250.0 (100%)
4.9	1125.0 (100%)	0	112.5 (79.1%)	29.7 (20.9%)	109.4 (30.4%)	250.0 (69.6%)
19.2	1125.0 (100%)	0	112.5 (79.1%)	29.7 (20.9%)	425.0 (63.0%)	250.0 (37.0%)
33.5	1125.0 (100%)	0	112.5 (79.1%)	29.7 (20.9%)	750.0 (75.0%)	250.0 (25.0%)
47.8	1125.0 (100%)	0	112.5 (79.1%)	29.7 (20.9%)	1075.0 (81.1%)	250.0 (18.9%)

- As SW NO3 increases, DO consumption via aerobic respiration remains about the same
- As SW NO3 increases, NO3 consumption via non-mixing dependent denitrification increases
- As SW NO3 increases, DOC consumption increases. The increase in DOC consumption is due to an increase in non-mixing dependent denitrification.

D.3.2 Homogeneous and Heterogeneous Hydraulic Conditions
D.3.2.1 Vary Hydraulic Conductivity

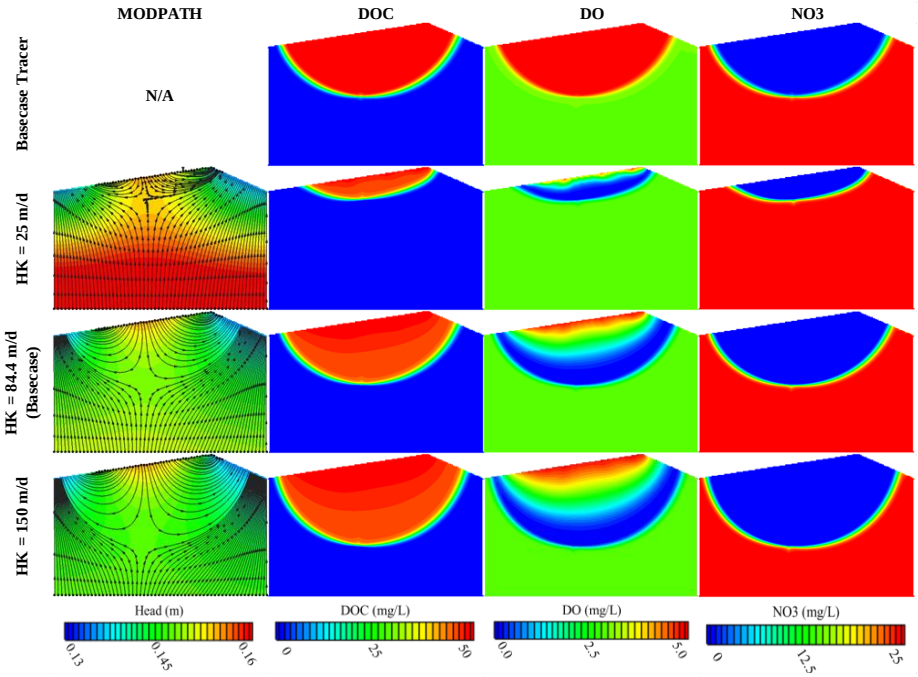

Figure D-58: MODPATH flow paths and DOC, DO, NO3 and tracer concentrations for varying hydraulic conductivity for the fine grid for basecase 2.

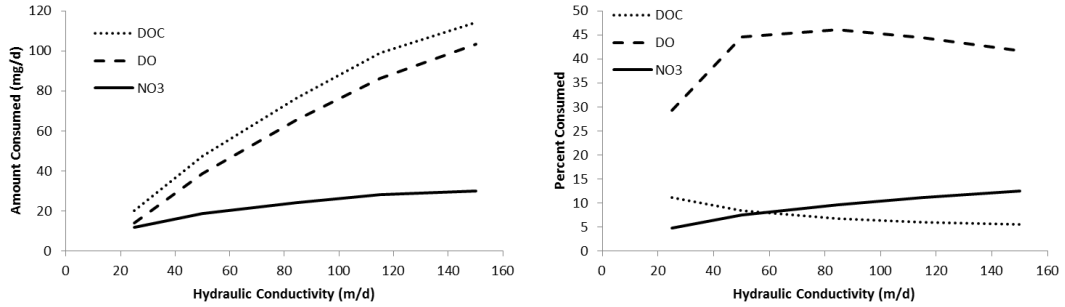

Figure D-59: Amount and percent of each solute consumed for varying hydraulic conductivity for the fine grid for basecase 2.

Table D-6: Amount of each solute entering the model from SW and GW for varying hydraulic conductivity for the fine grid for basecase 2.

HK (m/d)	DOC IN (mg/d)		DO IN (mg/d)		NO3 IN (mg/d)	
	from SW	from GW	from SW	from GW	from SW	from GW
25	183.7 (100%)	0	18.3 (37.9%)	30.1 (62.1%)	0	248.1 (100%)
50	567.2 (100%)	0	56.9 (65.6%)	29.9 (34.4%)	0	246.3 (100%)
84.4	1125.0 (100%)	0	112.5 (79.1%)	29.7 (20.9%)	0	250.0 (100%)
115	1655.2 (100%)	0	163.8 (84.4%)	30.2 (15.6%)	0	250.0 (100%)
150	2087.0 (100%)	0	217.4 (87.9%)	29.9 (12.1%)	0	239.1 (100%)

- As K increases, DOC and DO entering the model domain from SW increases a lot, and DO and NO3 entering the model domain from GW stays about the same.
- As K increases, consumption of DOC, DO and NO3 increases. DOC and DO consumption increase more than consumption of NO3 because their increase in inflow to the model is greater.

NO3 consumption increases due to the increase in SW DOC, indicating that mixing-dependent denitrification is SW DOC limited, consistent with what we saw when we varied SW DOC.

D.3.2.2 Vary Lower Bottom Flowrate

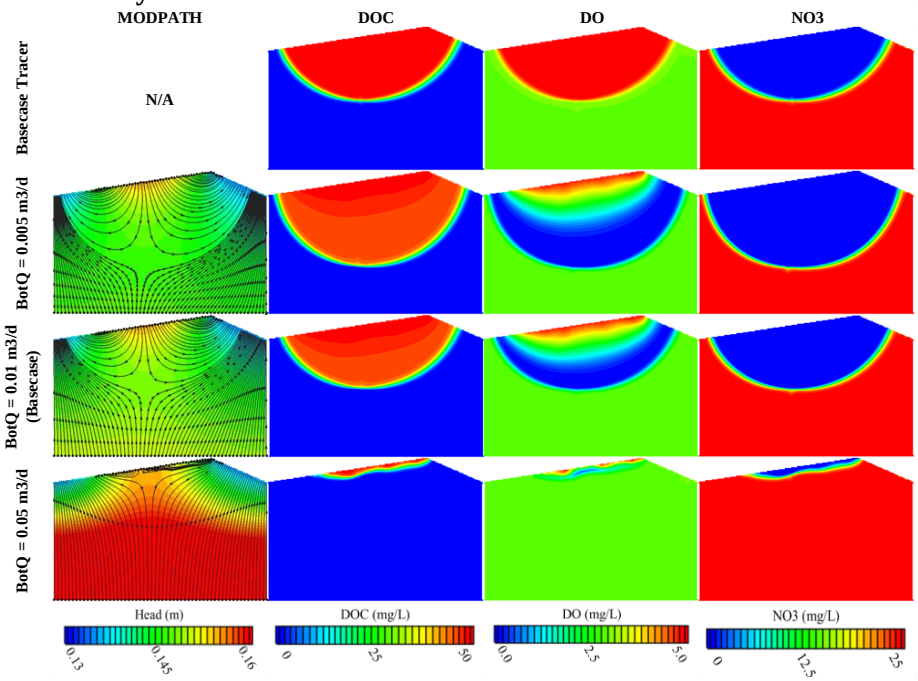

Figure D-60: MODPATH flow paths and DOC, DO, NO3 and tracer concentration for varying lower boundary flowrate for the fine grid for basecase 2.

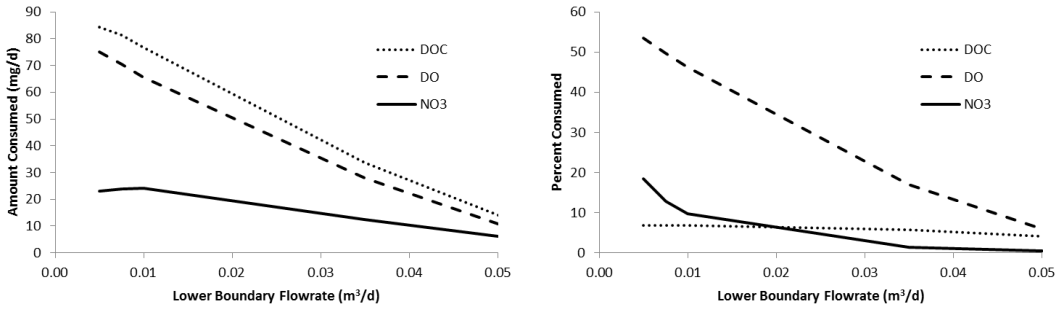

Figure D-61: Amount and percent of each solute consumed for varying lower boundary flowrate for the fine grid for basecase 2.

Table D-7: Amount of each solute entering the model from SW and GW for varying lower boundary flowrate for the fine grid for basecase 2.

Bot Q (m3/d)	DOC IN (mg/d)		DO IN (mg/d)		NO3 IN (mg/d)	
	from SW	from GW	from SW	from GW	from SW	from GW
0.0050	1225.0 (100%)	0	125.0 (89.1%)	15.2 (10.9%)	0	125.0 (100%)
0.0075	1175.0 (100%)	0	118.8 (84.0%)	22.7 (16.0%)	0	187.5 (100%)
0.0100	1125.0 (100%)	0	112.5 (79.1%)	29.7 (20.9%)	0	250.0 (100%)
0.0350	589.7 (100%)	0	59.3 (35.9%)	105.8 (64.1%)	0	871.8 (100%)
0.0500	342.8 (100%)	0	34.5 (18.9%)	147.4 (81.1%)	0	1230.8 (100%)

- As lower boundary flowrate increases, the amount of each solute coming from SW decreases and the amount of each solute coming from GW increases

- As lower boundary flowrate increases, GW NO3 flowing into the model increases, but SW DOC entering the model simultaneously decreases. These countervailing trends explain the non-monotonic nature of the trend of denitrification with lower boundary flowrate, but ultimately the decrease in SW DOC outweigh the increase in GW NO3 for an overall declining trend.
- The decreases in SW DOC and SW DO cause aerobic respiration within the hyporheic flow cell to decrease, leading to the monotonic decreases in DOC and DO consumption that we observed

D.3.2.3 Vary Variance of Hydraulic Conductivity

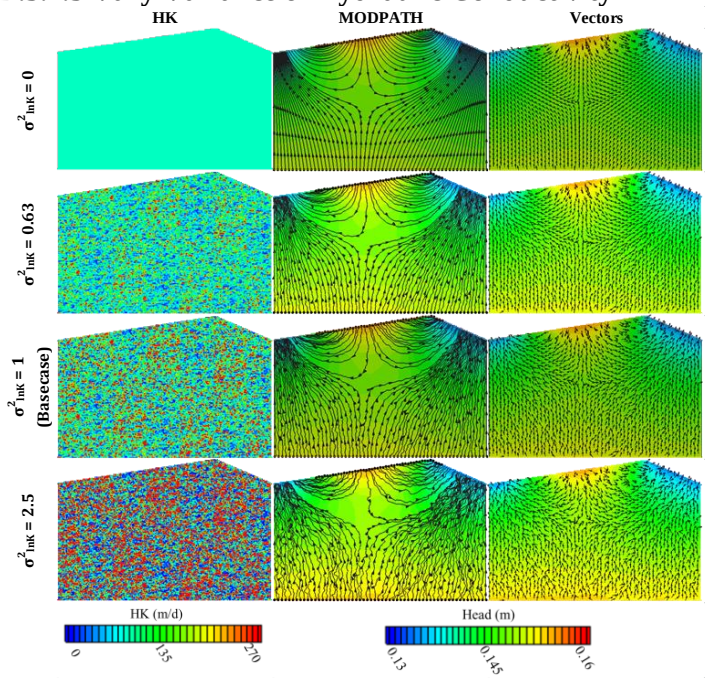

Figure D-62: Hydraulic conductivity and head (with particle tracking and vectors) for varying variance of hydraulic conductivity for the fine grid for basecase 2.

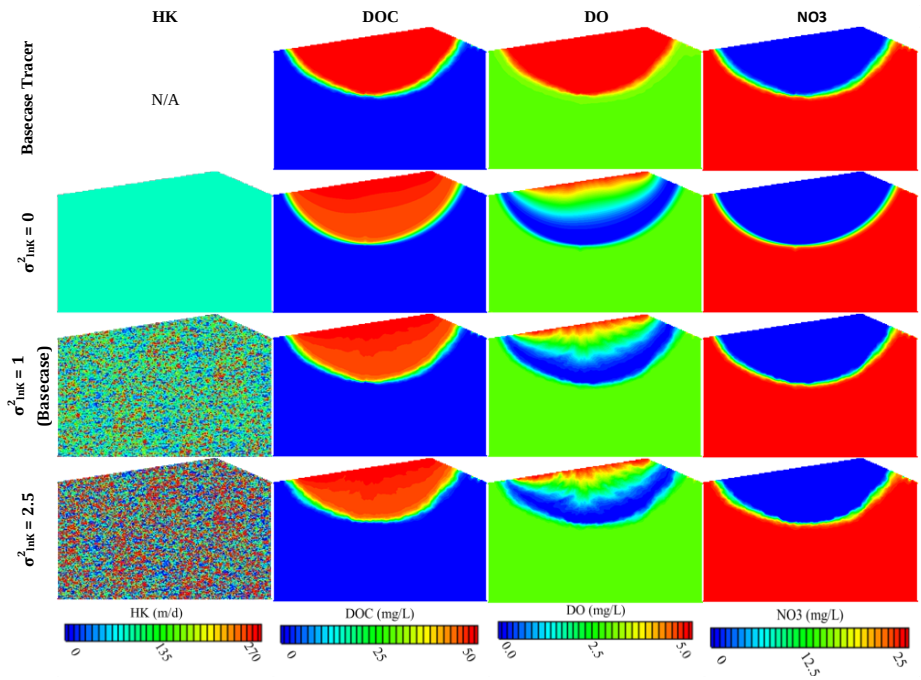

Figure D-63: Hydraulic conductivity fields and DOC, DO, NO3 and tracer concentration for varying variance of hydraulic conductivity for the fine grid for basecase 2.

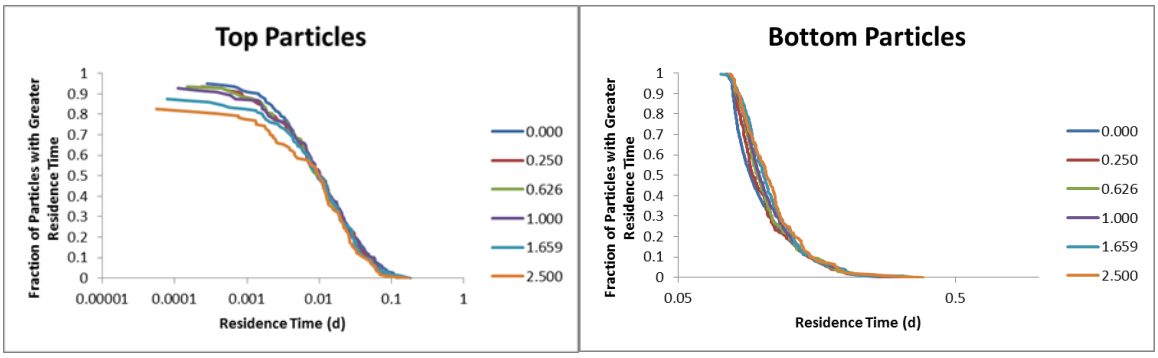

Figure D-64: Cumulative residence time distribution within model domain for particles released at the upper model boundary with SW (left) and at lower model boundary (right) for varying variance of hydraulic conductivity.

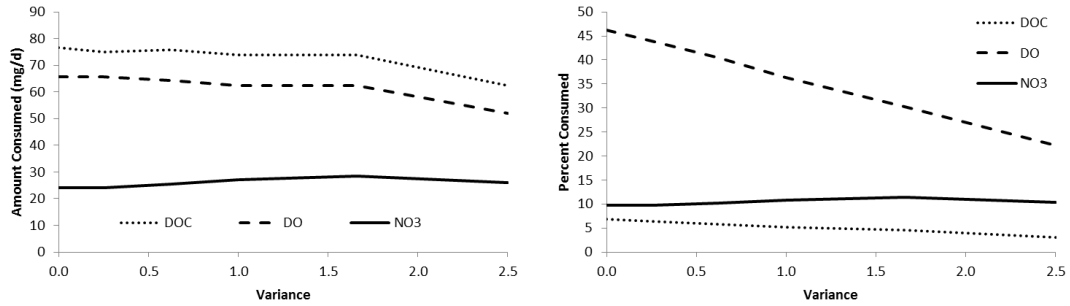

Figure D-65: Amount and percent of each solute consumed for varying variance of hydraulic conductivity for the fine grid for basecase 2.

Table D-8: Amount of each solute entering the model from SW and GW for varying variance of hydraulic conductivity for the fine grid for basecase 2.

Variance	DOC IN (mg/d)		DO IN (mg/d)		NO3 IN (mg/d)	
	from SW	from GW	from SW	from GW	from SW	from GW
0.000	1125.0 (100%)	0	112.5 (79.1%)	29.7 (20.9%)	0	250.0 (100%)
0.250	1175.0 (100%)	0	118.8 (79.6%)	30.5 (20.4%)	0	250.0 (100%)
0.626	1303.0 (100%)	0	128.8 (81.0%)	30.3 (19.0%)	0	250.0 (100%)
1.000	1409.1 (100%)	0	142.0 (82.6%)	29.8 (17.4%)	0	250.0 (100%)
1.659	1636.4 (100%)	0	174.8 (84.8%)	31.3 (15.2%)	0	250.0 (100%)
2.500	2000.0 (100%)	0	208.3 (88.9%)	26.0 (11.1%)	0	250.0 (100%)

- As variance increases, the amount of DOC and DO coming from SW increases and the amount of DO and NO3 coming from GW stays about the same.
    - Variance affects SW flux because the dune surface is not flat and flow paths are already entering the model at different angles (other than straight down). This gives the flow paths more opportunities to turn around and go back out of the model domain.
    - Variance does not affect GW flux because at the bottom, flow is coming straight up and therefore there is much less of a chance for the flow paths to turn around.
- Although the amount of SW solutes entering the model increases as variance increases, non-mixing dependent aerobic respiration of DOC and DO actually decreases (unlike when homogeneous K was varied). This can be explained by residence times and preferential flow paths
    - As variance increases, the amount of SW particles with short residence times increases (Figure 20). An increase in short residence times means that there are more flow paths that are coming into the model and then leaving the model very quickly. These quick flow paths contribute to SW solutes entering the model, but have very short residence times that are probably not long enough for substantial biodegradation.
    - As variance increases, preferential flow paths increase. This can be seen in the MODPATH column of Figure 18. When $\sigma^2_{lnK} = 0$, the SW particles are more or less evenly spaced. As variance increases, the path lines become more bunched together leaving more empty space. This means that water is traveling in preferential flow paths. These preferential flow paths likely are areas with higher homogeneous K, meaning they have shorter residence times resulting in less biodegradation, while still contributing to an increased amount of SW solutes entering the model domain.
    - The first effect above is due to a modeling artifact (the finite difference stair stepped dune face boundary) while the second effect appears to be a real phenomenon that would occur in the field
- As variance increases, there is an increase in short residence times. These short residence times are probably not allowing for as much non-mixing dependent biodegradation, leaving more DO in the model domain
- As variance increases, mixing dependent denitrification increases slightly and then decreases (at very high variances). *Hester et al.* [2013] showed that an increase in variance increased mixing between hyporheic water and GW. This is probably why denitrification increases initially. However, as explained above, an increase in variance decreased non-mixing dependent biodegradation leaving more DO in the model. The extra DO in the hyporheic water is probably inhibiting mixing dependent denitrification at higher variances.

D.3.2.4 Vary Horizontal Correlation Length of Hydraulic Conductivity

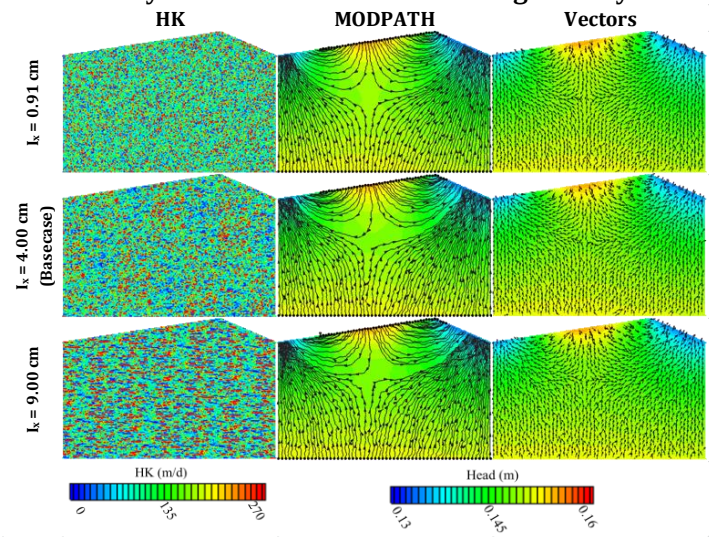

Figure D-66: Hydraulic conductivity and head (with particle tracking and vectors) for varying horizontal correlation length for the fine grid for basecase 2.

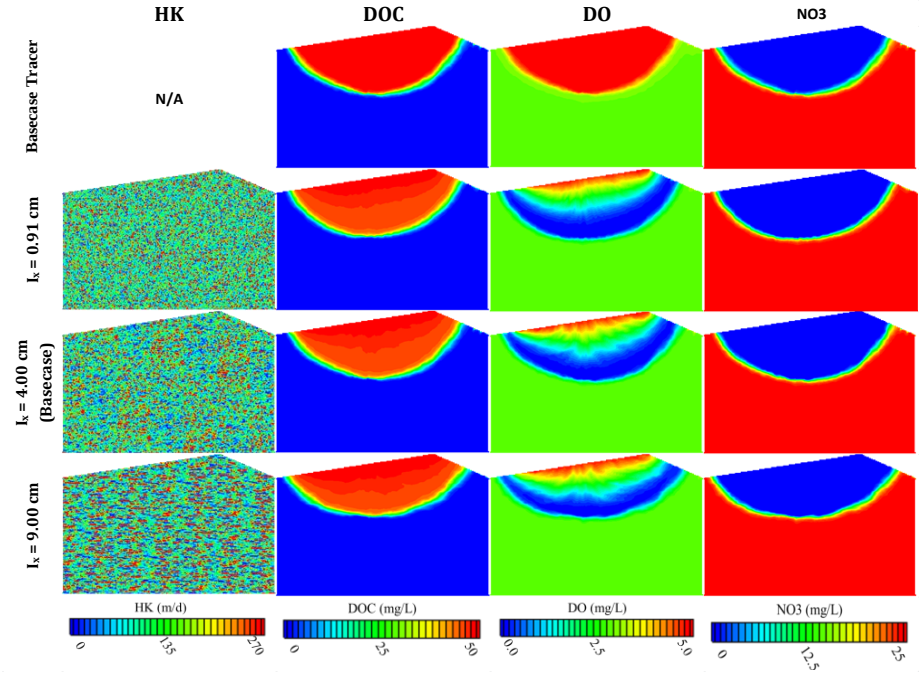

Figure D-67: Hydraulic conductivity fields and DOC, DO, NO3 and tracer concentrations for varying horizontal correlation length for the fine grid for basecase 2.

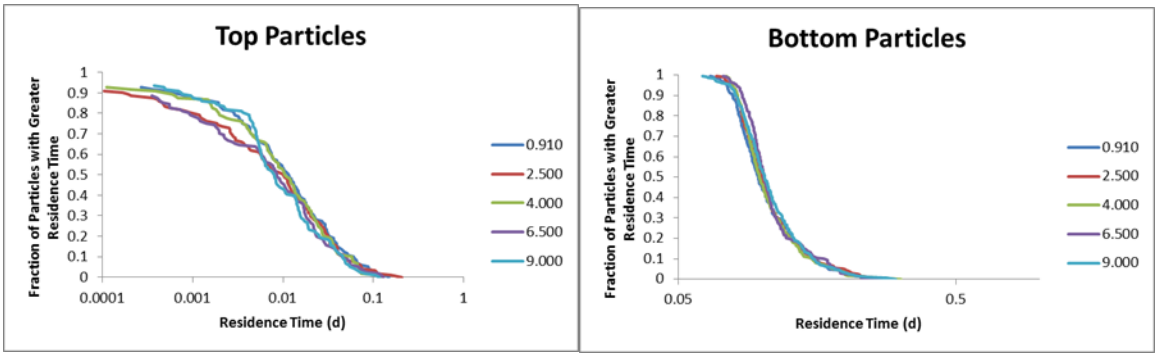

Figure D-68 Cumulative residence time distribution within model domain for particles released at the upper model boundary with SW (left) and at lower model boundary (right) for varying horizontal correlation length.

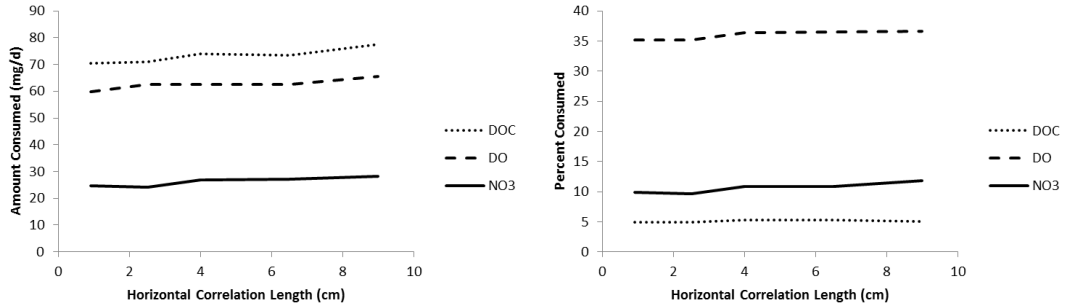

Figure D-69: Amount and percent of each solute consumed for varying horizontal correlation length for the fine grid for basecase 2.

Table D-9: Amount of each solute entering the model from SW and GW for varying horizontal correlation length for the fine grid for basecase 2.

H. Corr. Length	DOC IN (mg/d)		DO IN (mg/d)		NO3 IN (mg/d)	
(cm)	from SW	from GW	from SW	from GW	from SW	from GW
0.91	1416.7 (100%)	0	140.6 (82.4%)	29.9 (17.6%)	0	250.0 (100%)
2.5	1454.6 (100%)	0	147.7 (83.2%)	29.8 (16.8%)	0	250.0 (100%)
4.0	1409.1 (100%)	0	142.0 (82.6%)	29.8 (17.4%)	0	250.0 (100%)
6.5	1391.5 (100%)	0	141.3 (82.5%)	29.9 (17.5%)	0	250.0 (100%)
9.0	1523.8 (100%)	0	148.8 (83.3%)	29.8 (16.7%)	0	238.1 (100%)

- As horizontal correlation length increases, there is no pattern in change of SW residence times, GW residence times or flux of solutes entering the model from SW or GW
- As horizontal correlation length increases, consumption of all solutes increases slightly
- *Hester et al.* [2013] showed that an increase in correlation length increased mixing between hyporheic water and GW. This could be the cause of the slight increase in consumption of all solutes. Consumption of nitrate is from mixing dependent denitrification and consumption of oxygen is from a combination of mixing dependent and non-mixing dependent aerobic respiration. It's possible that consumption of mixing dependent reactions increase as correlation length increases due to an increase in mixing.